

Cascade Based Tracking Control of Quadrotors

S.J.A.M. van den Eijnden

DC 2017.012

Master's thesis

Coach: dr. ir. A.A.J. Lefeber

Supervisor: prof. dr. H. Nijmeijer

Eindhoven University of Technology
Department of Mechanical Engineering
Section Dynamics and Control

Eindhoven, January 9, 2017

Summary

Unmanned aerial vehicles (UAVs) provide the possibility to efficiently automate several processes, for example in the logistics sector. In many of such automated processes it is required for the drone to track a certain predefined trajectory without the intervention of a human operator. The design of appropriate tracking control algorithms is a crucial element in accomplishing such a task and is currently a very active topic of research. The main objective of this thesis is the design of tracking controllers for the autonomous flight of a specific type of UAV: the quadrotor. It is aimed for these controllers to guarantee sufficient tracking, not only for simple trajectories (e.g. hovering), but also in case of more aggressive acrobatic maneuvers. In this work, a nonlinear system dynamics description of the quadrotor is derived. In view of the cascaded nature of these dynamics, subsequently a full state feedback tracking controller is designed based on the theory of cascaded systems. Here, the complete system is divided into two independent subsystems, coupled with a nonlinear interconnection term, which are stabilized by means of several control techniques. Using known stability results for (time-varying) cascaded systems, almost-global uniform asymptotic stability of the complete interconnected closed-loop system is shown. The state feedback control framework is used for successive output feedback design, with the aim for a practical implementation on a quadrotor platform that is unable to provide velocity measurements. By means of a convergence analysis of the system in closed-loop with the dynamic output feedback law, similar convergence properties as in the state feedback case are guaranteed. The robustness of the final controller is first examined within a realistic simulation environment in which effects such as measurement noise and input saturation are taken into account. Simulation results show sufficient tracking performance in case of time-varying reference signals. As a final assessment, the feedback law is embedded within the Parrot AR Drone 2.0. Several experiments in which it is desired for the quadrotor to track a three dimensional circular reference trajectory are performed. Although the results show that the closed-loop system is able to perform stable circular maneuvers, a large deviation from the reference trajectory during flight remains. As a possible cause of this effect, unmodelled dynamics such as drag forces and torques are identified. Additional simulations in which such damping effects are taken into account, are conducted. The results show strong resemblance with the experiments, confirming the dominant effect of the unconsidered dynamics.

Contents

Summary	i
Nomenclature	iv
1 Introduction	1
1.1 Background	1
1.2 Literature Review	2
1.3 Motivation and Objectives	5
1.4 Outline of the Thesis	5
2 Preliminaries	7
2.1 Attitude Representations	7
2.2 Convergence Results	9
2.3 Cascaded Systems	10
3 System Dynamics	13
3.1 Degrees of Freedom	13
3.2 Dynamic Model	14
3.3 Concluding Remarks	17
4 State Feedback Control	19
4.1 Problem Formulation	20
4.2 Position Control Design	22
4.3 Attitude Control Design	25
4.4 Closed-loop Stability	29
4.5 Full State Stability	32
4.6 Concluding Remarks	33
5 Output Feedback Control	35
5.1 Problem Formulation	35
5.2 Observer Design	36
5.3 Dynamic Output Feedback	38
5.4 Observer Extension	40
5.5 Attitude Reconstruction	41
5.6 Concluding Remarks	43
6 Simulations and Experiments	45
6.1 Numerical Model	45
6.2 Simulation Results	47
6.3 Experimental Setup	52
6.4 Experimental Flights	55
6.5 Concluding Remarks	61

7	Conclusions and Recommendations	63
7.1	Conclusions	63
7.2	Recommendations	64
	Bibliography	67
A	Observer Extension: Proof	73
B	Attitude Reconstruction Algorithm	77
B.1	Roll and Pitch Angles	77
B.2	Yaw Angle	79
	Acknowledgements	81

Nomenclature

List of Symbols

\mathbb{N}	The set of nonnegative integers
\mathbb{R}^n	The n -dimensional Euclidian space
$SO(n)$	The n -dimensional Special Orthogonal group
\mathcal{B}	Right-handed orthonormal body-fixed coordinate frame
\mathcal{D}	Right-handed orthonormal desired direction frame
\mathcal{I}	Right-handed orthonormal inertial frame of reference
\mathcal{R}	Right-handed orthonormal tracking reference coordinate frame
x and \dot{x}	State of a system and its derivative with respect to time
x^\top or A^\top	The transpose of a vector or matrix
\hat{x}	State estimation
$\ x\ $	The Euclidean norm of an n -dimensional vector expressed as $\ x\ = \sqrt{x^\top x}$
e_ρ, e_ν	Position and velocity tracking errors, expressed with respect to \mathcal{R}
e_ω	Angular velocity tracking error, expressed with respect to \mathcal{B}
f	Total input thrust
\hat{f}, \hat{f}_d	Normalized thrust vectors
g	Standard gravitational acceleration
k_1, k_2, k_w, k_z	Control parameters
l_1, l_2, l_3	Observer parameters
t, t_0, t_k	Time, initial time and sampling time, respectively
u, u_d	Input and virtual input, respectively
$A(t), B, C$	State-space matrices
F, F_d	Thrust vectors
G	Gravitational force vector
I	The identity matrix of size $n \times n$
J	Inertia matrix
M	Mass matrix
P, Q	Symmetric positive definite matrices
R	Rotation matrix which transforms \mathcal{B} to \mathcal{I}
R_d	Rotation matrix which transforms \mathcal{D} to \mathcal{R}
R_r	Rotation matrix which transforms \mathcal{R} to \mathcal{I}
\hat{R}_e	Rotation matrix which transforms \mathcal{D} to \mathcal{B} (attitude tracking error)
S	Skew-symmetric matrix
ν, ν_r	Body-fixed velocities, expressed with respect to \mathcal{B} and \mathcal{R} respectively
ρ, ρ_r	Position of the origin of \mathcal{B} and \mathcal{R} respectively, relative to the center of \mathcal{I}

ϕ, θ, ψ	Roll, pitch and yaw angles
σ_n	Smooth saturation function of order n
τ	Torque
ω, ω_r	Angular velocities, expressed with respect to \mathcal{B} and \mathcal{R} respectively

Acronyms

ARE	Algebraic Riccati equation
GUAS (or GUES)	Global uniform asymptotic (exponential) stability
IMU	Inertial measurement unit
ISS	Input-to-state stability
LQR	Linear quadratic regulator
LTI	Linear time-invariant
PWM	Pulse width modulation
UAV	Unmanned aerial vehicle
UDP	User datagram protocol
ZOH	Zero-order-hold

Chapter 1

Introduction

1.1 Background

The interest in unmanned aerial vehicles (UAVs), often referred to as drones, has grown substantially in the past decades. Initially, these systems were developed for military purposes. Due to the relative indifference to terrain and greater range compared to ground vehicles, aerial systems are particularly useful for tasks such as surveillance, search and rescue missions, and reconnaissance of unknown regions [1–3]. Nowadays, the use of drones goes beyond military applications as this technology is increasingly used in various different civilian and research areas. One can think of the film and photography industry where drones provide a larger freedom of movement to capture certain aspects in a unique manner [4]. They can also be of great value for geo-scientific research, for example in the study of hurricanes [5]. Since drones can access regions that are often too dangerous for manned vehicles, important real-time data can be obtained in a more safe and convenient manner.

From a commercial perspective, one of the main advantages of UAVs is the possibility to automate several processes in a relatively easy and economic manner. For example, in the transport and delivery sector, drones can be utilized for the shipment of cargo. In fact, corporations such as Amazon, UPS and DHL are extensively researching the possibilities for transport by means of drones. The latter company has recently launched its delivery drone named "Parcelcopter" which is currently used for transporting medication to a remote German island [6]. Another example is found in agriculture, where drones are deployed for automating tasks such as the spraying of crops and monitoring of livestock [7]. Some of these commercial applications could highly benefit from a cooperative collaboration between drones. Compared to a single drone, a network of multiple drones may perform certain tasks more effectively. Think of the transport of large and fragile cargo or using a grid of drones for efficient watering of large areas. All mentioned examples illustrate the large contributions drones can provide within a wide variety of applications.

Due to the broad applicability and rapidly increasing advancements in UAV-technology, a large distinction in vehicle properties such as size and aerodynamic configuration can be made. A specific design of UAV that has received a considerable amount of attention is the multi-rotor vehicle, as shown in Figure 1.1. Due to the characteristic rotor configuration, these types of rotor-crafts exhibit many desirable properties such as high maneuverability, the capability of hovering and the ability for vertically take-off and landing. A particularly interesting multi-rotor vehicle is the quadrotor, as shown in Figure 1.1a. The characteristic cross-rotor configuration structure allows this vehicle to be compact and lightweight. Furthermore, the relative ease of operation and low-cost production availability makes this type of multi-rotor UAV one of the most popular choices for drone-based applications. Pioneering companies such as DJI and Parrot



Figure 1.1: Distinct types of multi-rotor vehicles.

have made qualitatively low-cost quadrotors available for hobby and recreational use.

Automating processes by means of either a single, or multiple drones requires some level of autonomy. Indeed, in most of these applications it is desired for the drones to perform a completely autonomous flight. This is often formulated in terms of a trajectory tracking problem in which it is desired for the considered UAV to move along a predefined path without the intervention of an external operator. The design of appropriate tracking control algorithms is a crucial element in accomplishing such a task and is the main topic of this research. Because of the many benefits and since quadrotors provide a very useful and intuitive research platform, in this thesis we are concerned with this specific type of UAV.

1.2 Literature Review

The tracking control problem of quadrotors has been extensively studied in the past years and appears to be rather challenging. Since there is a vast amount of literature available on the subject, it is impossible to review the complete topic here. Therefore, in this section we present a brief selection of the most commonly and recently proposed tracking control methods for quadrotor systems.

1.2.1 Modeling

Solving the tracking control problem starts with an appropriate formulation of the quadrotor's system dynamics. A large amount of mathematical model descriptions have been proposed in literature from which the majority is based on standard modeling frameworks such as the Newton-Euler method [8] and Euler-Lagrange approach [9, 10]. Strong differences in parametrization of the quadrotor's orientation (also denoted by attitude) are observed. In most of the work, the attitude is expressed in terms of Euler angles [9, 11], however, several alternative representations are proposed. For example, in [12] quaternions are used, whereas in [13] the attitude is parametrized by means of a rotation matrix. According to the authors in this latter work the use of rotation matrices is preferred as these can globally and uniquely represent the quadrotor's attitude. The remaining parametrization methods may contain mathematical singularities and ambiguities in case of large angular maneuvers. A common element in all models is the highly

nonlinear and under-actuated system characteristics. The latter is clear from the fact that since a quadrotor can only generate a thrust along its vertical body-fixed axis, a specific orientation is required for motion within the horizontal plane. For tracking control, this appears to be an essential property which is utilized by most proposed control strategies. As a result, the existing control frameworks usually exhibit a nested control structure consisting of an outer position control-loop and a significantly faster inner attitude control-loop [11]. Within this framework, a clear distinction between linear and nonlinear control methods can be found.

1.2.2 Linear Control

Most linear control strategies are based on a linearization of the nonlinear quadrotor dynamics around an operating point or trajectory. A key assumption that is made in this approach, is that the quadrotor is subject to small angular maneuvers. Using standard PID and LQR strategies, in [14–16] successful closed-loop tracking is obtained in case of hovering and straight line trajectories. In [17], LQR strategies are applied for tracking of a spiral reference trajectory. Experiments have been performed with a miniature quadrotor and a VICON positioning system, which has shown the effectiveness of the proposed controller. Here, the authors claim that their methodology could successfully be applied to slowly time-varying reference trajectories. There exist much more results which show the capability of tracking simple trajectories using a linear control approach. A main conclusion that is done from the work on linear trajectory control, is that such an approach provides sufficient results for applications in which the drone is subject to hovering or easy-to-follow trajectories. However, since this method confines the workspace to a small region of the complete configuration space, the tracking possibilities for a quadrotor are limited. Indeed, it is straightforward that in case of more aggressive maneuvers, linear control methods provide insufficient results. In order to overcome these limitations, several nonlinear control approaches have been proposed.

1.2.3 Nonlinear Control

A commonly used nonlinear control approach that is somewhat intuitive in combination with the characteristic dynamics of a quadrotor, is backstepping. In [18–20] the backstepping procedure is applied to obtain asymptotically stabilizing tracking controllers. Hereto, the combination of input thrust and orientation is considered as a virtual input for stabilizing the position control-loop. A new error variable is introduced as the difference between the virtual input and stabilizing behaviour, which constitutes new dynamics. Using augmented quadratic Lyapunov functions, an input thrust and torque are designed for which asymptotic convergence of the closed-loop states towards the reference is guaranteed. The authors have complemented their claims with numeric experiments, which illustrate the usefulness of the proposed backstepping methods. A drawback of the standard backstepping method is the lack of robustness against disturbances and modeling uncertainties. Various work exists in which the standard approach is complemented with integral backstepping techniques for improving the efficiency and robustness of the closed-loop system [21, 22]. In [23] an integral backstepping approach in combination with a nonlinear \mathcal{H}_∞ controller is proposed for stabilizing the position and the attitude loop respectively. Stability and convergence when the closed-loop system is subject to a constant disturbance and time-varying reference trajectory is claimed in this work. A numerical comparison is made between pure integral backstepping, backstepping complemented with \mathcal{H}_∞ control and

integral backstepping complemented with \mathcal{H}_∞ control. Here, an uncertainty has been added to the quadrotor's mass. A significantly increased performance and robustness against parametric uncertainties for the integral backstepping \mathcal{H}_∞ controller has been observed. The results from this work illustrate the possibility to obtain robust tracking by means of backstepping methods. Several alternative robust control methods have been proposed in combination with backstepping techniques, such as adaptive control [24] and sliding mode control [25]. Although backstepping methods provide a systematic and comprehensive approach for solving the tracking control problem of a quadrotor, tedious and complex control expressions are commonly obtained which often might be impractical for implementation [26].

In view of the characteristic quadrotor dynamics in which the orientation highly influences the position dynamics, a more natural approach to the tracking control problem is based on cascaded control. A cascade based control approach is appealing since it allows to divide the overall control problem into the stabilization of two independent subsystems. Arbitrary control methods can then be used for the stabilization of each subsystem. Compared to, for example backstepping, such control design might result in less complex structures as the coupling term is not explicitly taken into account [27]. In return, however, the stability properties of each subsystem do not directly guarantee stability of the overall closed-loop system but has to be derived a posteriori. In [28] a cascade based tracking controller is proposed. The resulting closed-loop system constitutes linear position and attitude subsystems, coupled by a nonlinear interconnection term. The authors have explicitly stated that the stability properties of the system essentially rely on the characteristics of the interconnection term, which strongly depends on the choice of the thrust. These results imply a certain deliberate design of the admissible input thrust. In more recent work [29], a cascade based controller has been proposed in which the position subsystem is controlled by means of a standard PID law, whereas feedback linearization and backstepping methods are used for attitude control. Asymptotic stability results are obtained in case of near hover flight, and the effectiveness of the controller has been shown through simulations and experiments on a Parrot AR Drone 2.0. Most of the cascade tracking controllers are based on a parametrization of the attitude by means of minimal coordinates (e.g. Euler angles). The authors in [13] claim that since such a representation exhibits mathematical singularities, the possibility for achieving complex flight maneuvers is significantly restricted. Although this work is concerned with general attitude control for rigid bodies, it has been shown that the use of rotation matrices provide the possibility for designing almost-globally stabilizing attitude controllers. As a result the configuration space of controlled attitudes is not limited by a mathematical representation.

A drawback of the previously mentioned research is the need of full-state information for the quadrotor. Generally this is not possible in practice as many experimental quadrotor setups are unable to provide direct measurements of all states (e.g. velocity). This requires the need for some state estimation mechanism. To the best of the author's knowledge, only a few works have thoroughly investigated the output feedback tracking control problem. For example, in [30] sliding mode observers are designed for estimating the quadrotor's unmeasurable velocity. A backstepping method is employed to generate a dynamic output feedback controller. In more recent work [31] the authors propose a non-model based angular and linear velocity filter in combination with a neural network-based robust controller. Through a Lyapunov-based stability analysis they claim semiglobal asymptotic tracking under uncertainties and disturbances. In most other works, Kalman filter algorithms in combination with measurements provided by an inertial measurement unit or external position detection sensor are used for estimating ve-

locity and attitude [32, 33]. The effectiveness of these approaches is often illustrated through simulations and experiments.

1.3 Motivation and Objectives

From the current research it is clear that a wide variety of tracking control laws is available for quadrotors, each with specific strengths and weaknesses. It appears that in many of the proposed control strategies, the full potential of trajectory tracking is limited, either by the chosen control method or representation of the system dynamics. Furthermore, some of the control methods might exhibit unnecessary complexities (e.g. backstepping compared to cascade control). As the demand for more aggressive maneuvers increases with an increase in drone-based applications, efficient nonlinear tracking controllers that are able to exploit the full capabilities of quadrotors are needed. In addition, with the aim for practical implementation, observer based controllers must be designed which are capable of using available measurements for appropriate state reconstruction. Motivated by these observations, the main objective of this research is the design of appropriate control laws that enable autonomous flight of a quadrotor. We aim for these controllers to guarantee sufficient tracking of a large variety of reference trajectories, ranging from steady-state hovering, to aggressive acrobatic maneuvers such that the controlled quadrotor is useful in many applications. Furthermore, we aim to design the control law in such a manner that it can be applied and tested on a real-world quadrotor platform.

As a means of addressing these objectives, a number of essential sub-objectives are considered in this work:

- Derivation of the system dynamics of a quadrotor. The aim of this objective is to obtain insight and understanding of the complex behaviour of these systems.
- Design of an intuitive full-state feedback tracking controller which guarantees desirable theoretical closed-loop system properties. This state-feedback framework can provide a foundation for further controller development.
- Design of appropriate state observers which can be used in combination with the full-state feedback framework for subsequent output feedback design. This sub-objective aims at a subtle transition from a theoretical control design towards the applicability in practice.
- Validate the effectiveness of the proposed controllers through simulations and provide a sufficient setup for experiments.

The objectives can be interpreted as consecutive steps in the iterative control design process. The last sub-objective might provide results which require the need for a re-assessment of the previous control design.

1.4 Outline of the Thesis

The thesis is organized as follows. Chapter 2 starts with some preliminary notions and results that are used extensively throughout this thesis. In particular, a stability theorem for time-varying cascaded systems is given which is fundamental for the design and subsequent analysis of

tracking controllers for a quadrotor. This chapter has been included in order to make the thesis more self-contained. In Chapter 3 a simplified mathematical model of the quadrotor dynamics is derived. Hereto, appropriate reference frames and degrees of freedom are introduced. The model description provides us with some useful insight in properties and the behaviour of a quadrotor. Next, in Chapter 4 a model-based full state-feedback tracking controller is designed. Using a cascade control approach, two independent subsystems are defined for which stabilizing sub-controllers are designed. Intermediate stability results are presented which are subsequently used for the closed-loop stability analysis of the complete interconnected system. In Chapter 5 the results from Chapter 4 are used as a foundation for output feedback control design. In this chapter a subtle transition from theory to practice is made as we omit the previous assumption that all states are directly available from measurement. Several observers are designed and the corresponding convergence results are presented accordingly. In Chapter 6 the effectiveness of the theoretically designed controllers is examined in simulations and subsequently verified through experiments performed on a Parrot AR Drone 2.0. This part of the work has been done in collaboration with colleague student N.L.M. Jeurgens. Finally, the conclusions of this work and recommendations for future research are presented in Chapter 7. Appendix A contains some additional stability proofs regarding observer extensions and in Appendix B a more detailed elaboration of the algorithm for attitude reconstruction is given.

Chapter 2

Preliminaries

In this chapter some nontrivial definitions and results which are used throughout this thesis, are recalled. First, several methods for parameterizing the orientation of a rigid body are discussed. Next, some lemmas and theorems useful for showing (uniform) asymptotic convergence are given. Finally, we present some theory on time-varying cascaded systems.

2.1 Attitude Representations

As the attitude representation of a quadrotor is a rather important aspect during control design, it seems appropriate to provide some preliminary information regarding this topic. In this section, the two attitude representations considered in this thesis are discussed: rotation matrices and Euler angles. For other representations (e.g. unit quaternions) the reader is referred to [34].

2.1.1 Rotation Matrix

Various methods exist for representing the orientation of a rigid body as a linear transformation between a frame of reference and a body-fixed frame. In this thesis we restrict ourselves to right-handed coordinate frames and assume that each frame is defined by $n \in \{2, 3\}$ orthogonal unit vectors ($n = 2$ for planar rotations and $n = 3$ for spatial rotations). The attitude of the rigid body can then be represented by an $n \times n$ matrix that maps a vector resolved in the body-fixed frame into its representation resolved in the reference frame, while preserving its length and handedness of the coordinate frames [35]. Such a matrix is denoted by rotation matrix R or direction cosine matrix. The set of all such $n \times n$ matrices is often referred to as the *Special Orthogonal* group of order n , denoted by the symbol $\mathcal{SO}(n)$. For any matrix $R \in \mathcal{SO}(n)$ the following properties hold [36]:

- $R^\top = R^{-1}$
- The columns (rows) of R are mutually orthogonal
- Each column (row) of R is a unit vector
- $\det(R) = 1$

We remark that there exist orthogonal rotation matrices for which $\det(R) = -1$. Such matrices correspond to improper rotations, which consist of a rotation followed by an inversion operation (mirroring). In this thesis we are not concerned with improper rotations as this is not a rigid body transformation. Furthermore, we consider spatial rotations such that $n = 3$.

One of the main advantages of rotation matrices is that the attitude can be represented globally and uniquely. From a mathematical perspective, it is an intuitive representation. On the other hand, rotation matrices give a redundant description of a body's orientation since they are characterized by nine elements which are not independent due to the orthogonality conditions $R^\top R = I$. Indeed, these constraints define six independent equations with nine unknowns, leaving three variables free. Many alternative methods exist for representing the attitude using a minimal set of coordinates consisting of only three independent quantities (e.g. Euler angles).

2.1.2 Euler Angles

The most commonly used method for representing the attitude of a rigid body is through three successive rotation angles $(\phi, \theta, \psi) \in \mathbb{R}^3$ about the sequentially displaced axes of a reference frame. These angles are generally referred to as Euler angles. Within this method, the order of rotation around the specific axes is of importance as the sequence of finite rotations is not commutative: performing three subsequent rotations around the x , y and z axis of a frame, in general, does not yield a similar orientation as if the order is z , y , x [37]. In the field of automotive and/or (aero)nautical research, the transformation from a body-fixed frame to an inertial frame is commonly described by means of a specific set of Euler angles, the so-called roll, pitch, and yaw angles (RPY). Here, first a rotation around the body-fixed x axis over the roll angle (ϕ) is done. Subsequently, we rotate around the resulting body-fixed y axis about the pitch angle (θ) and finally rotate about the z axis by the yaw angle (ψ). The roll-pitch-yaw angle approach is attractive since it can be easily visualized and interpreted in terms of a physical object. This rotation sequence is related to the rotation matrix through the composition of successive rotations around the single body-fixed axes as [34]

$$\begin{aligned}
 R &= R_z(\psi)R_y(\theta)R_x(\phi) \\
 &= \begin{bmatrix} c_\psi & -s_\psi & 0 \\ s_\psi & c_\psi & 0 \\ 0 & 0 & 1 \end{bmatrix} \begin{bmatrix} c_\theta & 0 & s_\theta \\ 0 & 1 & 0 \\ -s_\theta & 0 & c_\theta \end{bmatrix} \begin{bmatrix} 1 & 0 & 0 \\ 0 & c_\phi & -s_\phi \\ 0 & s_\phi & c_\phi \end{bmatrix} \\
 &= \begin{bmatrix} c_\theta c_\psi & s_\phi s_\theta c_\psi - c_\phi s_\psi & c_\phi s_\theta c_\psi + s_\phi s_\psi \\ c_\theta s_\psi & s_\phi s_\theta s_\psi + c_\phi c_\psi & c_\phi s_\theta s_\psi - s_\phi c_\psi \\ -s_\theta & s_\phi c_\theta & c_\phi c_\theta \end{bmatrix}
 \end{aligned} \tag{2.1}$$

where c_α denotes $\cos(\alpha)$, and s_α denotes $\sin(\alpha)$ with α referring to the corresponding RPY-angles. Note that R denotes the mapping from the body-fixed frame to the inertial reference frame whereas $R^\top = R_x^\top(\phi)R_y^\top(\theta)R_z^\top(\psi)$ is the mapping from inertial to body frame. In some aspects of this thesis, we adopt the RPY method for an explicit expression of the rotation matrix.

A disadvantage all minimal attitude representations contain is the possibility for geometric singularities. In case of RPY-angles this occurs at $\theta = \pi/2$, for which the roll and yaw angles are not uniquely defined anymore. This limits the global and unique representation of attitude by means of minimal coordinates. In literature the singular case is often referred to as Gimbal Lock.

2.2 Convergence Results

The following mathematical tool is commonly used for showing asymptotic convergence of a signal.

Lemma 2.2.1. (Barbalat, [38, Lemma 8.2]) *Let $f : \mathbb{R} \rightarrow \mathbb{R}$ be a uniformly continuous function on $[0, \infty)$. Suppose that $\lim_{t \rightarrow \infty} \int_0^t f(\tau) d\tau$ exists and is finite. Then*

$$\lim_{t \rightarrow \infty} f(t) = 0.$$

Whereas Barbalat's lemma only applies to uniformly continuous functions, in [39] a convergence result was presented which somewhat extends Barbalat's lemma to functions that are not uniformly continuous.

Lemma 2.2.2. (Micaelli and Samson, [39, Lemma 1]) *Let $f : \mathbb{R}_+ \rightarrow \mathbb{R}$ be any differentiable function. If $f(t)$ converges to zero as t approaches ∞ and its derivative satisfies*

$$\dot{f}(t) = f_0(t) + g(t) \quad \forall t \geq 0$$

where f_0 is a uniformly continuous function and $g(t)$ tends to zero as $t \rightarrow \infty$, then

$$\lim_{t \rightarrow \infty} \dot{f}(t) = 0 \quad \text{and} \quad \lim_{t \rightarrow 0} f_0(t) = 0.$$

The mentioned lemmas are of particular use in a Lyapunov based stability analysis of (non)linear time-varying systems, where the time-derivative of the considered Lyapunov function is semi-negative definite. Barbalat's lemma and the lemma of Micaelli and Samson are somewhat limited in the sense that only asymptotic convergence of a signal can be determined, whereas in some cases a more desirable property is *uniform* asymptotic convergence. In order to determine uniform asymptotic convergence properties of a signal, one may resort to Matrosov's theorem which, to some extent, can be considered as an invariance principle for time-varying systems.

Theorem 2.2.1. (Matrosov, [40, Theorem 1.1]) *Consider the non-autonomous system $\dot{x} = f(t, x)$ with $f(t, 0) = 0$ for all $t \geq 0$. Let $\mathcal{S} \in \mathbb{R}^n$ be an open connected region in \mathbb{R}^n which contains the origin. If there exist two \mathcal{C}^1 functions $V : [0, \infty) \times \mathcal{S} \rightarrow \mathbb{R}$, $W : [0, \infty) \times \mathcal{S} \rightarrow \mathbb{R}$; a \mathcal{C}^0 function $U : \mathcal{S} \rightarrow \mathbb{R}$; three class \mathcal{K} functions α, β, γ , such that, for every $(x, t) \in \mathcal{S} \times [0, \infty)$*

- (i) $\alpha_1(\|x\|) \leq V(t, x) \leq \alpha_2(\|x\|)$
- (ii) $\dot{V}(t, x) \leq U(x) \leq 0$
- (iii) $|W(t, x)|$ is bounded
- (iv) $\max(d(x, E), |\dot{W}(t, x)|) \geq \gamma(\|x\|)$
- (v) $\|f(t, x)\|$ is bounded

where $E = \{x \in \mathcal{S} | U(x) = 0\}$; choosing $c > 0$ such that $B_c = \{x \in \mathbb{R}^n | \|x\| \leq c\} \subset \mathcal{S}$, define for all $t \in [0, \infty)$

$$V_{t,c}^{-1} = \{x \in \mathcal{S} : V(t, x) \leq \alpha_1(c)\},$$

then

1. For all $x_0 \in V_{t,c}^{-1}$, $x(t) \rightarrow 0$ uniformly in $(0, x_0)$ as $t \rightarrow \infty$.
2. The origin is uniformly asymptotically stable.

Note that conditions (i) and (ii) imply uniform stability. Since condition (ii) requires that \dot{V} is only semi-negative definite, condition (iii) and (iv) are necessary for showing that no trajectory can stay identically in the set E other than the origin.

In order to verify condition (iv), a helpful lemma provided in [41] can be used.

Lemma 2.2.3. [41, Lemma 1] *Condition (iv) of Theorem 2.2.1 holds if the following conditions are satisfied*

- (iv-a) $\dot{W}(t, x)$ is continuous in t and x and depends on time in the following way: $\dot{W}(t, x) = g(x, a(t))$ where g is continuous in both its arguments, $a(t)$ is continuous and its image lies in a bounded set K .
- (iv-b) There exists a class \mathcal{K} function k , such that $|\dot{W}(t, x)| \geq k(\|x\|)$ for all $x \in E$ and $t \geq 0$.

2.3 Cascaded Systems

Throughout this thesis, extensive use is made of a result on the stability of cascaded systems as presented in [42] and [27]. For reasons of completeness, this result is stated here. Consider a nonlinear time-varying cascaded system of the form

$$\dot{x}_1 = f_1(t, x_1) + g(t, x_1, x_2)x_2 \quad (2.2a)$$

$$\dot{x}_2 = f_2(t, x_2) \quad (2.2b)$$

where $x_1 \in \mathbb{R}^n$, $x_2 \in \mathbb{R}^n$, $f_1(t, x_1)$ is continuously differentiable in (t, x_1) and $f_2(t, x_2)$ and $g(t, x_1, x_2)$ are continuous in their arguments, and locally Lipschitz in x_2 and (x_1, x_2) respectively. We define two nominal systems as

$$\Sigma_1 : \dot{x}_1 = f_1(t, x_1) \quad \text{and} \quad \Sigma_2 : \dot{x}_2 = f_2(t, x_2), \quad (2.3)$$

for which it is assumed that $f_1(t, 0) = 0$ and $f_2(t, 0) = 0$ for all $t \geq t_0$. It is straightforward to verify that the cascaded system (2.2) consists of Σ_1 , which is perturbed by the output of Σ_2 through the interconnection term $g(t, x_1, x_2)$. As was shown in [27], it does not necessarily hold in general that if both the subsystems Σ_1 and Σ_2 are uniformly asymptotically stable, the complete cascaded system is uniformly asymptotically stable. The following theorem presents sufficient conditions for the global uniform asymptotic stability of the equilibrium solution of nonlinear time-varying cascaded systems as in (2.2).

Theorem 2.3.1. (Panteley and Loria, [42, Theorems 1,2,4]) *Consider the following assumptions*

- A1.** *The subsystems Σ_1 and Σ_2 are both globally uniformly asymptotically stable (GUAS) and we know an explicit \mathcal{C}_1 Lyapunov function candidate $V(t, x_1)$, $\alpha_1, \alpha_2 \in \mathcal{K}_\infty$, $\alpha_4 \in \mathcal{K}$ and*

a positive semi-definite function $W(x_1)$ such that

$$\alpha_1(\|x_1\|) \leq V(t, x_1) \leq \alpha_2(\|x_1\|) \quad (2.4)$$

$$\frac{\partial V}{\partial t} + \frac{\partial V}{\partial x_1} f_1(t, x_1) \leq -W(x_1) \quad (2.5)$$

$$\left\| \frac{\partial V}{\partial x_1} \right\| \leq \alpha_4(\|x_1\|). \quad (2.6)$$

A2. For each fixed x_2 a continuous function $\lambda : \mathbb{R}_+ \rightarrow \mathbb{R}_+$ exists with $\lim_{s \rightarrow \infty} \lambda(s) = 0$ and such that

$$\left\| \frac{\partial V}{\partial x_1} g(t, x_1, x_2) \right\| \leq \lambda(\|x_1\|) W(x_1) \quad (2.7)$$

with V and W as in Assumption A1.

A3. Continuous functions $\theta_1 : \mathbb{R}_+ \rightarrow \mathbb{R}_+$ and $\alpha_5 : \mathbb{R}_+ \rightarrow \mathbb{R}_+$ exist such that

$$\|g(t, x_1, x_2)\| \leq \theta_1(\|x_2\|) \alpha_5(\|x_1\|) \quad (2.8)$$

and a continuous non-decreasing function $\alpha_6 : \mathbb{R}_+ \rightarrow \mathbb{R}_+$ and a constant $a \geq 0$ exist such that

$$\alpha_6(s) \geq \alpha_4(\alpha_1^{-1}(s)) \alpha_5(\alpha_1^{-1}(s)) \quad (2.9)$$

and

$$\int_a^\infty \frac{ds}{\alpha_6(s)} = \infty \quad (2.10)$$

with α_1, α_4 as in Assumption A1.

A4. For each $r > 0$, constants $\lambda > 0$ and $\eta > 0$ exist such that for all $t \geq t_0$ and all $\|x_2\| < r$

$$\left\| \frac{\partial V}{\partial x_1} g(t, x_1, x_2) \right\| \leq \lambda W(x_1) \quad \forall \|x_1\| \geq \eta. \quad (2.11)$$

A5. A function $\phi \in \mathcal{K}$ exists such that the solution $x_2(t)$ satisfies

$$\int_{t_0}^\infty \|x_2(t)\| dt \leq \phi(\|x_2(t_0)\|). \quad (2.12)$$

Then we can conclude

- If Assumption A1 and A2 hold, then the cascaded system (2.2) is globally uniformly asymptotically stable (GUAS).
- If Assumptions A1, A3 and A4 hold, then the cascaded system (2.2) is globally uniformly asymptotically stable (GUAS).
- If Assumption A1, A3 and A5 hold, then the cascaded system (2.2) is globally uniformly asymptotically stable (GUAS).

For the formal statements supporting this result, it is referred to [27] and [43] and the references therein.

In this chapter some preliminary definitions and mathematical results have been presented which are used in the sequel of this thesis. In the next chapter, the system dynamics of a quadrotor are derived, for which the background information on attitude representations, presented in Section 2.1, is of particular use. Hereafter, in chapters 4 and 5, state feedback and output feedback controllers are designed for which the presented convergence results and stability theory on cascaded systems provide important tools for the closed-loop stability analysis.

Chapter 3

System Dynamics

The design of appropriate controllers for quadrotors requires a fundamental knowledge and understanding of the dynamics of these systems. Quadrotors typically consist of four individual rotors attached to a rigid cross frame. Due to the characteristic design, this type of rotorcraft has many desirable properties such as high maneuverability and the ability for vertical take-off and landing. The relatively simple structure, however, imposes some limitations on the system's behaviour. In order for the quadrotor to perform maneuvers in the horizontal plane (i.e. the xy -plane) it must slightly tilt in the desired heading direction. This behaviour indicates a strong coupling between the quadrotor's inputs and states and, in addition, shows the under-actuation of the dynamics. Many efforts have been made in order to capture the dynamics of a quadrotor, for example by means of first principle modeling [11, 44, 45] and system identification tools [46]. In this chapter a step-by-step derivation of the simplified dynamics of a quadrotor, based on a theoretical Newton-Euler modeling framework is provided. We start Section 3.1 by defining appropriate reference frames and a suitable set of degrees of freedom in 3D-space. The actual system dynamics are derived in Section 3.2 where a distinction is made between a translational and attitude subsystem. In Section 3.3 a summary of the dynamics and some concluding remarks are presented.

3.1 Degrees of Freedom

First a right-handed orthonormal reference frame \mathcal{I} , with basis vectors $\{e_1, e_2, e_3\}$ and fixed with respect to the earth is introduced. Additionally, an orthonormal right-handed body-fixed frame \mathcal{B} with basis vectors $\{b_1, b_2, b_3\}$ is defined. The origin of this frame is fixed to the quadrotor's center of mass. A schematic representation of the quadrotor and corresponding frames is shown in Figure 3.1. For modeling the system dynamics, the following assumptions are made:

- *The quadrotor is axisymmetric;*
- *The quadrotor is a rigid body.*

As a direct consequence of the first assumption, the quadrotor's center of mass coincides with the body's geometrical center. The position of the center of mass relative to the inertial frame \mathcal{I} is denoted by $\rho = (x, y, z) \in \mathbb{R}^3$. Furthermore, we represent the orientation of the body-fixed frame with respect to the inertial frame by the rotation matrix $R \in \mathcal{SO}(3)$ with the special orthogonal group $\mathcal{SO}(3) = \{R \in \mathbb{R}^{3 \times 3} \mid R^\top R = I, \det(R) = 1\}$. In this thesis the attitude of the quadrotor is parametrized by means of R rather than, for example, Euler angles or quaternions. This choice is based on the fact that rotation matrices can represent all attitudes of a rigid body globally and uniquely in 3D-space, whereas other representations may contain kinematic singularities or are not globally defined. For a more detailed description of different attitude

representations, see Chapter 2. Additionally, a set of body-fixed linear and angular velocities is defined as $\nu = (u, v, w) \in \mathbb{R}^3$ and $\omega = (p, q, r) \in \mathbb{R}^3$ respectively. With the quadrotor's states properly defined, the kinematics and system dynamics can be formulated accordingly.

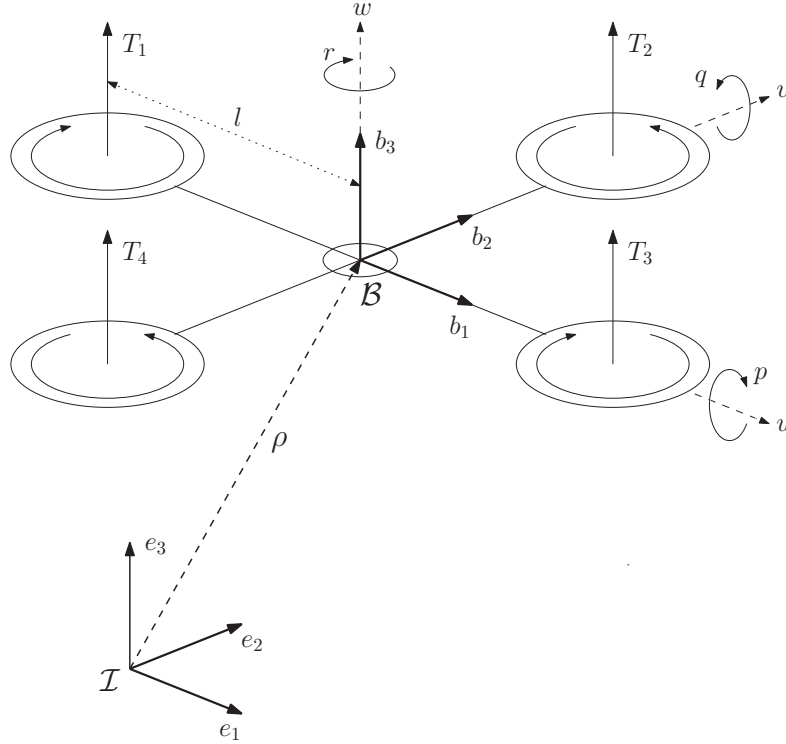


Figure 3.1: Schematic configuration of the quadrotor presented in the inertial reference frame \mathcal{I} and the body-fixed reference frame \mathcal{B} . By means of the rotation matrix R , the configuration in \mathcal{B} can be transformed to the configuration in \mathcal{I} .

3.2 Dynamic Model

For quadrotor systems it might be convenient to express the equations of motion in a body-fixed coordinate frame. This yields the possibility to take advantage of several assumptions such as axisymmetry. Moreover, since most quadrotors are equipped with inertial measurement units (IMU) consisting of accelerometers and gyroscopes, some states are measured with respect to the body-fixed frame (e.g. accelerations and angular velocities). The complete system dynamics are divided into a translational and an attitude subsystem.

3.2.1 Translational Subsystem

Without taking into consideration the effects of the mass and force on the body, the relation between the body-fixed linear velocities and inertial velocities is expressed as

$$\dot{\rho} = R\nu, \quad (3.1)$$

where $R : \mathcal{B} \rightarrow \mathcal{I}$. The equations of motion are derived using Newton's second law and are formulated as

$$\begin{aligned} \sum F &= \frac{d}{dt}(m\nu) \\ &= m(\dot{\nu} + \omega \times \nu), \end{aligned} \quad (3.2)$$

where m is the mass of the quadrotor and the term $\omega \times \nu$ is present due to the rotational motion of the body-fixed frame. The left-hand side of (3.2) represents the summation of the externally applied forces to the body. Initially, we do not take into account drag or wind induced forces nor do we consider aerodynamic effects such as rotor flapping. Such effects are usually difficult to model and may only be of interest at high velocities. The summation of all considered forces is expressed as

$$\sum F = B_f f + G, \quad (3.3)$$

where $f = \sum_{i=1}^4 T_i$ represents the summation of the thrust T_i of all individual rotors and $B_f = [0 \ 0 \ 1]^\top$. Moreover, G is the gravitational force expressed in the body-fixed reference frame, i.e.,

$$G = -MR^\top g e_3 \quad (3.4)$$

with $M = mI$ the mass matrix and g the standard gravitational acceleration. In order to express the equations of motion in a compact form, the following notation for the cross product operator is adopted

$$a \times b := S(a)b, \quad (3.5)$$

where $S(a)$ is a skew-symmetric matrix defined as

$$S(a) = -S(a)^\top = \begin{bmatrix} 0 & -a_3 & a_2 \\ a_3 & 0 & -a_1 \\ -a_2 & a_1 & 0 \end{bmatrix}. \quad (3.6)$$

Using this notation, the set of equations representing the quadrotor's translational motion is obtained as

$$\dot{\rho} = R\nu \quad (3.7a)$$

$$M\dot{\nu} + MS(\omega)\nu = B_f f + G. \quad (3.7b)$$

From the model description it is evident that this subsystem is under-actuated, i.e., the number of degrees of freedom exceeds the number of available inputs. This is due to the fact that the rotors are only capable of generating a thrust in the direction parallel to the b_3 -axis. Note that pre-multiplication of (3.7b) by R , and substitution of the kinematic relation (3.1) and its first derivative yields the quadrotor dynamics expressed within the inertial reference frame \mathcal{I} .

3.2.2 Attitude Subsystem

The attitude kinematics are derived by means of the Poisson equation as [37]

$$\dot{R} = RS(\omega), \quad (3.8)$$

where $S(\omega)$ is a skew-symmetric matrix containing the elements of the body-fixed angular velocity ω . The attitude dynamics are obtained as

$$\begin{aligned} \sum \tau &= \frac{d}{dt}(J\omega) \\ &= J\dot{\omega} + \omega \times J\omega, \end{aligned} \quad (3.9)$$

in which J is the matrix of moments of inertia about the center of mass. Due to the assumption of axisymmetry of the quadrotor, and the choice of \mathcal{B} such that the basis axes correspond to the quadrotor's principal axes of inertia, the off-diagonal terms of J are zero. Hence the inertia matrix reduces to $J = \text{diag}([J_x, J_y, J_z])$. The left-hand side of (3.9) represents the summation of externally applied torques. In this case, the only relevant torque results from the difference in thrust generated by the rotors. Therefore, we define

$$\tau = (\tau_1, \tau_2, \tau_3)^\top, \quad (3.10)$$

in which $\tau_1 = l(T_4 - T_2)$, $\tau_2 = l(T_3 - T_1)$ and $\tau_3 = d(T_1 + T_3 - T_2 - T_4)$. Furthermore, l is the distance from the rotors to the center of mass, and d is the rotational drag coefficient. By exploiting the notation for the cross product operator (3.5), the set of equations for the attitude subsystem is written in the following convenient form

$$\dot{R} = RS(\omega) \quad (3.11a)$$

$$J\dot{\omega} + S(\omega)J\omega = \tau. \quad (3.11b)$$

It is clear that the position dynamics (3.7) are affected by the attitude dynamics (3.11), whereas the reverse does not hold. This coupling indicates the cascaded character of the complete system dynamics, which is a central element in the subsequent design of tracking controllers. The cascaded structure is schematically shown in Figure 3.2.

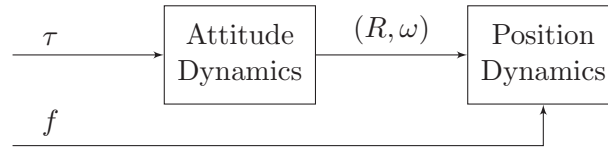


Figure 3.2: Cascaded structure of the quadrotor dynamics. The position dynamics (3.7) are coupled with the attitude dynamics (3.11).

An additional note is made on the system inputs f and τ . It is common to relate the individual input thrusts T_i and the individual rotor speeds Ω_i as $T_i = c\Omega_i^2$, where c is a positive constant depending on the rotor geometry. This results in the following relation between the input thrust, torques, and the rotor speeds respectively

$$\begin{bmatrix} f \\ \tau_1 \\ \tau_2 \\ \tau_3 \end{bmatrix} = \begin{bmatrix} c & c & c & c \\ 0 & -cl & 0 & cl \\ -cl & 0 & cl & 0 \\ cd & -cd & cd & -cd \end{bmatrix} \begin{bmatrix} \Omega_1^2 \\ \Omega_2^2 \\ \Omega_3^2 \\ \Omega_4^2 \end{bmatrix}, \quad (3.12)$$

in which d is a drag coefficient. Since the coupling matrix is nonsingular, it is straightforward that the inverse relation can be obtained. In the remaining part of this work, the system inputs are considered on thrust and torque level, rather than motor level. However, (3.12) provides a necessary relation for practical implementations.

3.3 Concluding Remarks

In this chapter a simplified mathematical model of the quadrotor dynamics has been derived. Hereto, first a suitable set of degrees of freedom is defined in which it is chosen to parameterize the attitude by means of a rotation matrix R rather than Euler-angles or unit-quaternions. This choice is based on the ambiguity-free, global characteristics of a rotation matrix representation. In order to be able to take advantage of several assumed properties such as axisymmetry, and since a number of states are measured with respect to the body-fixed reference frame \mathcal{B} , the dynamics are expressed with respect to \mathcal{B} . The complete quadrotor system dynamics are summarized as

$$\dot{\rho} = R\nu \tag{3.13a}$$

$$\dot{\nu} = -S(\omega)\nu + M^{-1}(B_f f + G) \tag{3.13b}$$

$$\dot{R} = RS(\omega) \tag{3.13c}$$

$$J\dot{\omega} = S(J\omega)\omega + \tau \tag{3.13d}$$

from which a cascaded structure can be recognized. In Chapter 4 this model is used for the design of appropriate state feedback tracking controllers. Here, the cascaded nature of the system provides a central element in the control design process.

Chapter 4

State Feedback Control

In this chapter the tracking control problem for a single quadrotor is studied. Due to the strongly coupled dynamics, and under-actuated system characteristics, design of appropriate control laws for this type of rotor craft is a complicated task. Various methods have been proposed to solve the tracking control problem, of which most are based on a linearization of the system dynamics around a trajectory [14, 16]. Although linear control laws have shown sufficient performance in case the quadrotor is subject to simple and "easy to-follow" trajectories, for more aggressive maneuvers such control design yields insufficient results. To overcome this limitation, several nonlinear control approaches are suggested [22, 47]. Since it is inherent to the quadrotor's system dynamics to use the attitude for performing certain maneuvers, most existing control methods (linear and nonlinear) are based on a hierarchical control approach. Here, the position is controlled in an outer loop for which a specific attitude is required. The control action necessary to track this new attitude reference is determined in the inner control loop. A visual representation of this common control method is shown in Figure 4.1.

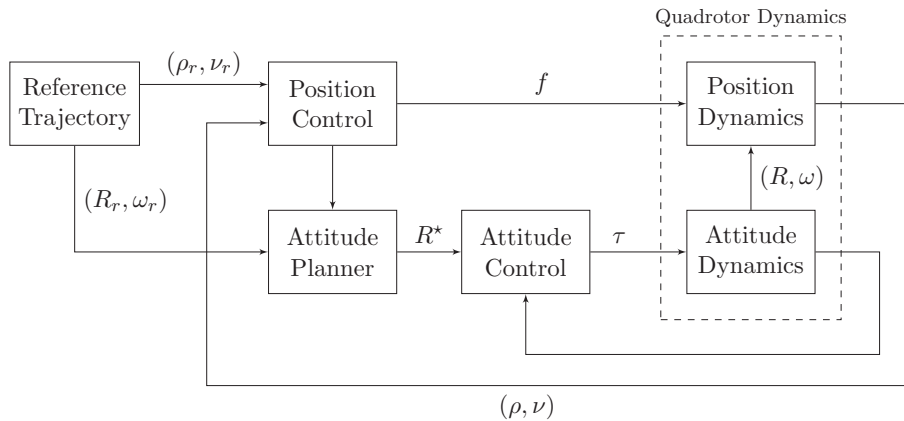


Figure 4.1: Commonly used hierarchical control structure. In the outer loop the position is controlled from which a new attitude reference R^* is determined. Attitude tracking control occurs within the inner control loop.

Backstepping methods and Lyapunov based control are widely used in combination with the hierarchical control method. However, this control scheme reveals a natural cascaded closed-loop structure. Indeed, if we consider R^* as a new attitude reference trajectory, it is clear that the position dynamics are influenced by the output of the attitude dynamics. Note that, in fact, the quadrotor's system dynamics admit a cascaded structure. These observations motivate controller design based on cascade control theory. Recently, in [29] such an approach has been proposed which was capable of global uniform asymptotic stabilization of the quadrotor under the assumption of near hover flight. Here, we present a nonlinear cascade based control

approach in which no small angle assumptions are made. In addition, since we parameterize the quadrotor's attitude in terms of rotation matrices rather than Euler angles or quaternions, we avoid singularities and ambiguities in the corresponding attitude dynamics and control. This chapter starts with a formal definition of the quadrotor's tracking control problem and a specific state transformation proposition. Additionally the cascade structure and control approach are motivated whereas in sections 4.2 and 4.3 the design of appropriate position and attitude controllers for the corresponding subsystems is discussed. In these sections, intermediate stability results are presented for each closed-loop subsystem, which are used in Section 4.4 where the stability result of the complete closed-loop cascaded system is given. Section 4.5 presents some additional, yet important, convergence results. Finally, some concluding remarks are given in Section 4.6.

4.1 Problem Formulation

It is assumed that a feasible reference trajectory is given by $(\rho_r, \nu_r, R_r, \omega_r, f_r, \tau_r)$, which satisfies the following dynamics

$$\dot{\rho}_r = R_r \nu_r \quad (4.1a)$$

$$\dot{\nu}_r = -S(\omega_r) \nu_r + M^{-1} (B_f f_r + G_r) \quad (4.1b)$$

$$\dot{R}_r = R_r S(\omega_r) \quad (4.1c)$$

$$J \dot{\omega}_r = S(J \omega_r) \omega_r + \tau_r, \quad (4.1d)$$

with initial conditions $(\rho_r(t_0), \nu_r(t_0), R_r(t_0), \omega_r(t_0))$. In addition we assume that the complete states of the quadrotor are available for measurement. We then formulate the state-feedback tracking control problem for a quadrotor as follows:

Problem 4.1.1. (State-feedback tracking control problem) *Consider the dynamics of a single quadrotor (3.13) and a reference trajectory which satisfies (4.1). Define the quadrotor states and reference states as $\mathcal{C}(t) := (\rho^\top, \nu^\top, R^\top, \omega^\top)$ and $\mathcal{C}_r(t) := (\rho_r^\top, \nu_r^\top, R_r^\top, \omega_r^\top)$ respectively. Find a suitable control law*

$$f = f(t, \mathcal{C}_r, f_r, \tau_r, \mathcal{C}) \quad (4.2a)$$

$$\tau = \tau(t, \mathcal{C}_r, f_r, \tau_r, \mathcal{C}) \quad (4.2b)$$

such that for the resulting closed-loop system (3.13),(4.2)

$$\lim_{t \rightarrow \infty} \varepsilon(t, \mathcal{C}, \mathcal{C}_r) = 0 \quad (4.3)$$

with $\varepsilon(t, \mathcal{C}, \mathcal{C}_r)$ some error measure (e.g. norm) between the actual states and reference states.

4.1.1 Tracking Error Coordinates

In most tracking control applications, it is common to express the measure $\varepsilon(t, \mathcal{C}, \mathcal{C}_r)$ for the translational dynamics in terms of the difference between states, defined with respect to an inertial frame \mathcal{I} . A drawback of this particular form of error coordinates is the dependence

on the choice of inertial reference frame. In order to overcome this possible disadvantage, the tracking error coordinates can be expressed with respect to a body-fixed frame. This was first proposed for mobile robots in [48]. For tracking control of a quadrotor this might, however, be inconvenient since the under-actuation of the system limits the control along the horizontal body-fixed axes. We therefore propose to express the coordinates in the tracking reference frame \mathcal{R} instead. This choice still yields independence from the choice of inertial frame, however, a more convenient combination of input thrust and orientation becomes apparent. The translational tracking error coordinates are therefore proposed as

$$e_\rho = R_r^\top (\rho_r - \rho) \quad (4.4)$$

$$e_\nu = \nu_r - R_r^\top R \nu. \quad (4.5)$$

with $R_r : \mathcal{R} \rightarrow \mathcal{I}$. In these coordinates, the tracking error dynamics become

$$\dot{e}_\rho = -S(\omega_r(t)) e_\rho + e_\nu \quad (4.6a)$$

$$\dot{e}_\nu = -S(\omega_r(t)) e_\nu + M^{-1} \left(B_f f_r(t) - R_r^\top R B_f f \right). \quad (4.6b)$$

By defining an augmented state-vector $e = (e_\rho, e_\nu)^\top \in \mathbb{R}^6$, this system can be rewritten in a standard linear time-varying format as

$$\dot{e} = A(t)e + Bu, \quad (4.7)$$

with

$$A(t) = \begin{bmatrix} -S(\omega_r(t)) & I \\ 0 & -S(\omega_r(t)) \end{bmatrix}, \quad B = \begin{bmatrix} 0 \\ I \end{bmatrix} \quad (4.8)$$

and $u = M^{-1} (B_f f_r(t) - R_r^\top R B_f f) \in \mathbb{R}^3$.

The representation of the attitude and angular velocity error functions are often given as

$$R_e = R_r^\top R \quad (4.9)$$

$$J\omega_e = J\omega - JR^\top R_r \omega_r, \quad (4.10)$$

with corresponding system dynamics

$$\dot{R}_e = R_r^\top R S(\omega_e) \quad (4.11a)$$

$$J\dot{\omega}_e = S(J\omega)\omega - JS(\omega_e)R^\top R_r \omega_r - JR^\top R_r \dot{\omega}_r + \tau. \quad (4.11b)$$

Note that the angular velocity error dynamics (4.11b) are expressed within the body-fixed reference frame and are fully actuated, which is convenient for control purposes.

4.1.2 Cascade Control

From the tracking error dynamics (4.6), (4.11) a cascade structure can be recognized due to the fact that the term u is dependent on the attitude error R_e . If we then define the error measure for the translational error coordinates as $\varepsilon_{\text{trans}} = \|e(t)\|_2$, it becomes intuitive to use u , and in turn R_e and f for stabilizing the zero solution of the translational error subsystem (4.7). By doing so, we impose a certain desired behaviour, denoted by (R_d, ω_d) , on the attitude

errors (R_e, ω_e) . This necessarily requires a newly defined attitude error functional, based on (R_e, ω_e) and (R_d, ω_d) , that has to be stabilized. The key structure is schematically presented in Figure 4.2.

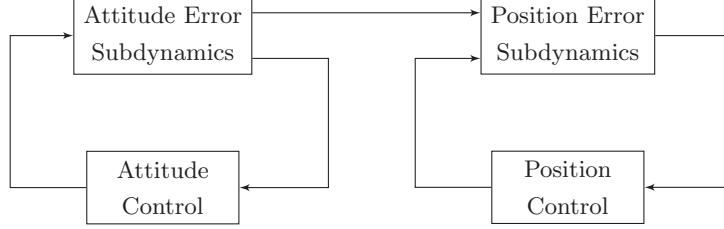


Figure 4.2: Closed-loop cascade control structure. The position error dynamics are as defined in (4.7). The attitude error dynamics result from a combination of the error dynamics in (4.11) and the newly defined attitude reference (R_d, ω_d) .

Remark 4.1.1. Note that this idea basically represents the first steps of a backstepping control approach. Here u can be considered as the virtual control for which a stabilizing function is designed. The resulting error variable, which results from the difference between u and the stabilizing function, is characterized in terms of the new attitude error.

In the next sections, we design stabilizing control laws for the translational error subsystem and the resulting attitude error subsystem respectively.

4.2 Position Control Design

In this section a control law which globally uniformly asymptotically stabilizes the zero solution of the translational error subsystem (4.7) is designed. The proposed control law is motivated through an analysis of its stabilizing properties. Consider u as the virtual input to the subsystem (4.7). An appropriate control-law is then given in the following proposition. We first note that the structure of the proposed control law is of a nonlinear PID form, in which the integrating action is based on the idea of conditional integrators, as is also used and illustrated in [49–53].

Proposition 4.2.1. Consider the linear time-varying system (4.7) in closed-loop with the control law

$$u = R_r^\top (k_z z + k_w w) - \frac{k_1}{\sqrt{1 + \|\bar{e}_\rho\|^2}} \bar{e}_\rho - \frac{k_2}{\sqrt{1 + \|\bar{e}_\nu\|^2}} \bar{e}_\nu, \quad (4.12)$$

where $\bar{e}_\rho = e_\rho + R_r^\top w$, $\bar{e}_\nu = e_\nu + R_r^\top z$ and w and z are solutions to the artificial subsystem

$$\begin{cases} \dot{w} = z \\ \dot{z} = -k_z z - k_w w + k_w R_r \sigma_n(\bar{e}_\rho), \end{cases} \quad (4.13)$$

with $(w(t_0), z(t_0)) = (0, 0)$. Here, $\sigma_n(\bar{e}_\rho)$ is a smooth saturation function of the form

$$\sigma_n(\bar{e}_\rho) = \frac{\bar{e}_\rho}{\left(1 + (\bar{e}_\rho^\top \bar{e}_\rho)^{\frac{n}{2}}\right)^{\frac{1}{n}}} \quad (4.14)$$

with $n \in 2\mathbb{N}$. If the control parameters are chosen such that $k_1 > k_w\sqrt{2} > 0$, and $k_2, k_z, k_w > 0$, and it is assumed that $\omega_r(t)$ is continuous and bounded for all $t \geq t_0$, then the zero solution $e = 0$ of the closed-loop system is uniformly asymptotically stable for all $\|(w(t_0), z(t_0))\| < \sqrt{1 + \left(\frac{k_w+1}{k_z}\right)^2}$ and $e(t_0) \in \mathbb{R}^6$.

Proof. We start the proof by defining the augmented state $q = (w, z)^\top \in \mathbb{R}^6$ and propose the following change of coordinates

$$\bar{e}_\rho = e_\rho + R_r^\top w \quad (4.15a)$$

$$\bar{e}_\nu = e_\nu + R_r^\top z. \quad (4.15b)$$

Using the state vector $\bar{e} = (\bar{e}_\rho, \bar{e}_\nu)^\top \in \mathbb{R}^6$, the corresponding dynamics are derived as

$$\dot{q} = \mathcal{A}q + B\gamma(\bar{e}_\rho) \quad (4.16a)$$

$$\dot{\bar{e}} = A(t)\bar{e} + B\left(u + R_r^\top \left(B^\top \mathcal{A}q + \gamma(\bar{e}_\rho)\right)\right) \quad (4.16b)$$

in which

$$\mathcal{A} = \begin{bmatrix} 0 & I \\ -k_w I & -k_z I \end{bmatrix}, \quad (4.17)$$

and $\gamma(\bar{e}_\rho) = k_w R_r \sigma_n(\bar{e}_\rho)$ is a bounded perturbation. The matrices $A(t)$ and B are defined as in (4.8). By substituting the proposed control-law (4.12) in (4.16), a cascaded structure can be recognized in which the q -dynamics are perturbed by the output of the \bar{e} -dynamics. It then remains to derive the stability properties of the closed-loop cascaded system (4.12), (4.16). Hereto, let us first consider the perturbed linear time-invariant system (4.16a). Choosing $k_w, k_z > 0$, the matrix \mathcal{A} is Hurwitz by construction and hence the unperturbed system (i.e. $\gamma(\bar{e}_\rho) = 0$) is globally uniformly exponentially stable. From converse Lyapunov theory we may therefore conclude that there exists $P = P^\top > 0$ which is the unique solution to the Lyapunov equation

$$\mathcal{A}^\top P + P\mathcal{A} = -Q \quad (4.18)$$

where Q is an arbitrary symmetric positive definite matrix. If we choose $Q = I$, solving the Lyapunov equation (4.18) then yields

$$P = \frac{1}{2} \begin{bmatrix} \left(\frac{k_z}{k_w} + \frac{(k_w+1)}{k_z}\right) I & \frac{1}{k_w} I \\ \frac{1}{k_w} I & \frac{(k_w+1)}{k_z k_w} I \end{bmatrix}. \quad (4.19)$$

Using $V(q) = q^\top P q$ as a candidate Lyapunov function for the perturbed system (4.16a), it immediately follows that the time-derivative of $V(q)$ satisfies

$$\dot{V} \leq -\|q\|^2 + r\|q\| \quad \text{with} \quad r = \sqrt{1 + \left(\frac{k_w+1}{k_z}\right)^2}. \quad (4.20)$$

Here we have used $\|\frac{\partial V}{\partial q} B \gamma(\bar{e}_\rho)\| \leq 2k_w \|PB\| \|q\|$. It is clear that (4.20) is negative for all $\|q\| > r$ from which we may conclude that solutions of (4.16a) remain uniformly bounded. In addition, if we choose $\|q(t_0)\| < r$ we can guarantee that independent of the \bar{e} behaviour, for all time $t \geq t_0$ the solutions remain within the set $\Omega_r = \{q \in \mathbb{R}^6 : \|q\| < r\}$. As a consequence the control input (4.12) is bounded.

Next, the stability result for the closed-loop subsystem (4.12), (4.16b) is derived. We propose a suitable candidate Lyapunov function for this system as

$$V(\bar{e}) = k_1 \sqrt{1 + \|\bar{e}_\rho\|^2} - k_1 - k_w \int_0^{\|\bar{e}_\rho\|} \sigma_n(s) ds + \frac{1}{2} \bar{e}_\nu^\top \bar{e}_\nu, \quad (4.21)$$

where $k_1 > k_w \sqrt{2} > 0$. Positive definiteness immediately follows from the observation that the first term of the right-hand side of (4.21) can be identified as the integral of a smooth saturation function of the form (4.14) with $n = 2$, evaluated on the domain $[0, \|\bar{e}_\rho\|]$. Differentiation of (4.21) along the solutions of (4.16b), and substitution of the proposed control law (4.12), yields the following result

$$\dot{V}(\bar{e}) = -\frac{k_2}{\sqrt{1 + \|\bar{e}_\nu\|^2}} \|\bar{e}_\nu\|^2 \leq 0, \quad (4.22)$$

where we have used the property $b^\top S(\omega_r(t)) b = 0$ for an arbitrary vector $b \in \mathbb{R}^3$. From this result we can conclude that $V(\bar{e})$ has a bounded limit for $t \rightarrow \infty$ and consequently the trajectories $\bar{e}(t)$ are uniformly bounded. Since $\dot{V}(\bar{e})$ is a uniformly continuous function, we may invoke Lemma 2.2.1 (Barbalat) and Lemma 2.2.2 (Micaelli and Samson) to conclude asymptotic stability of the transformed system (4.16b). Since the proposed Lyapunov function is weak (i.e. $V > 0$ and $\dot{V} \leq 0$) it is not possible to directly conclude the more desirable property of uniform asymptotic stability.

In order to conclude uniform asymptotic stability, we resort to Theorem 2.2.1 (Matrosov). Condition (i) of the theorem requires the proposed Lyapunov function (4.21) to be decrescent. We see that $V(\bar{e})$ is bounded by the functions

$$\alpha_1(\|\bar{e}\|) = k_3 \sqrt{1 + \|\bar{e}\|^2} - k_3 \quad k_3 \leq \min\{k_1 - k_w \sqrt{2}, \frac{1}{2}\}, \quad (4.23)$$

$$\alpha_2(\|\bar{e}\|) = k_4 \|\bar{e}\|^2 \quad k_4 \geq \max\{k_1, \frac{1}{2}\} \quad (4.24)$$

and thus condition (i) is satisfied. In addition, we see that condition (ii) is satisfied with

$$U(\bar{e}) = -\frac{k_2}{\sqrt{1 + \|\bar{e}_\nu\|^2}} \|\bar{e}_\nu\|^2, \quad (4.25)$$

such that uniform stability (US) can be concluded. Next, we define an auxiliary function

$$W(t, \bar{e}) = \kappa \bar{e}_\rho^\top \bar{e}_\nu, \quad (4.26)$$

with $\kappa > 0$. Since we have uniform stability, we can conclude that \bar{e}_ρ and \bar{e}_ν are bounded, and consequently $|W(t, \bar{e})|$ is bounded. Condition (iii) is therefore satisfied. To verify (iv), we use Lemma 2.2.3. It follows that

$$\dot{W}(\bar{e}) = \kappa \left(\bar{e}_\nu^\top \bar{e}_\nu - k_1 \frac{\bar{e}_\rho^\top \bar{e}_\rho}{\sqrt{1 + \|\bar{e}_\rho\|^2}} - k_2 \frac{\bar{e}_\rho^\top \bar{e}_\nu}{\sqrt{1 + \|\bar{e}_\nu\|^2}} + k_w \bar{e}_\rho^\top \sigma_n(\bar{e}_\rho) \right), \quad (4.27)$$

where we have used the property that $-\bar{e}_\nu^\top S(\omega_r(t)) \bar{e}_\rho - \bar{e}_\rho^\top S(\omega_r(t)) \bar{e}_\nu = 0$. Since \dot{W} is continuous and independent of time t , condition (iv-a) is satisfied. Furthermore, in the set $E = \{\bar{e} \in \mathcal{S} \mid U(\bar{e}) = 0\}$ it holds that $\bar{e}_\nu = 0$, and (4.27) reduces to

$$\dot{W}(\bar{e}) = -\kappa \left(k_1 \frac{\bar{e}_\rho^\top \bar{e}_\rho}{\sqrt{1 + \|\bar{e}_\rho\|^2}} - k_w \bar{e}_\rho^\top \sigma_n(\bar{e}_\rho) \right) \quad \forall \bar{e} \in E. \quad (4.28)$$

Therefore, (iv-b) and consequently condition (iv) is satisfied. From the assumption that $\omega_r(t)$ is bounded for all t , and the trajectories of \bar{e} are bounded, it immediately follows that condition (v) is satisfied. Additionally, we can find a c and \mathcal{S} for arbitrary initial conditions, such that $x_0 \in V_{t,c}^{-1}$. Note that although $V(\bar{e})$ being radially unbounded implies that we can choose c and \mathcal{S} arbitrary large, condition (v) limits this choice for \mathcal{S} to a bounded region. It follows from Matrosov's theorem that the origin of the transformed closed-loop subsystem (4.12), (4.16b) is globally uniformly asymptotically stable (GUAS). Since solutions of the cascaded system (4.16) remain bounded, uniform asymptotic stability of this system immediately follows. The results hold for all $\|q(t_0)\| < r$ and all $\bar{e}(t_0) \in \mathbb{R}^6$. As a direct consequence of the state-transformation (4.15), the tracking errors $(e_\rho, e_\nu)^\top$ uniformly asymptotically converge to zero for all $e(t_0) \in \mathbb{R}^6$. This completes the proof. \square

Remark 4.2.1. We observe that for sufficiently small \bar{e}_ρ , the saturation (4.14) behaves linearly such that $\sigma_n(\bar{e}_\rho) \approx \bar{e}_\rho$ and hence $\dot{z} \approx -k_z z + k_w R_r e_\rho$. Assuming e_ρ to be constant, the solution can be approximated by $z \approx \frac{k_w}{k_z} R_r e_\rho$. By construction we have $R_r e_\rho = \rho_r(t) - \rho(t)$ and consequently $w \approx \frac{k_w}{k_z} \int_0^t (\rho_r(s) - \rho(s)) ds$. The resulting control input can then be approximated by the PID control law

$$u = -\frac{k_w}{k_z} (k_1 - k_w) e_I - \left(k_1 - k_w + \frac{k_2 k_w}{k_z} \right) e_\rho - k_2 e_\nu, \quad (4.29)$$

where $e_I = R_r^\top \left(\int_0^t (\rho_r(s) - \rho(s)) ds \right)$ is a natural extension of the tracking error coordinates proposed in (4.4) and (4.5). Due to $k_1 > k_w$, the effective control gains are positive.

Since we have defined u as a virtual input, its stabilizing function (desired behaviour) is then defined as

$$u_d = R_r^\top (k_z z + k_w w) - \frac{k_1}{\sqrt{1 + \|\bar{e}_\rho\|^2}} \bar{e}_\rho - \frac{k_2}{\sqrt{1 + \|\bar{e}_\nu\|^2}} \bar{e}_\nu. \quad (4.30)$$

From the original definition of u , we recognize a new input vector as $R_r^\top R B_f f$. It then becomes intuitive to use R and f for letting u attain the desired behaviour of the nonlinear PID control law (4.30). In the next section the design of the actual inputs f and τ , based on the virtual control law is discussed.

4.3 Attitude Control Design

Consider the stabilizing function u_d (4.30). Let us rewrite the linear time-varying system (4.7) as

$$\dot{e} = A(t)e + B u_d + B(u - u_d). \quad (4.31)$$

A new error variable appears as $u - u_d$ which can be separated in terms of a new input vector F and a desired vector F_d

$$F = \left(R_r^\top R B_f \right) f \quad \text{and} \quad F_d = B_f f_r - M u_d, \quad (4.32)$$

such that $u - u_d = M^{-1}(F_d - F)$. Note that F and F_d are expressed within the tracking reference frame \mathcal{R} , and can be interpreted as the quadrotor's actual and desired thrust vectors respectively. By letting F converge to F_d , we actually steer the quadrotor in the appropriate

heading direction towards the trajectory. As a first step to obtain this objective, the magnitude of the thrust can be used for setting $\|F\|_2 = \|F_d\|_2$. Since the magnitude of a vector is invariant under a rotational transformation, it holds that $\|F\|_2 = f$. Therefore, we choose the input thrust as

$$f = \|F_d\|_2 = \|B_f f_r(t) - M u_d\|_2. \quad (4.33)$$

It is assumed that $0 < f_{\min} \leq f_r(t) \leq f_{\max}$. In order to guarantee $\|F_d\|_2 > 0$, $\forall t$ we might impose a condition on the stabilizing function as $\|u_d\| \leq \frac{f_{\min}}{m}$, i.e.,

$$\|u_d\| \leq k_z + \frac{(k_w + 1)^2}{k_z} + k_1 + k_2 < \frac{f_{\min}}{m}. \quad (4.34)$$

By choosing the initial conditions of the q -subsystem (4.13) as $\|q(t_0)\| < r$, with r the bound defined in (4.20), and k_w , k_z , k_1 and k_2 such that (4.34) is satisfied, it can be guaranteed that $f > 0$. The physical relevance of this condition is that the quadrotor's propellers always generate a non-negative, positive thrust during flight. Note that the bound on u_d is inversely proportional to k_z . By choosing k_z arbitrarily small, the bound increases, whereas by choosing k_z arbitrarily large this also happens. A deliberate choice for k_z must therefore be made. For fixed k_w , k_1 and k_2 , there is a minimum at $k_z = k_w + 1$.

Next, $R_r^\top R$ is used for controlling the orientation of F , with the aim to align F and F_d . Hereto, consider the following two normalized thrust vectors

$$\hat{f} = \frac{F}{\|F\|} = R_r^\top R B_f \quad \text{and} \quad \hat{f}_d = \frac{F_d}{\|F_d\|} = R_d B_f, \quad (4.35)$$

which are well-defined due to the properties of u_d . From the definition of \hat{f}_d , a new coordinate frame is introduced, and is denoted by the heading direction frame \mathcal{D} . The origin of this frame coincides with the origin of the body-fixed frame \mathcal{B} . The rotation matrix $R_d \in \mathcal{SO}(3)$ maps the desired heading reference frame \mathcal{D} to the tracking reference frame \mathcal{R} .

The construction of R_d is based on the property that the columns of a rotation matrix are orthogonal. Since the third column of R_d is specified by \hat{f}_d , the orthogonal matrix is defined as

$$R_d = \begin{bmatrix} \frac{r_{1d}}{\|r_{1d}\|} & \frac{r_{2d}}{\|r_{2d}\|} & r_{3d} \end{bmatrix} \in \mathcal{SO}(3), \quad (4.36)$$

where

$$r_{1d} = r_{2d} \times r_{3d}, \quad r_{2d} = r_{3d} \times \hat{i} \quad \text{and} \quad r_{3d} = \hat{f}_d \quad (4.37)$$

and $\hat{i} = [1, 0, 0]^\top$. Note that \hat{f}_d is always defined and the third component is always positive. This property guarantees that \hat{f}_d and \hat{i} are never parallel and hence $\|r_{3d} \times \hat{i}\| > 0$. Moreover, we have by definition that r_{2d} is perpendicular to the plane spanned by r_{3d} and \hat{i} . Therefore, r_{2d} is never parallel to \hat{f}_d , which guarantees $\|r_{2d} \times r_{3d}\| > 0$. This result implies that the columns of R_d are well defined. Furthermore, by construction it holds that $\hat{f}_d = [0, 0, 1]^\top$ implies $R_d = I$.

Since we want to align the actual and desired thrust vectors \hat{f} and \hat{f}_d , the definition of these normalized thrust vectors in (4.35) allows for an intuitive set of error coordinates

$$e_f = R^\top R_r (\hat{f}_d - \hat{f}) = (\hat{R}_e - I) B_f, \quad (4.38)$$

$$J e_\omega = J R^\top R_r (\omega_d + \omega_r) - J \omega, \quad (4.39)$$

where

$$\hat{R}_e = \left(R^\top R_r \right) R_d \quad \text{and} \quad \omega_d = \frac{F_d \times \dot{F}_d}{\|F_d\|^2}. \quad (4.40)$$

Note that this set of error coordinates is expressed with respect to the body-fixed frame \mathcal{B} . This choice shows to be convenient for control design purposes, as is discussed hereafter. Due to the definition of (4.38) and (4.39), the objective of letting \hat{f} converge to \hat{f}_d can now be characterized in terms of a standard attitude tracking control problem.

As a result of the previous definitions, the following attitude dynamics are considered

$$\dot{\hat{R}}_e = S(e_\omega) \hat{R}_e \quad (4.41a)$$

$$J\dot{e}_\omega = -JS(\omega_e)R^\top R_r(\omega_d + \omega_r) + JR^\top R_r(\dot{\omega}_d + \dot{\omega}_r) + S(\omega)J\omega - \tau, \quad (4.41b)$$

where $\omega_e = \omega - R^\top R_r \omega_r$ is the angular velocity difference between the body-fixed frame \mathcal{B} and the tracking reference frame \mathcal{R} , expressed in \mathcal{B} . The attitude tracking control problem is stated as follows:

Problem 4.3.1. (Attitude tracking control problem) *Consider the attitude system (4.41). Assume that the desired equilibrium of this system is given as $(I, 0) \in \mathcal{SO}(3) \times \mathbb{R}^3$. Find an appropriate control law*

$$\tau = \tau \left(t, \hat{R}_e, e_\omega \right) \quad (4.42)$$

such that for the resulting closed-loop system (4.41), (4.42)

$$\lim_{t \rightarrow \infty} \hat{R}_e = I \quad \text{and} \quad \lim_{t \rightarrow \infty} e_\omega = 0.$$

The attitude tracking control problem has been studied extensively [35, 54]. A main result from the available research is that no globally asymptotically stabilizing control law that is also continuously dependent on the attitude in $\mathcal{SO}(3)$ exists [55, 56]. Due to the fact that the configuration manifold $\mathcal{SO}(3)$ is compact, every continuous vector field on it necessarily possesses more than one equilibrium which restricts the possibility for global stabilization of a single equilibrium solution [57].

Several continuous feedback control schemes using minimal coordinates (e.g. Euler angles) or quaternions have been suggested to globally asymptotically stabilize motion in \mathbb{R}^3 or \mathbb{S}^3 . This, however, does not imply global asymptotic stability in $\mathcal{SO}(3)$. Recent studies propose continuous time feedback control laws that render the closed-loop attitude system of a rigid body *almost-globally* asymptotically stable in $\mathcal{SO}(3)$ [58]. These control algorithms have been applied to problems such as stabilization of a 3D inverted pendulum [59] or attitude tracking of small satellites [60]. In [13], the control structure is used for attitude control of a quadrotor. In this thesis we adopt the smooth feedback control law proposed in [56] and [57] and adapt it to our specific requirements. The result is based on this work and presented as follows.

Proposition 4.3.1. *Consider the attitude dynamics (4.41) with \hat{R}_e , ω_d and e_ω defined in (4.40) and (4.39) respectively. The continuous control law*

$$\tau = S(\omega)J\omega + J(\lambda - \mu) \quad (4.43)$$

with

$$\lambda = -S(\omega_e)R^\top R_r(\omega_d + \omega_r) + R^\top R_r(\dot{\omega}_d + \dot{\omega}_r) \quad (4.44)$$

and

$$\mu = -c_1 \sum_{i=1}^3 \sigma_i \left(s_i \times \hat{R}_e s_i \right) - c_2 e_\omega, \quad (4.45)$$

where s_i , $i \in \{1, 2, 3\}$ are the respective columns of the identity matrix I , σ_i distinct positive numbers and $c_1, c_2 > 0$ almost-globally uniformly asymptotically stabilizes the solutions of the closed-loop system (4.41), (4.43) to $\hat{R}_e = I$ and $e_\omega = 0$. That is, with the exception of solutions starting in a set $\mathcal{M} \subset \mathcal{SO}(3) \times \mathbb{R}^3$ with zero Lebesgue measure, all trajectories converge to the desired equilibrium $(I, 0)$. As a direct consequence, the actual thrust vector F asymptotically converges to its desired behaviour F_d for almost all initial conditions.

Proof. The proof is based on the results in [56] and [57] in which a similar closed-loop attitude system is analyzed. Consider the attitude error dynamics defined in (4.41). By defining τ as in (4.43) it can be seen that the angular error dynamics (4.41b) are feedback linearized to $J\dot{e}_\omega = J\mu$. Substitution of μ as in (4.45), the following closed-loop system is obtained

$$\dot{\hat{R}}_e = S(e_\omega)\hat{R}_e \quad (4.46a)$$

$$\dot{e}_\omega = -c_1 \sum_{i=1}^3 \sigma_i \left(s_i \times \hat{R}_e s_i \right) - c_2 e_\omega. \quad (4.46b)$$

We choose a similar candidate Lyapunov function for this system as in [56, 57] as

$$V(\hat{R}_e, e_\omega) = \frac{1}{2} e_\omega^\top e_\omega + c_1 \Psi(\hat{R}_e), \quad (4.47)$$

where $\Psi(\hat{R}_e)$ is an error function, defined as

$$\Psi(\hat{R}_e) = \sum_{i=1}^3 \sigma_i \left(1 - s_i^\top \hat{R}_e s_i \right). \quad (4.48)$$

The parameters σ_i are distinct and positive. The elements of this function are analogous to the magnitude $\frac{1}{2} \|\hat{R}_e s_i - s_i\|^2 = 1 - \cos(\theta_i)$, where θ_i is the angle between $\hat{R}_e s_i$ and s_i . This function can therefore be interpreted as the distance between \hat{R}_e and I on $\mathcal{SO}(3)$. Furthermore, since $\Psi(\hat{R}_e) > 0$ for all $\hat{R}_e \neq I$ and $\Psi(I) = 0$ positive definiteness of $V(\hat{R}_e, e_\omega)$ directly follows. Differentiating $V(\hat{R}_e, e_\omega)$ with respect to time along the solutions of (4.41) yields

$$\dot{V}(\hat{R}_e, e_\omega) = e_\omega^\top \left(\mu + c_1 \sum_{i=1}^3 \sigma_i \left(s_i \times \hat{R}_e s_i \right) \right). \quad (4.49)$$

Substitution of μ (4.45) results in

$$\dot{V}(\hat{R}_e, e_\omega) = -c_2 e_\omega^\top e_\omega \leq 0, \quad (4.50)$$

hence the origin $(I, 0)$ is a stable equilibrium. Since the closed-loop dynamics (4.46) are time-invariant, and we have that the set

$$\Omega = \left\{ \left(\hat{R}_e, e_\omega \right) \in \mathcal{SO}(3) \times \mathbb{R}^3 : V(\hat{R}_e, e_\omega) \leq V(\hat{R}_e(t_0), e_\omega(t_0)) \right\} \quad (4.51)$$

is a positively invariant set, by a direct application of LaSalle's invariant set theorem [38, Theorem 4.4] we may conclude that the only solution that can identically stay in the set [56]

$$E = \{(\hat{R}_e, e_\omega) \in \mathcal{SO}(3) \times \mathbb{R}^3 \mid \dot{V}(\hat{R}_e, e_\omega) = 0\} \subset \Omega \quad (4.52)$$

is the solution $e_\omega = 0$ and $\sum_{i=1}^3 \sigma_i (s_i \times \hat{R}_e s_i) = 0$. Due to the orthogonality property and the cross-product operator, the latter equality holds if and only if $s_i = \pm \hat{R}_e s_i$. Since we consider rotation matrices in the special orthogonal group, and thus $\det(\hat{R}_e) = 1$, this implies $\hat{R}_e \in \mathcal{E}$ with

$$\mathcal{E} = \{I, \text{diag}([-1, -1, 1]), \text{diag}([-1, 1, -1]), \text{diag}([1, -1, -1])\} \subset \mathcal{SO}(3). \quad (4.53)$$

Note that the last three equilibria denote a rotation by $|\pi|$ radians around the positive axis. From these results we can conclude that all solutions of the closed-loop system asymptotically converge to one of the four equilibria $\hat{R}_e \in \mathcal{E}$ and $e_\omega = 0$. Let us denote $\hat{R}_e = I$ as the desired equilibrium such that the set $\mathcal{E} \setminus \{I\}$ contains the undesired equilibria. We continue the proof by analyzing the local stability properties of each equilibrium. Hereto, the closed-loop system (4.46) is linearized around the corresponding equilibria. The linearization method is adopted from [35, 61] where the infinitesimal variation of \hat{R}_e is expressed as $\delta \hat{R}_e = S(\theta) \hat{R}_e$. This yields the following linearized dynamics,

$$\begin{bmatrix} \dot{\theta} \\ \delta \dot{e}_\omega \end{bmatrix} = \begin{bmatrix} S(e_\omega) & I \\ -c_1 N & -c_2 I \end{bmatrix} \begin{bmatrix} \theta \\ \delta e_\omega \end{bmatrix} \quad \text{with} \quad N = \sum_{i=1}^3 \sigma_i \left[(s_i^\top \hat{R}_e s_i) I - s_i (\hat{R}_e s_i)^\top \right]. \quad (4.54)$$

It follows that at the desired equilibrium N is diagonal and positive definite such that the linearized matrix is Hurwitz. For the other equilibria, N is diagonal and has at least one negative real eigenvalue. This result implies local exponential stability of the desired equilibrium and the undesired equilibria are unstable. Moreover, since the scalars σ_i are distinct, all eigenvalues have nonzero real part, and at least one eigenvalue has positive real part. The unstable equilibria are hyperbolic, and therefore we can conclude that for each undesired equilibrium there exists a stable and unstable invariant manifold, that is, solutions starting in the stable manifold converge to the equilibrium, whereas solutions starting outside the stable manifold diverge from the equilibrium. According to [35, 56, 59, 61] the dimension of the union \mathcal{M} of stable manifolds is less than the dimension of the tangent space of $\mathcal{SO}(3)$, and therefore it has zero measure. This completes the proof. \square

4.4 Closed-loop Stability

In the previous sections, stabilizing control laws for the translational subsystem (4.7) and the attitude subsystem (4.41) are designed. In this section the stability properties of the complete closed-loop system are derived. Hereto, consider the following closed-loop structure

$$\dot{q} = \mathcal{A}q + B\gamma(e, q) \quad (4.55)$$

$$\dot{e} = A(t)e + Bu_d + BM^{-1}(F_d - F) \quad (4.56)$$

$$\dot{\eta} = \Sigma(\eta) \quad (4.57)$$

where $q = (w, z)^\top \in \mathbb{R}^6$, $e = (e_\rho, e_\nu)^\top \in \mathbb{R}^6$, $\eta = (e_f, e_\omega)^\top \in \mathbb{R}^6$ and

$$\Sigma(\eta) = \begin{bmatrix} S(e_\omega) \hat{R}_e B_f \\ -c_1 \sum_{i=1}^3 \sigma_i (s_i \times \hat{R}_e s_i) - c_2 e_\omega \end{bmatrix}. \quad (4.58)$$

From the system description (4.55)–(4.57) two cascaded structures can be recognized since the q -subdynamics are perturbed by the output of the e -subdynamics whereas the e -dynamics are perturbed by the output of the η -dynamics. In order to obtain a more convenient closed-loop system description, we must rewrite the perturbation term $F_d - F$ as follows. It has previously been shown that the magnitude of F can be directly manipulated such that $\|F\| = \|F_d\| = f(t, e, q)$. Additionally, the definition of e_f (4.38) allows us to write

$$\begin{aligned} F_d - F &= f(t, e, q) R_r^\top R e_f \\ &= f(t, e, q) R_r^\top R H \eta \end{aligned} \quad (4.59)$$

with $H = [I \ 0]$. The following cascaded structure is then obtained

$$\dot{q} = \mathcal{A}q + B\gamma(e, q) \quad (4.60a)$$

$$\dot{e} = h(t, e, q) + d(t, e, q)\eta \quad (4.60b)$$

$$\dot{\eta} = \Sigma(\eta) \quad (4.60c)$$

with

$$h(t, e, q) = A(t)e + Bu_d \quad (4.61)$$

$$d(t, e, q) = f(t, e, q) B M^{-1} R_r^\top R H. \quad (4.62)$$

The result is presented as follows.

Proposition 4.4.1. *Solutions of the closed-loop system (4.60) are uniformly asymptotically stable. In addition, if $\|q(t_0)\| < \sqrt{1 + \left(\frac{k_w+1}{k_z}\right)^2}$ solutions of the subsystems (4.60b)–(4.60c) uniformly asymptotically converge to the origin, for all $e \in \mathbb{R}^6$, all $e_\omega \in \mathbb{R}^3$ and all e_f starting outside a set with measure zero.*

Proof. For the first part of the proof we again adopt the coordinate transformation (4.15), for which the dynamics can be written in an equivalent cascaded-structure as (4.60)

$$\dot{q} = \mathcal{A}q + B\gamma(\bar{e}) \quad (4.63a)$$

$$\dot{\bar{e}} = \bar{h}(t, \bar{e}) + d(t, e, q)\eta \quad (4.63b)$$

$$\dot{\eta} = \Sigma(\eta) \quad (4.63c)$$

with

$$\bar{h}(t, \bar{e}) = A(t)\bar{e} + B \left(u_d + R_r^\top \left(B^\top \mathcal{A}q + \gamma(\bar{e}_\rho) \right) \right). \quad (4.64)$$

We first consider the result from the proof of Proposition 4.2.1, in which it was shown that by choosing the initial conditions of (4.63a) as

$$\|q(t_0)\| < \sqrt{1 + \left(\frac{k_w+1}{k_z}\right)^2} \quad (4.65)$$

the solutions remain uniformly within a desired bound. This is an important result since it is used to show boundedness of the coupling term $d(t, e, q)$ in (4.63b). Next, assume (4.65) holds and consider the system (4.63b)–(4.63c) which has a standard cascaded structure. In order to derive its convergence properties, we resort to Theorem 2.3.1 presented in Chapter 2, in which several necessary assumptions are given to guarantee boundedness of the solutions of a cascaded system. In the proofs of Proposition 4.2.1 and Proposition 4.3.1 it has been shown that the subsystems $\dot{\bar{e}} = \bar{h}(t, \bar{e})$ and $\dot{\eta} = \Sigma(\eta)$ are GUAS and almost-GUAS respectively. Let us first consider the domain in which the solutions of the attitude subsystem converge to the desired equilibrium and denote this by D_1 . Within this domain, the following observations are made:

1. The subsystems $\dot{\bar{e}} = \bar{h}(t, \bar{e})$ and $\dot{\eta} = \Sigma(\eta)$ are GUAS with respect to the considered domain D_1 . Furthermore, the Lyapunov function $V(t, \bar{e})$ as defined in (4.21) satisfies the conditions in Assumption A1 from Theorem 2.3.1 with $\alpha_1(\|\bar{e}\|)$, $\alpha_2(\|\bar{e}\|)$ and $W(\bar{e})$ as defined in (4.23), (4.24) and (4.25) respectively, and

$$\alpha_4(\|\bar{e}\|) = k_5\|\bar{e}\| \quad k_5 \leq \max\{(k_1 + k_w), 1\}. \quad (4.66)$$

2. The coupling term $d(t, e, q)$ defined in (4.62) satisfies the upper bound

$$\begin{aligned} \|d(t, e, q)\| &\leq f(t, e, q)\|BM^{-1}R_r^\top RH\| \\ &\leq k_z + \frac{(k_w + 1)^2}{k_z} + k_1 + k_2 + \frac{1}{m}f_{\max} := d_{\max} \end{aligned} \quad (4.67)$$

provided the initial conditions of the q -subsystem are chosen according to (4.65). Here, we have used the properties $\|B\| = 1$, $\|R_r^\top R\| = 1$, $\|H\| = 1$ and $\|u_d\| \leq k_z + \frac{(k_w+1)^2}{k_z} + k_1 + k_2$.

3. The system is forward complete, that is the solutions are defined over the complete time-interval, and thus do not have a finite escape-time. In order to see this, let us observe that for this case we have

$$\alpha_1^{-1}(s) = \sqrt{\left(\frac{s}{k_3} + 1\right)^2 - 1} \quad \text{and} \quad \alpha_5 = d_{\max}. \quad (4.68)$$

Choosing

$$\alpha_6(s) = d_{\max}k_5 \left(\frac{s}{k_3} + 1\right) \quad (4.69)$$

and integrating the fraction $\frac{1}{\alpha_6(s)}$ over the domain (a, ∞) , where we choose $a = 0$, yields

$$\lim_{k \rightarrow \infty} \int_0^k \frac{ds}{\alpha_6(s)} = \lim_{k \rightarrow \infty} \left(\ln \left(\frac{k}{k_3} + 1 \right) \right) \frac{k_3}{d_{\max}k_5} = \infty, \quad (4.70)$$

such that assumption A3 from Theorem 2.3.1 is satisfied.

4. Since the solutions do not escape in finite-time, it can be concluded that for all $t \geq t_0$

$$\frac{\partial V}{\partial t} + \frac{\partial V}{\partial \bar{e}} \bar{h}(t, \bar{e}) + \frac{\partial V}{\partial \bar{e}} d(t, e, q)\eta \leq -\|\bar{e}_\nu\| \left(\frac{k_2}{\sqrt{1 + \|\bar{e}_\nu\|^2}} \|\bar{e}_\nu\| - d_{\max}\|\eta\| \right). \quad (4.71)$$

Due to the asymptotic convergence properties of the attitude dynamics, we know that after some time $t_1 \geq t_0$ the solutions of the second subsystem satisfy $\|\eta\| < \frac{k_2}{d_{\max}}$ and thus $\dot{V} \leq 0$ for all sufficiently large $\|\bar{e}_\nu\|$. This implies global uniform boundedness of the solutions \bar{e} .

According to the observations, assumptions A1, A3 and A4 of Theorem 2.3.1 hold and therefore the transformed closed-loop cascade system (4.63b)–(4.63c) is GUAS with respect to the domain D_1 .

As a result, we obtain that solutions of the system (4.63) are uniformly bounded. If we then consider (4.63) as a cascaded system in which the output of the \bar{e} -dynamics perturbs the q -dynamics, we may directly conclude from cascaded system theory that (4.63) is uniformly asymptotically stable. Since $q(t_0)$ is chosen according to (4.65), due to the global convergence properties of the subsystem (4.63b)–(4.63c), this result holds for all $\bar{e}(t_0) \in \mathbb{R}^6$ and all $\eta(t_0) \in D_1$. As a direct corollary from the coordinate transformation (4.15), it follows that the tracking errors $(e_\rho(t), e_\nu(t))^\top$ uniformly asymptotically converge to zero for all initial conditions.

As a final note, it is shown that the domain D_1 can be extended with the region of attraction of the undesired equilibrium $R_u = \text{diag}([-1, -1, 1])$. From the definition of e_f , and the subdynamics (4.58) it is evident that, for position tracking, only the last column of \hat{R}_e is of importance. Whenever \hat{R}_e converges to the considered undesired equilibrium, it still holds that e_f converges to zero. The previous observations are therefore true for this situation and hence the closed-loop cascaded system is uniformly asymptotically stable in the domain $D = D_1 \cup \mathcal{M}_u$ where \mathcal{M}_u is the region of attraction of R_u . Physically, this can be interpreted as the quadrotor heading in the specified direction, though the frame is rotated by π radians around the thrust axis. If \hat{R}_e converges to one of the other two undesired equilibria, it follows that $\|\eta\| \rightarrow 2$. As a result, the quadrotor is upside down and since the direction of the thrust is defined to be along the positive b_3 -axis, the quadrotor falls towards the ground. The translational tracking errors increase and we conclude that all solutions starting in the set \mathcal{M}^* which consists of the regions of attraction of the last two undesired equilibria, grow unbounded. \square

4.5 Full State Stability

In the previous sections it is shown that the available control inputs, f and τ are used for position tracking of the quadrotor but not for direct attitude control. The results showed that for almost all initial conditions, the quadrotor's position and body velocity, expressed within the tracking reference frame, converges to the reference behaviour. Since no pure attitude tracking (that is, attitude tracking with the purpose of letting $(R, \omega) \rightarrow (R_r, \omega_r)$) has been applied, convergence of e does not necessarily imply that the complete behaviour of the quadrotor converges to the reference behaviour. In order to verify convergence of the systems behaviour, let us first assume that solutions start in the domain D_1 . Then due to the uniform asymptotic convergence properties of the closed-loop system we can conclude that

$$\lim_{t \rightarrow \infty} \{q(t), e_\rho(t), e_\nu(t), e_f(t), e_\omega(t)\} = \{0, 0, 0, 0, 0\}. \quad (4.72)$$

As a direct consequence, we obtain $\lim_{t \rightarrow \infty} F_d(t) = f_r(t)B_f$ and $\hat{f}_d = [0, 0, 1]^\top$. In order to verify if R_d converges to I , let us first consider the following vectors

$$r_{1d} = r_{2d} \times \hat{f}_d \quad (4.73)$$

$$r_{2d} = \hat{f}_d \times \hat{i} \quad (4.74)$$

with $\hat{i} = [1, 0, 0]^\top$. It immediately follows that r_{2d} is a linear function of the last two elements of \hat{f}_d , i.e. $r_{2d} = [0, \hat{f}_{d3}, -\hat{f}_{d2}]^\top$. Due to boundedness of \hat{f}_d , this vector remains bounded

and converges to $r_{2d} = [0, 1, 0]^\top$. From the cross-product operator we furthermore observe that

$$r_{1d} = \left[\hat{f}_{d_2}^2 + \hat{f}_{d_3}^2 \quad -\hat{f}_{d_1} \hat{f}_{d_2} \quad -\hat{f}_{d_1} \hat{f}_{d_3} \right]^\top. \quad (4.75)$$

Since all elements of \hat{f}_d remain bounded, we may conclude that r_{1d} eventually converges to $[1, 0, 0]$. Due to the definition, it then follows that R_d converges to I . In the considered domain we have that \hat{R}_e approaches I such that we are able to conclude that

$$\lim_{t \rightarrow \infty} R(t) = R_r(t). \quad (4.76)$$

Recall that the position and translational velocity errors are defined as $e_\rho = R_r^\top (\rho_r - \rho)$ and $e_\nu = \nu_r - R_r^\top R\nu$ respectively. Hence from (4.72) and (4.76) we may conclude that

$$\lim_{t \rightarrow \infty} (\rho(t), \nu(t)) = (\rho_r(t), \nu_r(t)). \quad (4.77)$$

It then remains to show convergence of the quadrotor's angular velocity ω . Hereto we observe the fact that since $e_\omega \rightarrow 0$ and the orientation converges to its desired behaviour, results in $\omega = \omega_d + \omega_r$. The desired angular velocity ω_d is defined as

$$\omega_d = \frac{F_d \times \dot{F}_d}{\|F_d\|^2} \quad (4.78)$$

where we can identify

$$\dot{F}_d = B_f \dot{f}_r - \frac{d}{dt} \left(R_r^\top (k_z z + k_w w) \right) + M \left(\frac{\partial K_\rho(\bar{e}_\rho)}{\partial \bar{e}_\rho} \dot{\bar{e}}_\rho + \frac{\partial K_\nu(\bar{e}_\nu)}{\partial \bar{e}_\nu} \dot{\bar{e}}_\nu \right) \quad (4.79)$$

with K_ρ and K_ν the respective saturation functions defined in (4.12). It can then be verified that since F_d and the derivatives of the saturation functions remain bounded, \dot{F}_d approaches $\dot{f}_r B_f$ and as a consequence ω_d approaches 0. This result is straightforward since ω_d denotes the required angular velocity for alignment of F and F_d . Finally, we may observe that

$$\lim_{t \rightarrow \infty} \omega(t) = \omega_r(t) \quad (4.80)$$

such that it can be concluded that the behaviour of the quadrotor completely converges to the reference behaviour, provided that the trajectories start in D_1 . If the trajectories of the attitude controller start in \mathcal{R}_u , a similar analysis can be done from which the following is concluded:

$$\lim_{t \rightarrow \infty} \{\rho(t), R(t), \nu(t), \omega(t)\} = \{\rho_r(t), TR_r(t), T\nu_r(t), T\omega_r\} \quad (4.81)$$

with $T = \text{diag}([-1, -1, 1])$ a matrix that rotates the quadrotor's frame by π -radians around the thrust axis. Note that if the quadrotor is perfectly axisymmetric this still provides the desired result. In practice, however, this is not the case and if, for example a camera is fixed to the quadrotor for image capturing purposes, an incorrect image might be obtained.

4.6 Concluding Remarks

In this chapter the tracking control problem for a quadrotor has been considered. The proposed control law is partially based on the commonly used hierarchical control structure, in which the

position control-loop determines a new reference attitude. A cascade structure can be recognized from this control scheme, which motivates cascade based control design. By expressing the tracking error coordinates in the tracking reference frame, rather than the inertial or body-fixed frame, the control law is independent of the choice of inertial reference frame. Moreover, a convenient cascade-structure for the tracking error dynamics is obtained.

The error dynamics can be separated in a position error subsystem, and an attitude error subsystem. First, a stabilizing virtual control input has been designed for the position subsystem. It has been shown by Lyapunov analysis that the closed-loop subsystem is globally uniformly asymptotically stable. Since the virtual control input imposes some desired behaviour on the attitude dynamics, a new set of attitude error coordinates is introduced. An *almost*-globally uniformly asymptotically stabilizing control law has been proposed for the corresponding attitude error dynamics. By means of cascade theory, it has been shown that the interconnected closed-loop system is uniformly asymptotically stable, with a region of attraction that covers the complete configuration space with the exception of a set of measure zero. It has furthermore been shown that when the system trajectories enter the remaining region of the configuration space, the quadrotor turns upside down and falls towards the ground.

Since we actually use the available inputs for position tracking only, it is not straightforward that the complete behaviour of the quadrotor (that is translational and attitude behaviour) converges to the reference. However, by examining all relevant signals, it is shown that the quadrotor's behaviour completely converges to the reference behaviour provided the trajectories start in the appropriate domain.

In this chapter it has been assumed that all states of the quadrotor are directly available from measurements. In practice, however, this is not necessarily true which limits the use of the proposed full-state feedback controller. In order to overcome this issue, an output feedback control law is presented in Chapter 5, which is based on the state-feedback control structure.

Chapter 5

Output Feedback Control

In the previous chapter, a state feedback controller has been designed for which it is assumed that all states are available for control. This assumption necessitates the use of specific sensor equipment by means of which all quadrotor states can directly be measured. Commercially available quadrotors are often equipped with a set of inertial measurement units (IMUs). This set usually consists of an accelerometer, magnetometer and gyroscope from which the attitude can be reconstructed. In addition, most of these quadrotors contain an ultrasound sensor and internal cameras which can potentially be used for three dimensional position determination. In most cases, however, there is no specific sensor by means of which the body-fixed velocity ν can be measured. This limits the use of the full state feedback tracking control law designed in Chapter 4 since the error state e_ν , which is directly dependent on ν , is unavailable. In order to overcome this issue, in this chapter an observer based feedback control law is proposed which inherits its structure from the previously designed state-feedback controller. We start by formulating the output feedback tracking control problem in Section 5.1. Next, in Section 5.2 a full state observer for the translational tracking error dynamics (4.6), based on the position measurements is proposed. In Section 5.3 we propose a dynamic output feedback control law and derive the closed-loop stability properties accordingly. With the aim for practical implementation, an extension of the observer is proposed in Section 5.4 in which sampled measurements are considered. The subject of attitude reconstruction is briefly discussed in Section 5.5 and some concluding remarks are given in Section 5.6.

5.1 Problem Formulation

Let us consider the time-varying linear system (4.6) and assume that the body-fixed velocities ν are unavailable from measurements. We define the translational error system as

$$\dot{e} = A(t)e + Bu(t) \quad (5.1a)$$

$$y = Ce. \quad (5.1b)$$

with the corresponding matrices

$$A(t) = \begin{bmatrix} -S(\omega_r(t)) & I \\ 0 & -S(\omega_r(t)) \end{bmatrix}, \quad B = \begin{bmatrix} 0 \\ I \end{bmatrix} \quad \text{and} \quad C = [I \quad 0]. \quad (5.2)$$

Furthermore $u(t) = M^{-1} (B_f f_r(t) - R_r^\top R B_f f(t)) \in \mathbb{R}^3$ where $f_r(t)$ and $f(t)$ are the reference input thrust and actual input thrust respectively. Moreover R_r and R are the reference attitude matrix and actual attitude matrix, and $B_f = [0, 0, 1]^\top$.

The output function of the translational tracking error system is denoted by $y \in \mathbb{R}^3$ and corresponds to the linear transformation of measured states to tracking errors, i.e. $y = R_r^\top (\rho_r - \rho)$. Here, the reference states ρ_r and R_r are always known and ρ is the measured position. The output feedback tracking control problem for this system is formulated as follows:

Problem 5.1.1. (Output-feedback tracking control problem) *Consider the translational error coordinates (5.1a) with the corresponding measurement output function (5.1b).*

Find an appropriate dynamic control law

$$u = u(t, \mathcal{C}, \mathcal{C}_r, y, \hat{z}) \quad (5.3a)$$

$$\dot{\hat{z}} = \gamma(t, \mathcal{C}, \mathcal{C}_r, y, \hat{z}), \quad (5.3b)$$

such that for the closed-loop system

$$\lim_{t \rightarrow \infty} \|e(t)\| = 0. \quad (5.4)$$

Here, \hat{z} is some combination of estimated states which are desired to converge to the actual states.

Note that the output feedback control problem is only considered in terms of the translational error dynamics. We initially assume that the attitude states (R, ω) can be perfectly reconstructed from the measurements and are therefore available. In Section 5.5 attitude reconstruction is discussed in more detail.

5.2 Observer Design

Since we consider the tracking control problem in terms of tracking error coordinates, it is appropriate to design an observer for the translational tracking error dynamics rather than the actual quadrotor dynamics. In order to increase the robustness against measurement noise and constant disturbances to some extent, a full state proportional integral Luenberger-type observer is proposed as

$$\dot{\hat{e}} = A(t)\hat{e} + Bu(t) + L_p(y - \hat{y}) - By_I \quad (5.5a)$$

$$\dot{y}_I = -S(\omega_r(t))y_I - L_I(y - \hat{y}) \quad (5.5b)$$

$$\hat{y} = C\hat{e}, \quad (5.5c)$$

where $L_p = [L_1 \ L_2]^\top \in \mathbb{R}^{6 \times 3}$ and $L_I \in \mathbb{R}^{3 \times 3}$. The last term in (5.5a) consists of the integral of the estimation error and corresponds to the error between the actual and estimated position integral. This correction term acts directly on the velocity error dynamics, since these are most sensitive to modeling errors. Although the observer structure is of a simple form, it can provide some useful insight for constructing more complex observers as discussed in the sections hereafter. Since it is assumed that the reference trajectory is completely known for all t , the system matrix $A(t)$ is fully known. In addition, since we assume that R is (indirectly) available from measurements and since the quadrotor's input thrust $f(t)$ can be directly manipulated, the term $u(t)$ is always known.

5.2.1 Observer Error Dynamics

In order to analyze the convergence behaviour of the proposed observer, we define an observer error $e_o = e - \hat{e}$ and an augmented state vector $\xi = (e_o, y_I)^\top \in \mathbb{R}^9$. The corresponding dynamics are derived as

$$\dot{\xi} = (A_\xi(t) - \bar{L}\bar{C}) \xi, \quad (5.6)$$

with

$$A_\xi(t) = \begin{bmatrix} A(t) & B \\ 0 & -S(\omega_r(t)) \end{bmatrix}, \quad \bar{L} = \begin{bmatrix} L_p \\ L_I \end{bmatrix} \quad \text{and} \quad \bar{C} = [C \ 0], \quad (5.7)$$

and $A(t)$, B and C as in (5.2). A result regarding the convergence properties of this linear time-varying dynamics is given by:

Proposition 5.2.1. *The solutions of (5.6) globally uniformly exponentially converge to zero provided the observer gains are chosen as $\bar{L}^\top = [l_1 I \ l_2 I \ l_3 I]$ with $l_1, l_2 > 0$ and $l_1 l_2 > l_3 > 0$. As a direct result, the estimated error states converge to the actual errors.*

Proof. In order to formulate the proof, we first make the following observation. The time varying matrix $A_\xi(t)$ as defined in (5.7) can be subdivided in a time-varying part and a constant component as

$$A_\xi(\omega_r(t)) = \bar{S}(t) + \bar{A}, \quad (5.8)$$

in which

$$\bar{S}(t) = \begin{bmatrix} -S(\omega_r(t)) & 0 & 0 \\ 0 & -S(\omega_r(t)) & 0 \\ 0 & 0 & -S(\omega_r(t)) \end{bmatrix} \quad \text{and} \quad \bar{A} = \begin{bmatrix} 0 & I & 0 \\ 0 & 0 & I \\ 0 & 0 & 0 \end{bmatrix}. \quad (5.9)$$

The observer-error dynamics (5.6) are then rewritten as

$$\dot{\xi} = (\bar{A} - \bar{L}\bar{C}) \xi + \bar{S}(t)\xi, \quad (5.10)$$

which can be considered as a perturbed linear time-invariant (LTI) system. Let us choose the observer gain matrix as $\bar{L}^\top = [l_1 I \ l_2 I \ l_3 I]$ with l_1, l_2, l_3 nonzero scalars, such that the characteristic polynomial of the time-invariant matrix $\bar{A} - \bar{L}\bar{C}$ is written as

$$(\lambda^3 + l_1 \lambda^2 + l_2 \lambda + l_3)^3. \quad (5.11)$$

Choosing the observer parameters l_1, l_2 and l_3 as

$$l_1 > 0 \quad (5.12a)$$

$$l_2 > 0 \quad (5.12b)$$

$$l_1 l_2 > l_3 > 0 \quad (5.12c)$$

renders the polynomial (5.11) Hurwitz and hence the unperturbed linear system is globally exponentially stable (GES). From Lyapunov theory it then follows that there exists a $P = P^\top > 0$ which is the unique solution to the Lyapunov equation

$$(\bar{A} - \bar{L}\bar{C})^\top P + P (\bar{A} - \bar{L}\bar{C}) = -Q, \quad (5.13)$$

with Q an arbitrary symmetric positive definite matrix. If we set $Q = I$, the Lyapunov equation can be solved and we obtain a matrix P that consists of nine sub-matrices of the form $p_{ij}I \in \mathbb{R}^{3 \times 3}$ with indices $(i, j) \in \{1, 2, 3\}$, and where p_{ij} are scalars defined as

$$p_{11} = \alpha (l_2 (l_2 + 1) + l_3 (l_3 + l_1)) \quad (5.14a)$$

$$p_{22} = \alpha (l_1 (l_1 + l_3) + l_2 + 1) \quad (5.14b)$$

$$p_{33} = \alpha (l_1 (l_1^2 + l_1 + l_2^2 + 1) - l_2 + 1) \quad (5.14c)$$

$$p_{12} = p_{21} = -\frac{1}{2} \quad (5.14d)$$

$$p_{13} = p_{31} = -p_{22} \quad (5.14e)$$

$$p_{23} = p_{32} = -\frac{1}{2} \quad (5.14f)$$

and $\alpha = \frac{1}{2} \frac{1}{(l_1 l_2 - l_3)}$. We then propose $V(\xi) = \xi^\top P \xi$ as a candidate Lyapunov function for the perturbed linear system (5.10). Due to the specific form of the matrix P , the following convenient relation holds:

$$\bar{S}(t)^\top P + P \bar{S}(t) = 0, \quad (5.15)$$

such the time-derivative of $V(\xi)$ along the solutions of (5.10) satisfies

$$\dot{V}(\xi) = -\xi^\top \xi. \quad (5.16)$$

Since the Lyapunov function and its corresponding time-derivative are strictly positive definite and negative definite respectively, it follows that by choosing the observer gains according to (5.12), the observer error dynamics (5.6) are globally uniformly exponentially stable (GUES). \square

5.3 Dynamic Output Feedback

Based on the designed state feedback control law in Chapter 4 and the observer design (5.5) the following dynamic output feedback is proposed.

Proposition 5.3.1. *Consider the dynamic output-feedback*

$$\hat{u}_d = R_r^\top (k_z z + k_w w) - \frac{k_1}{\sqrt{1 + \|\hat{e}_\rho\|^2}} \hat{e}_\rho - \frac{k_2}{\sqrt{1 + \|\hat{e}_\nu\|^2}} \hat{e}_\nu, \quad (5.17)$$

where $\hat{e}_\rho = \hat{e}_\rho + R_r^\top w$, $\hat{e}_\nu = \hat{e}_\nu + R_r^\top z$, w and z are solutions to the artificial subsystem

$$\begin{cases} \dot{w} = z \\ \dot{z} = -k_z z - k_w w + k_w R_r \sigma_n(\hat{e}_\rho), \end{cases} \quad (5.18)$$

and the states $(\hat{e}_\rho, \hat{e}_\nu)$ are generated by the observer (5.5). By choosing the control gains as $k_1 > k_w \sqrt{2} > 0$, and $k_2, k_w, k_z > 0$, and the observer gains as $\bar{L}^\top = [l_1 I \quad l_2 I \quad l_3 I]$ with $l_1, l_2 > 0$ and $l_1 l_2 > l_3 > 0$, the tracking error dynamics (5.1) in closed-loop with the output feedback (5.17) and attitude controller (4.43) are uniformly asymptotically stable for all $\|(w(t_0), z(t_0))\| < \sqrt{1 + \left(\frac{k_w + 1}{k_z}\right)^2}$, $e(t_0) \in \mathbb{R}^6$, all $e_w(t_0) \in \mathbb{R}^3$ and all attitude errors starting outside a set with measure zero. In addition, the observer errors globally uniformly exponentially converge to zero.

Proof. The closed-loop stability proof has strong resemblance with the proof of Proposition 4.4.1 and for reasons of conciseness, in some parts of the proof we therefore make a reference to the previously obtained results.

Define a state transformation of similar form as in the state feedback case

$$\hat{e}_\rho = \hat{e}_\rho + R_r^\top w \quad (5.19a)$$

$$\hat{e}_\nu = \hat{e}_\nu + R_r^\top z. \quad (5.19b)$$

By constructing the composite state $\hat{e} = (\hat{e}_\rho, \hat{e}_\nu)^\top \in \mathbb{R}^6$ and using $q = (w, z)^\top$ the corresponding dynamics can be compactly written as

$$\dot{q} = \mathcal{A}q + B\gamma(\bar{e}_\rho) \quad (5.20a)$$

$$\dot{\hat{e}} = h(t, \hat{e}) + B(u - \hat{u}_d) + D\xi, \quad (5.20b)$$

in which \mathcal{A} is defined in (4.17), $\gamma(\bar{e}_\rho) = k_w R_r \sigma_n(\hat{e}_\rho)$ a bounded perturbation,

$$h(t, \hat{e}) = A(t)\hat{e} + B\left(\hat{u}_d + R_r^\top \left(B^\top \mathcal{A}q + \gamma(\hat{e}_\rho)\right)\right), \quad (5.21)$$

and $D = [L_p C \quad -B]$. If we then adopt the attitude control scheme proposed in Section 4.3 for letting u attain the behaviour of the stabilizing function \hat{u}_d , we can proceed similarly as in Section 4.4 to obtain the following closed-loop cascaded system

$$\dot{q} = \mathcal{A}q + B\gamma(\bar{e}_\rho) \quad (5.22a)$$

$$\dot{\hat{e}} = h(t, \hat{e}) + D\xi + d(t, \hat{e}, q)\eta \quad (5.22b)$$

$$\dot{\xi} = (A_\xi(t) - \bar{L}\bar{C})\xi \quad (5.22c)$$

$$\dot{\eta} = \Sigma(\eta), \quad (5.22d)$$

with

$$d(t, \hat{e}, q) = f(t, \hat{e}, q)BM^{-1}R_r^\top RH \quad (5.23)$$

$$f(t, \hat{e}, q) = \|B_f f_r(t) - M\hat{u}_d\|, \quad (5.24)$$

and $H = [I \quad 0]$. The attitude dynamics (5.22d) are identical to (4.57) with $\eta = (e_f, e_\omega)^\top$. From the proof of Proposition 4.2.1 it follows that if we choose the initial conditions of the subsystem (5.22a) according to (4.65), that is,

$$\|q(t_0)\| < \sqrt{1 + \left(\frac{k_w + 1}{k_z}\right)^2}, \quad (5.25)$$

the solutions q remains within a desired bound for all $t \geq t_0$.

As a next step in the proof, we derive the convergence properties of the cascaded system (5.22b)–(5.22d). Since the subsystem $\dot{\hat{e}} = h(t, \hat{e})$ has an identical structure to the considered system in the proof of Proposition 4.2.1, we can immediately conclude that this subsystem is GUAS with a Lyapunov function

$$V(\hat{e}) = k_1 \sqrt{1 + \|\hat{e}_\rho\|^2} - k_1 - k_w \int_0^{\|\hat{e}_\rho\|} \sigma_n(s) ds + \frac{1}{2} \hat{e}_\nu^\top \hat{e}_\nu, \quad (5.26)$$

which is analogous to (4.21). Furthermore, according to Propositions 4.3.1 and 5.2.1 the η -dynamics and ξ -dynamics are almost-GUAS and GUES respectively. Assumption A1 from Theorem 2.3.1 is therefore satisfied. The perturbing states (ξ, η) in (5.22b) enter the \hat{e} -dynamics through D and $d(t, \hat{e}, q)$. Since these coupling terms can be upper bounded by a constant, and due to the properties of the Lyapunov function (5.26), we can immediately conclude that Assumption A3 is satisfied (for further details on this claim it is referred to observation 3 in the proof of Proposition 4.4.1).

It then remains to show that the solutions of (5.22b) are uniformly bounded. Hereto, we choose (5.26) as a candidate Lyapunov function for (5.22b). Since the system is forward complete, we have that $\forall t \geq t_0$ the corresponding time-derivative along the closed-loop solutions satisfies

$$\dot{V}(\hat{e}) \leq -\frac{k_2}{\sqrt{1 + \|\hat{e}_\nu\|^2}} \|\hat{e}_\nu\|^2 + \left\| \frac{\partial V}{\partial \hat{e}} \right\| \left(\|D\| \|\xi\| + \|d(t, \hat{e}, q)\| \|\eta\| \right). \quad (5.27)$$

One can verify that there exist $\beta > 1$ and $l > 0$ such that for all $\|\hat{e}_\nu\| \geq l$, the partial derivative of V satisfies

$$\begin{aligned} \left\| \frac{\partial V}{\partial \hat{e}} \right\| &\leq \sqrt{(k_1 + k_w)^2 + \|\hat{e}_\nu\|^2} \\ &\leq \beta \|\hat{e}_\nu\|. \end{aligned} \quad (5.28)$$

Due to the convergence properties of the ξ - and η -dynamics, we know that there exists a time moment $t_1 \geq t_0$ at which $\|\xi\| < \frac{k_2}{2\beta\|D\|}$ and $\|\eta\| < \frac{k_2}{2\beta d_{\max}}$ such that for sufficiently large $\|\hat{e}_\nu\|$ we have $\dot{V} \leq 0$. Since this holds for all initial \hat{e} , ξ and η , the solutions remain globally uniformly bounded (globally with respect to \hat{e} , ξ and η). Assumption A4 is then satisfied and as a result the cascaded subsystem (5.22b)–(5.22d) is GUAS.

Solutions of (5.22) are uniformly bounded, and due to the system (5.22a) being input-to-state stable (ISS) with respect to \hat{e} we immediately conclude that the complete system is uniformly asymptotically stable for all $\|q(t_0)\| < \sqrt{1 + \left(\frac{k_w+1}{k_z}\right)^2}$, all $\hat{e}(t_0), \xi(t_0) \in \mathbb{R}^6$ and all $\eta(t_0) \in D_1$. As a direct corollary from the state transformation (5.19) the estimated errors \hat{e} uniformly asymptotically converge to zero. Convergence of the observer error ξ then implies that $\hat{e} \rightarrow e$ and therefore e uniformly asymptotically converges to zero. The result holds globally with respect to the tracking errors e , observer errors ξ and almost all attitude errors η . This completes the proof. \square

5.4 Observer Extension

In the previous sections it has been assumed that the attitude and position measurements are continuously available from the sensors. In practice this is not the case as the signals are sampled and possibly delayed due to software or hardware limitations. In this section we propose an extension of the designed observers concerning sampled position measurements.

5.4.1 Sampled Measurements

The position of a quadrotor is mostly determined by means of cameras, which sample images at a certain rate. The position measurements are therefore available at each sampling time

$t_k, k \in \mathbb{N}$. Under this consideration, the output of the translational system description (5.1) can be reformulated as

$$y(t_k) = Ce(t_k) \quad (5.29)$$

where $e(t_k) \in \mathbb{R}^6$. Intuitively, the sampled position measurements could be used in the observer (5.5) in a zero-order-hold (ZOH) fashion, i.e the signal $y(t)$ in the innovation term of the observer is kept constant for $t \in [t_k, t_{k+1})$. Such an approach, however, could result in largely non-smooth state estimates, particularly in the case of small sampling rates or packet transmission losses. Inspired by the work on high-gain continuous-discrete observers for nonlinear systems [62–64], it is proposed to smoothen the state estimates to some extent by estimating the system output based on the expected system behaviour, within a time-period where no new output is available, i.e. $t \in (t_k, t_{k+1})$. The previously proposed observer is then extended as follows

$$\dot{\hat{e}}(t) = A(t)\hat{e}(t) + Bu(t) + L_p(\varphi(t) - \hat{y}(t)) - By_I(t) \quad (5.30a)$$

$$\dot{y}_I(t) = -S(\omega_r(t))y_I(t) - L_I(\varphi(t) - \hat{y}(t)) \quad (5.30b)$$

$$\hat{y}(t) = C\hat{e}(t), \quad (5.30c)$$

where $\varphi(t)$ is the prediction of the system output, which is continuous in the interval $t \in (t_k, t_{k+1})$ and is updated with the available output at time t_k . We define the output predictor as a hybrid system of the form

$$\begin{cases} \dot{\varphi}(t) = -S(\omega_r(t))\hat{e}_\rho(t) + \hat{e}_\nu(t) \\ \varphi(t_k^+) = y(t_k) \end{cases} \quad (5.31)$$

By analyzing the observer behaviour, it follows that the estimated states globally uniformly exponentially converge to the actual states provided the maximum sampling interval $t_{k+1} - t_k$ remains within a certain bound. A formal proof of this claim is given in Appendix A.

Note that an advantage of this structure is that the inter sample predictor is re-initialized at every measurement update, whereas the observer dynamics are only initialized once at $t = t_0$. This results in the (numeric) solutions of (5.30) to be continuous (non-smooth) over the complete time interval.

5.5 Attitude Reconstruction

An essential element for tracking control which has not yet been considered, is reconstructing the quadrotor's attitude. Previously, it has been assumed that R and ω are directly available for control, whereas in practice these states have to be reconstructed from the available measurements. A commonly used method for attitude reconstruction is based on the accelerometer, magnetometer and gyroscopic measurements [65]. In order to see the usefulness of these sensor outputs, we define the following sensor output description in the absence of noise and bias

$$S_a = R^\top (\ddot{p} + ge_3) \quad (5.32)$$

$$S_m = R^\top m_{\mathcal{I}} \quad (5.33)$$

$$S_\omega = \omega, \quad (5.34)$$

in which S_a , S_m and S_ω represent the accelerometer, magnetometer and gyroscopic output respectively. Moreover, g and $m_{\mathcal{I}}$ are the gravitational acceleration and the earth's magnetic

field vector, expressed in an inertial frame of reference. It is assumed that these quantities are constant and known. If the quadrotor is subject to small accelerations such that $\ddot{\rho} \approx 0$, (e.g. hovering) and small magnetic field disturbances, the absolute attitude information provided by (5.32) and (5.33) is apparent. In addition, it is clear that the gyroscopes directly provide the angular velocity. Using the (possibly noisy and disturbed) measurements in combination with a standard linear Kalman filter algorithm, estimates of the body fixed gravitational accelerations and magnetic field vector can be obtained. These are subsequently used to determine the quadrotor's roll, pitch and yaw angles. A direct disadvantage of this method is the restrictive usefulness when the quadrotor is subject to high accelerations or large magnetic disturbances. In this case S_a and S_m do not provide correct attitude information. In order to overcome this issue, a decisive algorithm has been proposed in [65], which determines if the measurements are reliable by comparing the norm of the sensor outputs with the expected values. As a result, only the low-frequency components of the accelerometer and magnetometer data is used, and are complemented by the high-frequency parts of the gyroscopes. The method is schematically illustrated in Figure 5.1. Here, we have furthermore augmented this method with the heading angle of the quadrotor, obtained by means of an external camera. Note that the sensors possibly have distinct sampling rates. The decisive algorithm can somewhat compensate for this effect by relying more on the most recently updated signals.

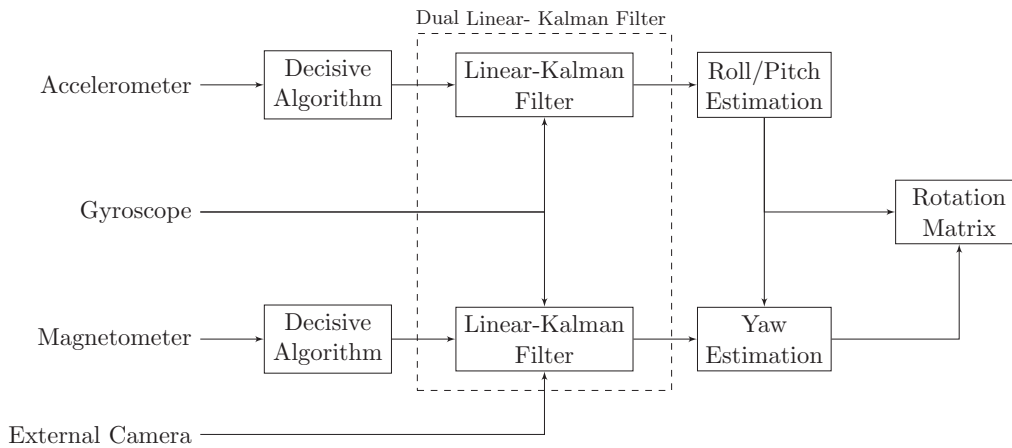


Figure 5.1: Schematic illustration of the dual-linear Kalman filter in which accelerometer and magnetometer measurements are integrated with the gyroscopic measurements. Moreover, the sensor data is augmented with the heading angle determined from external camera measurements. The decisive algorithm determines whether to use or disregard the accelerometer and magnetometer data.

The effectiveness of this method has been shown repeatedly in experiments [65] and we adopt it for our numerical simulations and experiments as is discussed in Chapter 6. For reasons of completeness, the complete attitude reconstruction algorithm is presented in Appendix B.

Remark 5.5.1. Various other attitude observers have been proposed in literature from which the structure presented in [11] is worth mentioning here since it is based on the sensor data

provided by the IMU of a Parrot AR Drone:

$$\dot{\hat{R}} = \hat{R}S(\omega_m) - S(\alpha) \quad (5.35)$$

$$\alpha = \frac{k_g}{g^2} \left(\left(\hat{R}^\top B_f \right) \times a_m \right) + \frac{k_m}{\|m_{\mathcal{I}}\|} \left(\left(\hat{R}^\top m_{\mathcal{I}} \right) \times m_m \right), \quad (5.36)$$

in which $k_g, k_m > 0$. It is claimed that for almost all initial conditions, the attitude estimate \hat{R} exponentially converges to R . It is furthermore proposed to tune the observer gains k_g and k_m online in a similar manner as is done in the previously described decisive algorithm. Using this observer structure in combination with the proposed continuous-discrete translational observer (5.30), it is expected that the GUAS property of the closed-loop system is preserved due to the exponential convergence properties of the attitude observer. Correct attitude estimation is crucial for good tracking performance, since the horizontal motion of a quadrotor relies heavily on its orientation. Further analysis and improvement of attitude observers is therefore a useful and interesting topic for further research.

5.6 Concluding Remarks

In this chapter the output feedback tracking control problem for a quadrotor has been considered. Here, with the aim for a practical implementation, it has been assumed that the body-fixed velocities of the quadrotor are unavailable from measurements limiting the use of the previously proposed full state feedback controller. In order to overcome this issue, a full state linear observer has been proposed. The design has been complemented with an integrating term such that robustness with respect to constant or slowly time-varying disturbances can be guaranteed to some extent. By means of standard Lyapunov techniques, it has been shown that the observer error globally uniformly exponentially converges to zero.

The dynamic output feedback controller is based on the previously proposed full state feedback controller, in which the estimated states are generated by the proportional integral observer. Adopting a similar approach for the corresponding attitude tracking as in the state-feedback case, it has been shown by means of cascade stability theory that the solutions of the complete closed-loop system asymptotically converge to the origin for all initial times, and almost all initial conditions with the exception of a nowhere dense set. This result corresponds to the state-feedback case.

In practice, the measurements used for driving the observer dynamics are sampled and possibly delayed due to hardware limitations. In order to improve the state estimates, it is proposed to extend the proportional integral observer with an inter sample predictor which predicts the system output within a sampling interval, based on the expected behaviour. It has been shown that the estimated states exponentially converge to the actual states provided the sampling interval remains bounded.

As a final note, we have briefly discussed the algorithms that are used for correct attitude estimation, based on the measurements provided by the IMU. The effectiveness of these algorithms in combination with the proposed output feedback controller is shown through a numerical and experimental analysis in Chapter 6.

Chapter 6

Simulations and Experiments

The dynamics and control of a quadrotor have previously been considered within a theoretical framework. In this chapter, a transition from theory to practice is made as the designed cascaded output feedback controller is implemented in a simulation environment, and subsequently embedded within the commercially available Parrot AR Drone 2.0. The combination of simulation and experimental results can provide valuable insight for further developments. This part of the presented work has been done in collaboration with colleague student N.L.M Jeurgens and is organized as follows. First a simulation study is done with the main objective to analyze the closed-loop system behaviour when the controller is discretized, and in the presence of sensor noise and model uncertainties. Hereto, the numerical model developed in [66] is used. Since the sensory behaviour and actuator dynamics of a Parrot AR Drone are included in this model, it provides a realistic simulation environment. We start this chapter with a brief description of the model in Section 6.1. Next, in Section 6.2 the results from several numerical experiments are presented and discussed accordingly. In the second part of this chapter the performance of the controller is studied in a real-world quadrotor application. In Section 6.3 we discuss the experimental setup, whereas in Section 6.4 the results from several experiments in which it is desired for the drone to track a certain trajectory are considered. We finish this chapter with some concluding remarks in Section 6.5.

6.1 Numerical Model

In this section the key structure and the fundamental elements of the model used for simulating the closed-loop response of a Parrot AR Drone are briefly presented. The general model structure is illustrated in Figure 6.1 and implemented within a SIMULINK environment.

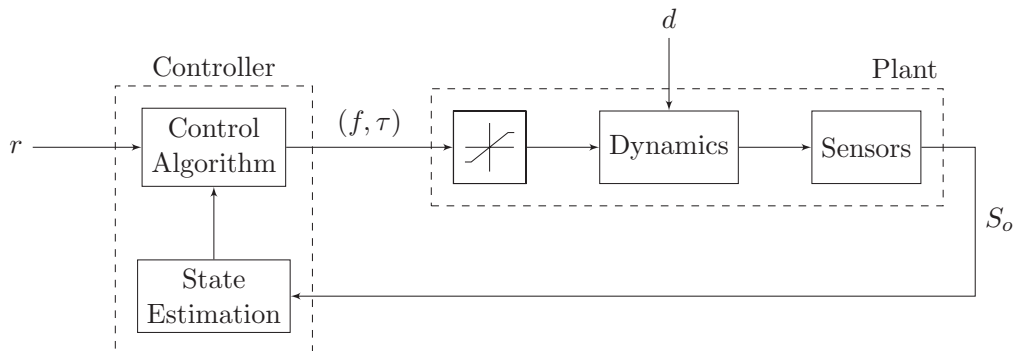


Figure 6.1: General outline of the closed-loop model structure implemented in a SIMULINK environment. Here, r , d and S_o represent the reference trajectory, external disturbances and measurement output respectively.

For simulation purposes, the mathematical system description (3.13) as derived in Chapter 3 is used. Here, the gyroscopic effects of the rotors τ_d are linearly added to the right-hand side of the rotational dynamics (3.13d) as an additional disturbance d . The gyroscopic effect of the rotors is modeled as [11]

$$\tau_d = -J_r S(\omega) b_3 \sum_{i=1}^4 \Omega_i, \quad (6.1)$$

in which J_r is the moment of inertia of a rotor, and Ω_i is the individual rotor speed. Since the motion of a quadrotor is heavily dependent on its orientation, it is expected that each disturbance in this subsystem might affect the closed-loop response. The disturbed dynamics are implemented in the plant structure.

6.1.1 Sensors

In practice, the states of a quadrotor are not continuously available for control since information is obtained in a discretized manner. Moreover, the measurement data might be biased and corrupted by sensor noise. In order to be able to analyze the robustness of the controller in the absence of perfect state measurements, the sensory behaviour has been incorporated into the model. As is discussed in the experimental setup in more detail, the Parrot AR Drone 2.0 is equipped with an inertial measurement unit (IMU) which consists of an accelerometer, magnetometer and gyroscope. Furthermore, an ultrasound sensor is available. In [66, 67] the sensory behaviour and corresponding noise characteristics have been determined by means of extensive experiments. According to this work, the output of the IMU can be modeled as

$$S_a = 4 \text{ round} \left(\frac{128}{g} R^\top (\ddot{p} + g e_3) + \mathcal{N}(t, \sigma_a) \right) \quad (6.2)$$

$$S_m = \text{round} \left(R^\top B_m \frac{\sqrt{1.35 \cdot 10^4}}{\|B_m\|} + \mathcal{N}(t, \sigma_m) \right) \quad (6.3)$$

$$S_\omega = \text{round} \left(\omega \frac{180}{\pi} \frac{2^{16}}{4000} + \mathcal{N}(t, \sigma_\omega) \right) \quad (6.4)$$

in which g is the gravitational acceleration and B_m the geomagnetic field vector as calculated by MATLAB's function `wrldmagm.m()`. Moreover, $\mathcal{N}(\sigma_k) \in \mathbb{R}^3$ with k the corresponding sensor index denotes measurement noise which is modeled as a normally distributed random signal with standard deviations $\sigma_k \in \mathbb{R}^3$. The additional factors result from the necessary conversion of sensor inputs to outputs with physical resemblance. The output of the ultrasound is modeled as

$$S_z = \text{round} (z + \mathcal{N}(t, \sigma_z)). \quad (6.5)$$

The IMU signals (6.2)-(6.4) are sampled at 400 Hz whereas the output of the ultrasound (6.5) is sampled at 25 Hz. These rates are in accordance with the actual sampling rates on the AR Drone. Regarding the experimental setup as is described in more detail in Section 6.3, we consider modeling an external camera for horizontal position detection. Hereto, the xy -position obtained from the dynamic model description is sampled at 30 Hz and delayed by 0.1 seconds. We assume very low noise levels, such that noise is omitted from the camera model. The delay is introduced in the system due to an image processing algorithm. For a more extensive elaboration of the sensor dynamics and output descriptions, we refer to [66, 67].

The sensor outputs are subsequently used for state reconstruction. The output of the external camera and ultrasound are used for position and velocity estimation. Whereas previously it has been assumed that all position measurements are available at similar time-instances, as is clear from the sensor models, the horizontal position and altitude are sampled at different rates. In order to be able to use all measurement data in the observer, an update mechanism is therefore implemented as follows: each time a change in measurement data is detected, a trigger state is updated from 0 to either 1, 2 or 3. Here, 1 corresponds to an update in xy , 2 corresponds to an update in z and 3 corresponds to an update in all position measurements. Based on the trigger state, the vector of position measurements is updated. The outputs of the inertial measurement unit are used for attitude reconstruction. The observer and controller algorithms have been extensively discussed in chapters 4 and 5 and are implemented within the controller block. Due to the fact that in practice the speed of each rotor is limited, the generated thrusts are also limited. As a result, the admissible input thrust f and torque τ are bounded. This physical limitation is embedded within the numerical model in the following manner. First, the calculated thrust and torque are converted to the corresponding individual rotor speeds by means of the motor matrix relation (3.12). Subsequently, a conversion from rotor speeds to pulse width modulation (PWM) signals is made [66]. The PWM signals are confined to range between 0 and 100. The signals are converted back to f and τ , which are then indirectly saturated and used as an input to the system dynamics.

6.1.2 System Parameters

The relevant parameters used for simulations are listed in Table 6.1. These parameters have been experimentally determined in [67]. In order to introduce deviations in the system's parameters, we add a discrepancy of 5 percent between the actual mass of the quadrotor m and the expected mass m_r . The remaining parameters are assumed to be perfectly known. Since all on-board processes of the Parrot AR Drone 2.0 run at a rate of 400 Hz, the simulation model is executed with a sampling time of 1/400 seconds. For a more detailed discussion about the numerical model, software and implementation practicalities, a reference is made to [66].

Table 6.1: Relevant parameter values used for simulations.

Parameter	Description	Value	Unit
m	Actual mass	0.4560	kg
m_r	Expected mass	0.4800	kg
J_x	Moment of inertia around x -axis	0.0022	kg m ²
J_y	Moment of inertia around y -axis	0.0025	kg m ²
J_z	Moment of inertia around z -axis	0.0045	kg m ²
J_r	Inertia of the rotor	$2.2 \cdot 10^{-5}$	kg m ²
g	Gravitational acceleration	9.81	ms ⁻²

6.2 Simulation Results

In this section, a number of simulation studies are performed and the results are presented accordingly. The main purpose of these simulations is as follows. Although it has been shown that the controller is able to stabilize a quadrotor in continuous time with no specific assumptions

made on the physical limits of the rotors, it is not guaranteed that the stabilizing properties are preserved if the control law is implemented within a discretized environment and the input thrust and torques are limited. Furthermore, the addition of external disturbances, measurement noise and time-delays might significantly affect the closed-loop behaviour. Using the previously described numerical model which provides a rather realistic simulation environment, the performance of the control law in the presence of the discussed effects can be analyzed. In addition, since the integrating action has been implemented in the control structure in a relatively unconventional manner, the effectiveness of this approach is illustrated through a numerical experiment. Due to the fact that the GUAS-property of the theoretical closed-loop system (see Proposition 5.3.1) gives rise to some robustness and since the sampling rate appears to be relatively large, it is expected that in the absence of perfect measurements, the closed-loop system is practically stable, that is, the tracking errors converge to some region near the origin. We expect that in the case of delayed measurements, this region is larger than without time-delay.

For all numerical experiments, it is chosen to let the quadrotor track a three-dimensional circular trajectory parametrized as

$$\rho_r(t) = [\cos(t) \quad \sin(t) \quad 1.5 + \sin(t)]^\top. \quad (6.6)$$

The remaining reference states are generated according to (4.1). Hereto, we first transform the translational dynamics (4.1a)–(4.1b) from the tracking reference frame to the inertial frame of reference. The reference input thrust $f_r(t)$ can then be calculated as

$$f_r(t) = m_r \sqrt{\ddot{x}_r(t)^2 + \ddot{y}_r(t)^2 + (\ddot{z}_r(t) + g)^2}, \quad (6.7)$$

in which $\ddot{x}_r(t)$, $\ddot{y}_r(t)$ and $\ddot{z}_r(t)$ are the second order derivatives of the respective components of $\rho_r(t)$. It is worth remarking here that if we confine $\ddot{z}_r(t) > -g$, it follows that $f_r(t) > 0$ and is always defined (conform the previous assumption that $0 < f_{\min} \leq f_r(t)$). Furthermore, note that due to the dynamic constraints, the last column of R_r must necessarily satisfy

$$R_r B_f = f_r(t)^{-1} m_r (\ddot{\rho}_r(t) + g B_f), \quad (6.8)$$

where $B_f = [0, 0, 1]^\top$. Using this result and a similar approach as in Section 4.3, the remaining columns of R_r are then calculated based on the properties of rotation matrices. By means of (numerical) differentiation, \dot{R}_r is determined which is used in combination with the attitude kinematics (4.1c) for calculating $\omega_r(t)$. The reference torque $\tau_r(t)$ can then be calculated by differentiating $\omega_r(t)$. From the position kinematics (4.1a) the body-fixed reference velocity ν_r is calculated. The complete set of relevant reference states $(\rho_r(t), \nu_r(t), R_r(t), \omega_r(t), f_r(t), \tau_r(t))$ is then obtained.

6.2.1 Control Parameters

The control parameters used for simulations are shown in Table 6.2. These parameters are determined in an iterative manner and are chosen such that condition (4.34) is satisfied.

Table 6.2: Control parameters used in simulations.

Parameter	Description	Value
k_w	Integral gain	0.4
k_z	Integral gain	1
n	Saturation level	2
k_1	Position gain	3
k_2	Velocity gain	2
c_1	Attitude gain	70
c_2	Attitude gain	30

Regarding the observer parameter tuning we use an LQR approach as a starting point. Hereto, we consider the observer error-dynamics (5.6) with $\omega_r(t) = 0$. Using a standard Linear Quadratic Regulator (LQR) optimization approach, the optimal observer gain matrix is determined as

$$\bar{L} = P\bar{C}^\top \bar{R}^{-1}, \quad (6.9)$$

in which P is a solution to the observer algebraic Riccati equation (ARE)

$$A_\xi P + PA_\xi^\top + Q - P\bar{C}^\top \bar{R}^{-1} \bar{C}P = 0 \quad (6.10)$$

and the positive definite weight matrices

$$\bar{Q} = \begin{bmatrix} 10I & 0 & 0 \\ 0 & 20I & 0 \\ 0 & 0 & 5I \end{bmatrix} \in \mathbb{R}^{9 \times 9} \quad \text{and} \quad \bar{R} = \bar{r}I \in \mathbb{R}^{3 \times 3}. \quad (6.11)$$

Here, \bar{r} is chosen as $\bar{r} = 0.05$. Using MATLAB's LQR command `lqr(A_ξ^\top , \bar{C}^\top , \bar{Q} , \bar{R})` we arrive at the (optimal) observer gains which are subsequently fine-tuned and listed in Table 6.3.

Table 6.3: Observer parameters used in simulations.

Parameter	Description	Value
l_1	Observer gain	15
l_2	Observer gain	30
l_3	Observer gain	10

The initial conditions for all experiments are set to

$$\rho(t_0) = [-0.5, 0, 0]^\top, \quad \nu(t_0) = [0, 0, 0]^\top, \quad R(t_0) = I \quad \text{and} \quad \omega(t_0) = [0, 0, 0]^\top.$$

The simulation results are presented in figures 6.2 to 6.5. Note that figure 6.2 additionally presents the results of a simulation in which no integral action is added to the control structure (i.e. $k_w = 0$, $k_z = 0$ and $q(t_0) = 0$). It is furthermore chosen to complement these results with an illustration of the Euclidean-norm of the position error, as shown in Figure 6.3. This quantity provides a certain measure for comparing the system's performance with and without integrating action.

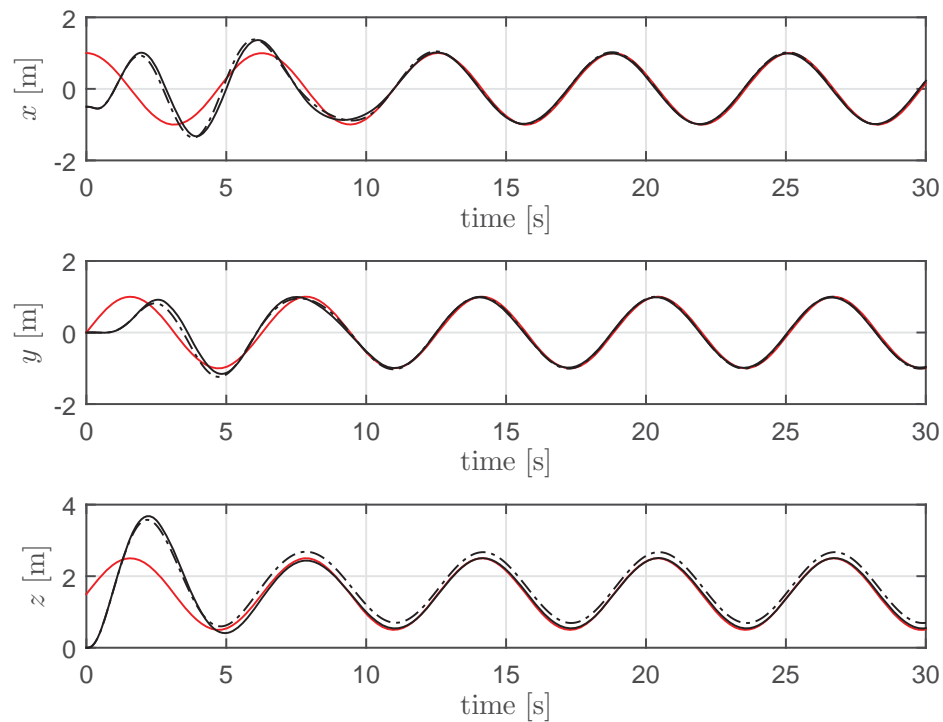


Figure 6.2: Position $\rho(t)$ without integral control (dashed), with integral control (black) and reference position $\rho_r(t)$ (red).

The effect of the integrating action immediately follows from the altitude z in Figure 6.2. In case no integral action is added to the controller, the quadrotor consistently remains at a larger altitude than desired. This results from the fact that since it is assumed that the quadrotor is heavier than in reality, an excessive reference thrust is generated by the system. The increase in tracking performance can additionally be observed from the error norm in Figure 6.3. Here, we see that the steady state error is reduced if integral control is added.

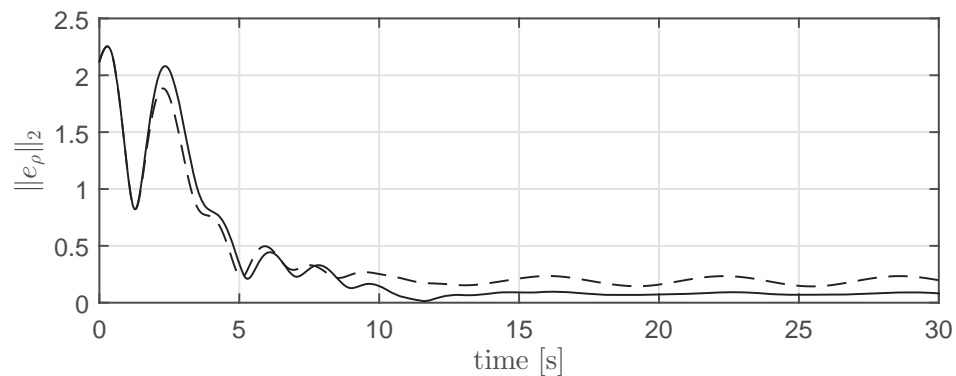


Figure 6.3: Norm of the position error $e_\rho = R_r^\top (\rho_r - \rho)$ for the system without integral control (dashed) and with integral control (solid).

Comparing the actual position with the reference position in Figure 6.2 and examining the error norm in Figure 6.3, it is observed that the quadrotor is able to track the reference, however, a certain error remains. It is found that the delayed position measurements are somewhat contributing to this difference between the reference and actual trajectories. As a consequence of the delay, the estimated states converge to the measurements rather than the actual states. This effect is illustrated in Figure 6.4 in which the difference between the actual position and estimations, and the difference between the measured position and the estimations is shown. The control action is therefore somewhat delayed, as it compensates for previous positions. It is expected that in case of fast, aggressive reference trajectories, time-delays have a larger effect on the closed-loop performance than for slow trajectories. These observations motivate the idea to (partially) incorporate the time-delay in the observer. Moreover, one could examine possibilities to reduce the time-delay, for example by adopting a more efficient image processing algorithm.

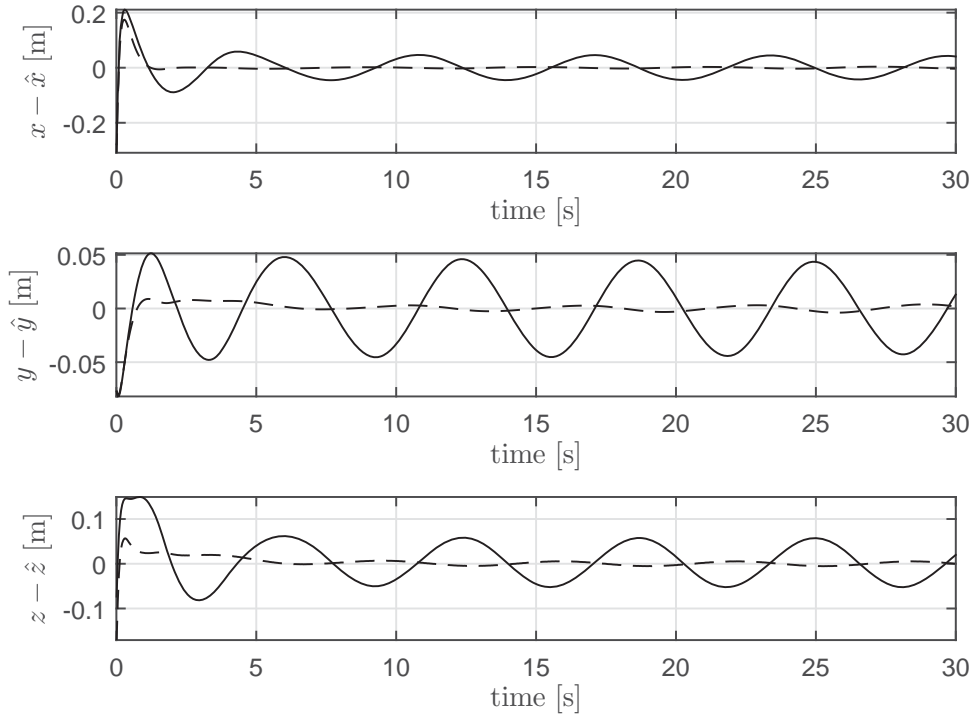


Figure 6.4: Difference between the actual position and estimates (solid) and difference between the measured position and estimates (dashed).

Recall from Chapter 4 that for position tracking it is necessary to align the two normalized vectors $\hat{f} = R_r^\top R B_f$ and $\hat{f}_d = R_d B_f$, which represent the actual and desired thrust vectors of the quadrotor expressed within the tracking reference frame \mathcal{R} . In order to align these vectors, as a control objective it is chosen to let $R_r^\top R$ approach R_d . In Figure 6.5 the attitude $R_r^\top R$ and desired attitude R_d are characterized in terms of roll, pitch and yaw angles and expressed with respect to the tracking frame of reference. From this figure we observe that in the presence of corrupted measurements, the quadrotor is still able to track the attitude

accurately. Furthermore, as expected, the desired attitude is small, since the quadrotor is within a small vicinity of the desired trajectory. Therefore, there is no need for a large angle maneuver to track the position.

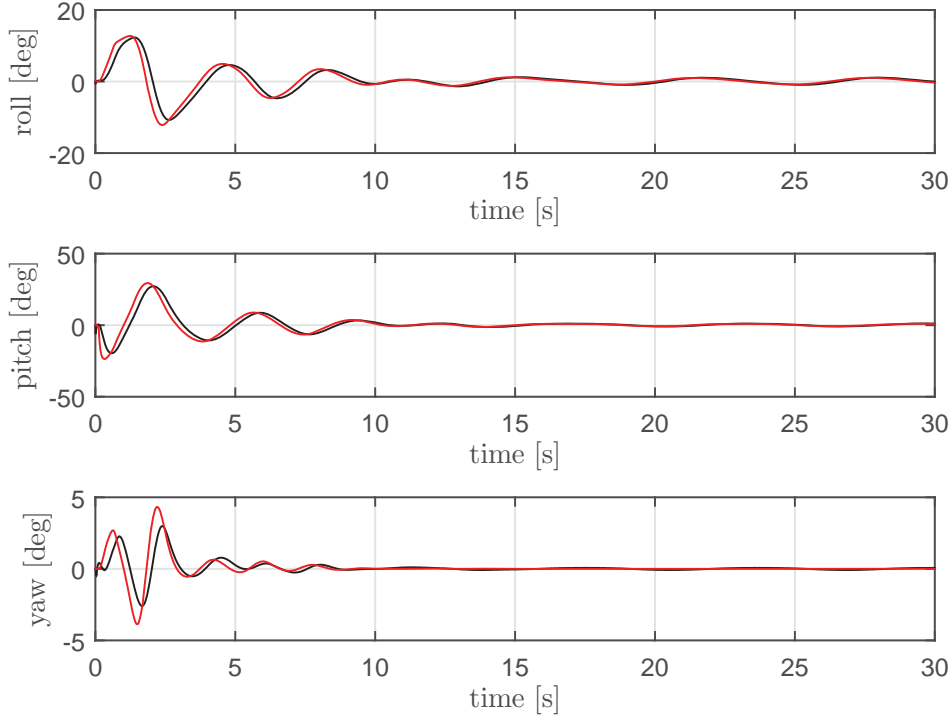


Figure 6.5: Attitude of the quadrotor $R_r^\top R$ (black) and the desired attitude R_d (red), characterized in terms of roll, pitch and yaw angles and expressed with respect to the tracking frame of reference.

The overall simulation results are as expected: in case the system is subject to small constant disturbances (e.g. difference in actual and expected mass) and sampled, delayed and disturbed measurements, the closed-loop stability is maintained and the corresponding tracking errors converge to some region near the origin.

In the next sections, the performance of the output feedback controller is examined within a real-world quadrotor platform. We first discuss the setup used for experiments, and subsequently present the experimental results.

6.3 Experimental Setup

Experiments are performed at the RoboCup soccer field location at Eindhoven University of Technology. In order to perform safe flights, this area has been surrounded by nets such that the quadrotor remains within a confined region. A fixed right-handed frame is defined at the center of the soccer field and serves as the inertial frame of reference.

6.3.1 Hardware

As a test setup we use the commercially available Parrot AR Drone 2.0 which is shown in Figure 6.6. This quadrotor consists of a carbon fiber X-shaped frame to which four rotors are attached and actuated by means of brushless motors. The AR Drone contains an on-board computer that runs a Linux operating system and is capable of self-generating a WiFi hotspot through which it can communicate with any supporting client device (e.g. smartphone or laptop). The system is powered by a lithium polymer battery pack and provides approximately twelve minutes of flight time.



Figure 6.6: Parrot AR Drone 2.0 with protective hull and LED identifiers.

The quadrotor is equipped with the following low-cost sensors [67, 68]:

- **Three-axis accelerometer:** measures the body-fixed linear accelerations with ± 50 mg precision;
- **Three-axis magnetometer:** measures the components of the earth's magnetic field vector, with respect to the body-fixed frame with a precision of 6° ;
- **Three-axis gyroscope:** measures the body-fixed angular accelerations with 2000° /second precision;
- **Ultrasound:** measures the altitude, up to 6 meters;
- **Barometer:** measures the surrounding pressure with a precision of 10 Pa.

The accelerometer, magnetometer and gyroscope constitute the inertial measurement unit which runs at 400 Hz. The ultrasound, however, samples at 25 Hz. In [66] it is found that the sensors in the IMU are temperature dependent. In order to provide correct state measurements, this temperature dependency is compensated for (see [66]).

In addition to the sensors, the quadrotor contains two internal HD cameras: a front-facing camera (30 frames per second), and a down-facing camera (60 frames per second). Although the internal cameras can potentially be used for position detection, the horizontal position of the quadrotor is determined by means of the external Prosilica GE1900 camera. This high-resolution

camera is located above the RoboCup soccer field and covers an area of approximately 11×7.5 m². Images are sampled at a rate of 30 frames per second. The camera communicates through a Gigabit Ethernet connection with a laptop, on which raw snapshot data is retrieved by means of the GigE vision toolbox in MATLAB. A LED-strip, visible to the camera, is attached to the protective hull of the quadrotor as is also shown in Figure 6.6. In [29] an image processing algorithm has been developed, which extracts the horizontal position and yaw-angle relative to the earth-fixed reference frame from the camera image. This information is subsequently sent from the laptop to the quadrotor via a UDP connection. The position detection method is discussed in more detail in [29]. A second laptop on which a graphical user interface (GUI) runs within a SIMULINK environment, connects to the quadrotor through a WiFi channel. By means of the GUI, the control parameters can be conveniently adjusted on-line, and supervisory commands that overrule all local control processes can be transmitted to the quadrotor.

6.3.2 Local Control Structure

For reasons of efficiency, all processes of state estimation and control run locally on the quadrotor. Hereto, a SIMULINK model is compiled and build into binary code, which is uploaded to the Parrot AR Drone. The particular local structure is shown in Figure 6.7.

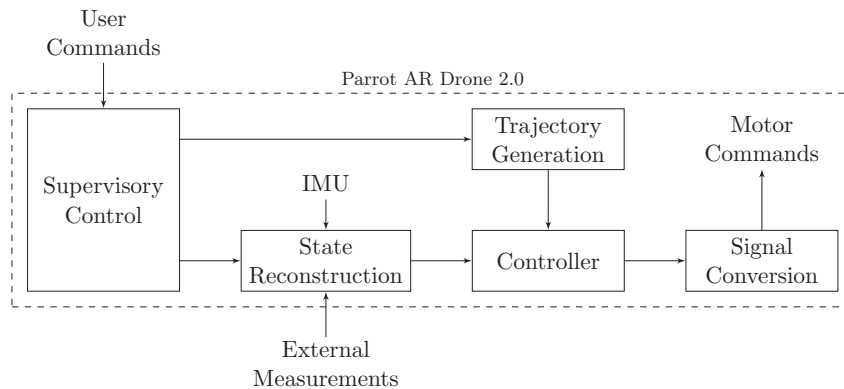


Figure 6.7: Schematic overview of the local control structure embedded within the Parrot AR Drone 2.0.

In addition to the tracking controller, a supervisory controller is added to the structure which serves the purpose to ensure safe flights and proper functioning of the quadrotor [66]. This controller has the structure of a finite-state automaton in which the states and transition conditions are predefined, and is schematically illustrated in Figure 6.8.

After uploading the compiled model to the Parrot AR Drone, we enter the state *Initialise*. We remain within this idle state for a predefined amount of time such that a self-calibrating procedure can be executed. Here, the sensor values (e.g. gyroscopic output) are averaged, and extracted from the measurements such that possible bias can be reduced. After this specific time, the state switches to *Wait* and remains there until a start command is provided. If the battery can supply sufficient voltage, we then continue to the state *Lift-Off* which lets the quadrotor vertically take off to a predefined height. If the altitude has been reached, the

supervisory control state switches to *Flight*, in which the output feedback tracking controller is used for letting the quadrotor track a desired trajectory.

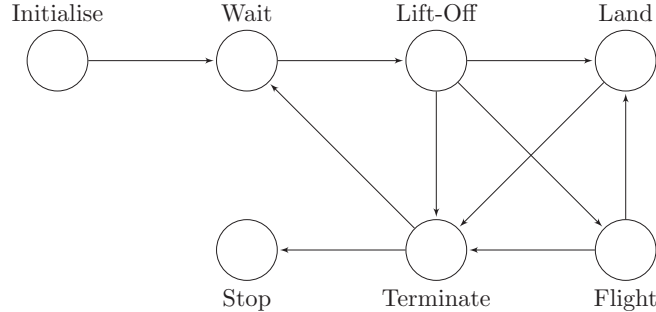


Figure 6.8: Supervisory control structure.

In this mode, it is possible to provide an external command for switching between different trajectories. If the user demands the quadrotor to land, the state continues to *Land*, in which the altitude is gradually decreased. Note that the supervisory controller also enters this state if during lift-off or flight mode the battery is unable to supply sufficient voltage. If the quadrotor has landed successfully, the state reaches *Terminate* and the motors are disarmed. The *Terminate* state can be reached from any other flight operating state, and acts as an emergency stop. If unsafe situations occur, for example, when the rotors are blocked by some object, the state switches to *Terminate* and all processes are aborted.

6.4 Experimental Flights

In this section the results from various experimental flights are presented. In order to solve all problems regarding software and implementation, and to verify proper functioning of the sensors and hardware, we initially consider a simple trajectory in which it is desired to let the quadrotor hover above the center of the RoboCup soccer field, at a height of 1 meter. During the hovering experiments, similar control parameters are used as in Table 6.2 with the exception of the integral gains that are set to $k_w = 0.3$ and $k_z = 0.3$. The results are presented in figures 6.9 and 6.10. From the position measurements in Figure 6.9 it can be seen that the Parrot AR Drone is able to reach the desired position through a stable maneuver. Overshoot is limited and the quadrotor settles after approximately 20 seconds and slightly oscillates around the desired point. The oscillations result from small deviations in the quadrotor's estimated orientation (\hat{R}) and desired orientation (R_d) as can be seen in Figure 6.10. Note that in case of hovering $R_r = I$ such that the roll, pitch and yaw angles can be considered with respect to the inertial frame of reference. Moreover, the desired attitude has been calculated retroactively. It is remarkable that the desired and measured pitch angle of the quadrotor remain positive, whereas it is expected that these angles oscillate around zero. This difference might be caused by a misalignment of the sensors or propellers, such that a constant disturbance acts in the horizontal position. The position integral controller compensates for this and as a result, a small angle is necessary to prevent drift. Furthermore, note the small deviation from zero in the yaw angle. For position control, it is understood that this angle is irrelevant and therefore a small error does not have a significant effect.

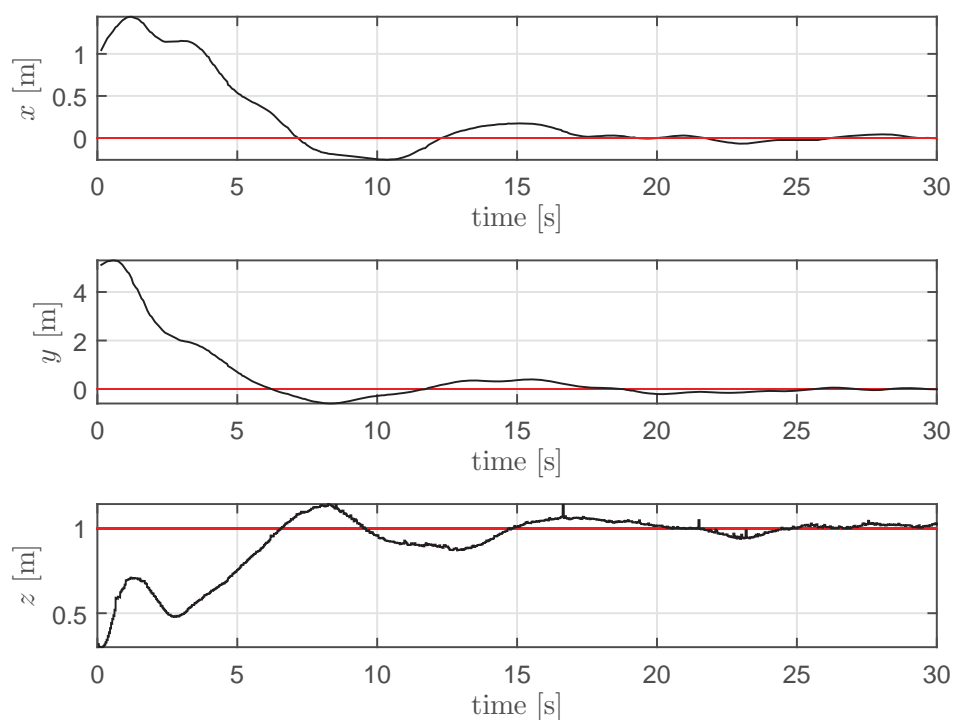


Figure 6.9: Measured position $\rho(t)$ (black) and reference position $\rho_r(t)$ (red) as a function of time.

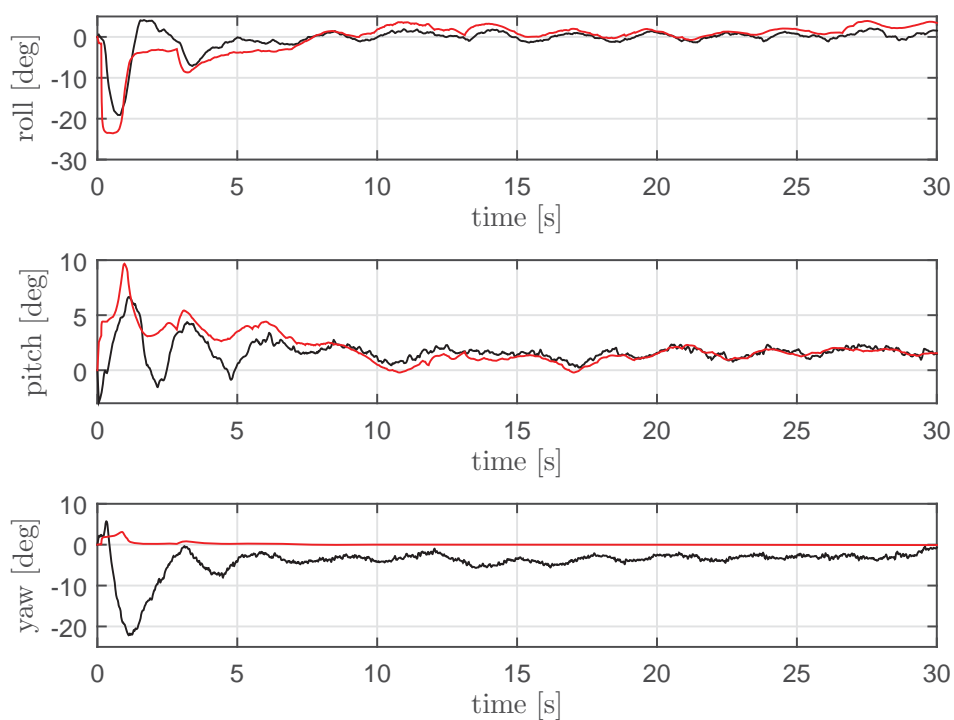


Figure 6.10: Reconstructed attitude $R_r^T \hat{R}$ (black) and desired orientation R_d (red) characterized in terms of roll, pitch and yaw angles and expressed with respect to the tracking frame of reference.

During experiments at the RoboCup soccer field it is found that the magnetometer is heavily biased by external magnetic fields, which might be caused by iron elements in the floor. We have therefore chosen to discard the magnetometer for attitude determination in subsequent experiments, such that we rely more on the gyroscopes and external camera for reconstructing the attitude of the quadrotor.

6.4.1 Circular Reference Trajectory

Since the hovering trajectory is time-invariant (constant), the control action and tracking error dynamics are not explicitly dependent on time. In order to verify the effectiveness of the controller in case it is desired to track more aggressive, time-varying maneuvers, an experiment is performed in which it is desired for the Parrot AR Drone to track a three-dimensional circular reference trajectory. This trajectory is parametrized as

$$\rho_r(t) = [\cos(t) \quad \sin(t) \quad 1.5 + \sin(t)]^T. \quad (6.12)$$

The control parameters used for the experiments are similar as presented in Table 6.2 with the exception of the integral gains, which are set to $k_w = 0.03$ and $k_z = 1$. Note the difference with the choice for integral gains in the hovering experiment. It appears that a larger integral action results in a more oscillatory response. The resulting flight trajectory is shown in figures 6.11 and 6.12. Note that in these figures, it is chosen for reasons of clarity to use the discretized data as obtained from the camera and altimeter and represent these as a continuous signal.

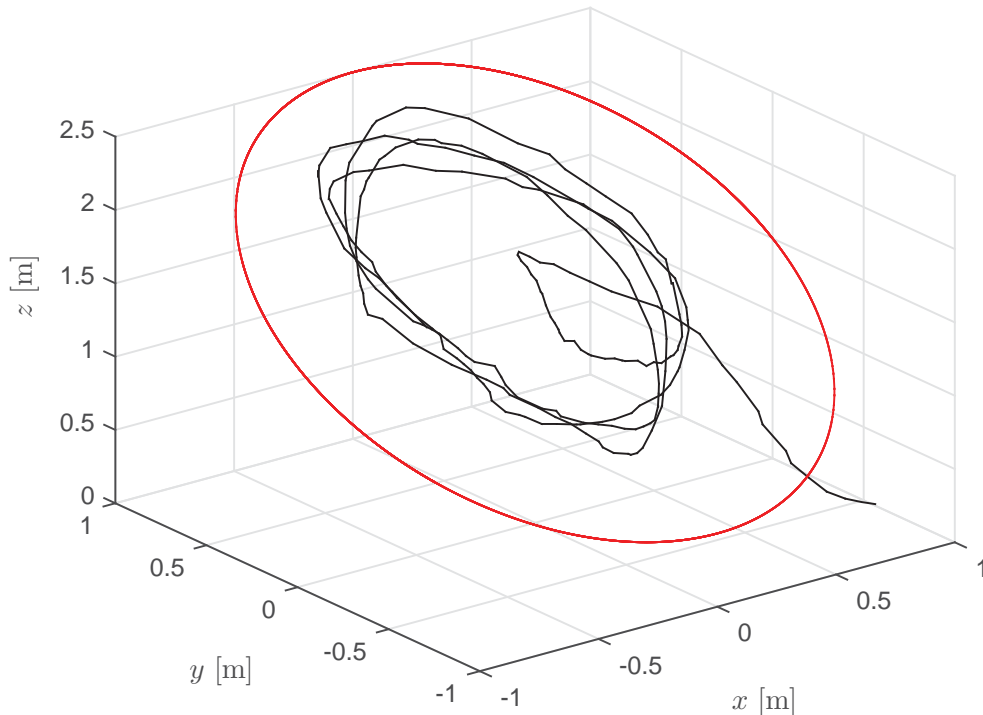


Figure 6.11: Spatial representation of the flight trajectory of the Parrot AR Drone (black) and the reference trajectory (red).

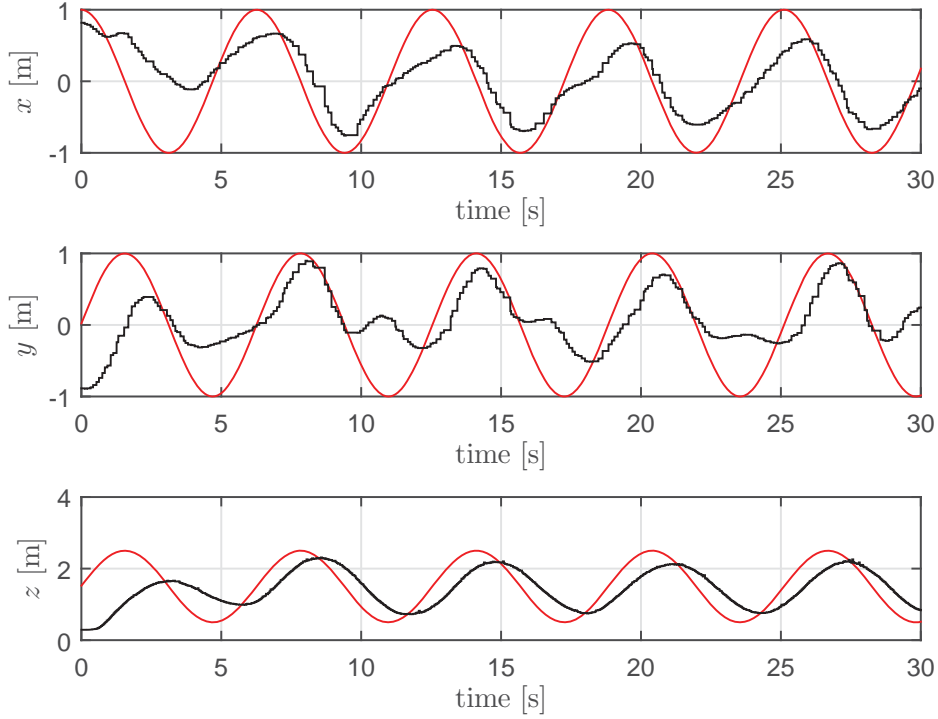


Figure 6.12: Measured position $\rho(t)$ (black) and reference position $\rho_r(t)$ (red) as a function of time.

Two direct observations can be made from the results in Figure 6.12. First, we can conclude that the closed-loop system is able to perform a stable three-dimensional circular maneuver. Second, it can be seen that the quadrotor remains within a significant distance from the reference trajectory, that is, the amplitude of the quadrotor's trajectory remains smaller than desired. Intuitively it can be expected that some form of damping is present within the system. In order to examine this hypothesis, an additional set of numerical experiments is performed where a generalized, motion dependent damping force is added to the dynamics as

$$F_D = -\text{sign}(\nu) \frac{1}{2} \rho_a C_D \nu \circ \nu \quad (6.13)$$

in which ρ_a is the density of air and $C_D = \text{diag}([c_x, c_y, c_z])$ a diagonal matrix consisting of drag coefficients in x , y , and z -directions, respectively. These coefficients are estimated by means of an optimization algorithm in which the difference between simulation and experimental data is minimized through tuning of the drag coefficients. Here, experimental data in which the quadrotor performed some maneuver (e.g. navigation towards a desired hovering location) is used, and the coefficients are found to be $c_x = 2.5$, $c_y = 1.3$, $c_z = 1.3$.

We remark the large difference between c_x and c_y , whereas intuitively it is expected that these coefficients are somewhat similar. As the damping force (6.13) is considered as a generalized disturbance force, other non-modeled dynamics might strongly affect motion in the x -direction. We note that the actual value of the coefficients is not particularly of importance here, as the

addition of F_D is purely to illustrate the influence of unconsidered effects. It is therefore more appropriate to consider the coefficients as weight coefficients. The density of the surrounding air is set to $\rho_a = 1.2 \text{ kg/m}^3$.

In Figure 6.13 we compare the results from a simulation with drag, with the results from the numerical experiments without drag, and the experimental results.

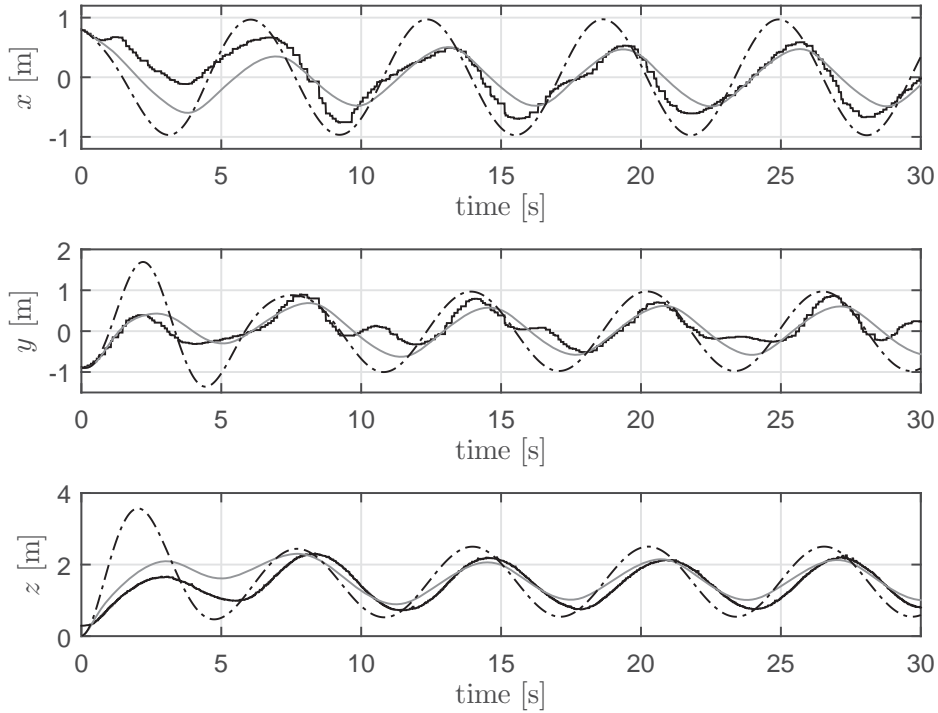


Figure 6.13: Comparison between the experimental results (solid), simulation results without drag (dashed) and simulations with drag (gray).

From this figure it is clear that by adding a generalized drag force to the system, the simulation model resembles the physical system more accurately. The results confirm the expectation: the closed-loop performance is largely affected by the unmodeled, motion dependent dynamics. Such dynamics have a larger contribution in case the quadrotor is subject to faster motion. Therefore, it is recommended to incorporate these effects in the quadrotor's mathematical system description (3.13) and expand the output feedback controller such that damping effects can be compensated for. Hereto, an algorithm could for example be used to estimate the disturbance on-line. A feedforward structure can subsequently be added to the controller to compensate for these effects. It is expected that such an approach can significantly increase the tracking performance. We furthermore remark here that since the damping effect is motion dependent, the tracking performance is ultimately limited by the hardware. If it is desired for the quadrotor to track a very fast trajectory, the damping force might increase with the increasing velocity. The possibility could then occur that the rotors are incapable of generating the necessary thrust for compensating this effect. Since the amplitude of the quadrotor's flight trajectory during the

conducted experiments approximately ranges between 0.5 and -0.5 meters, and the period time is roughly 2π seconds, the velocity in x , y and z -directions can be estimated as 0.5 meters per second. This suggests that the damping force is of order 0.4 Newton, which is well within the physical limits of the thrust.

6.4.2 Additional Effects

So far, only damping effects in the translational motion of the system have been identified as a source for the diminishing tracking performance, however, the motion of the Parrot AR Drone is heavily dependent on its orientation. We therefore examine the attitude behaviour during flight in more detail. In Figure 6.14 the estimated attitude $R_r^\top \hat{R}$ and the desired attitude R_d necessary for position tracking are shown in terms of roll, pitch and yaw angles and considered with respect to the tracking frame of reference \mathcal{R} .

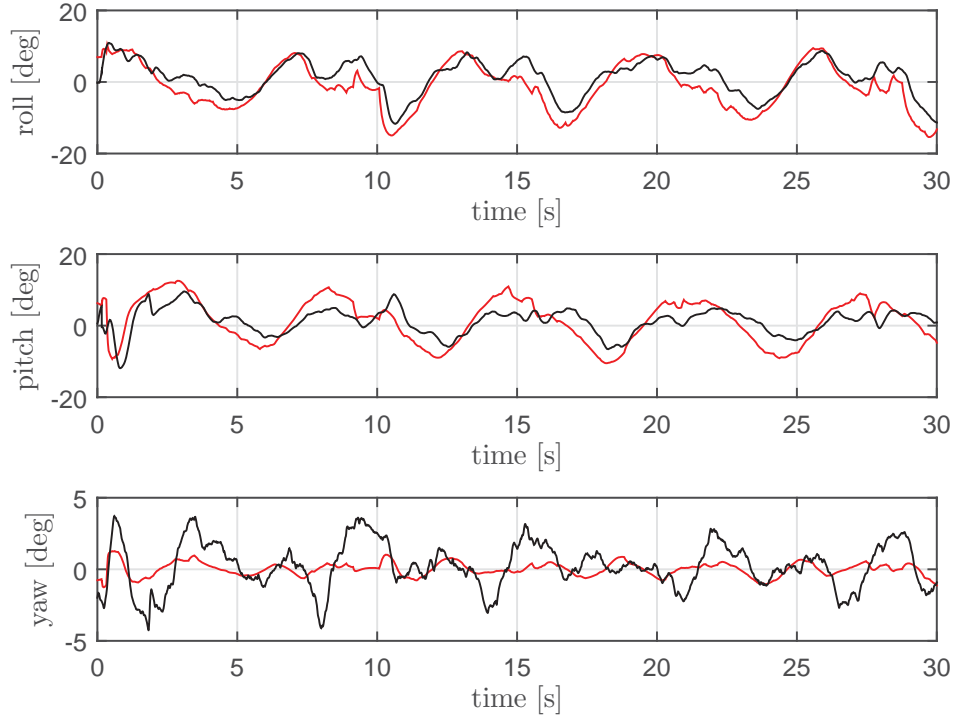


Figure 6.14: Estimated attitude $R_r^\top \hat{R}$ (black) and desired orientation R_d (red) characterized in terms of roll, pitch and yaw angles and expressed with respect to the tracking reference frame.

It can be seen that the attitude follows the desired behaviour to some extent, however, the overall roll and pitch response appear to be suppressed. A possible cause for this effect could be the damping in the attitude subdynamics. Indeed, considering the protective hull of the Parrot AR Drone, which is constructed of lightweight polystyrene foam, it is found that this hull is not rigid, and not rigidly attached to the frame. During high angular accelerations, these properties of the hull might counteract the quadrotor's motion which results in damping. An

other source of rotational damping could be the air resistance during rotational motion, causing an additional drag torque in the system.

We remark that in [66] the motor-rotor behaviour has been measured in case the AR Drone is fixed. During flight in varying airflow, the motor performance might be different than expected, and possibly affects the performance of the Parrot AR Drone.

Although including a generalized drag force into the model improves the accuracy, there are still significant differences visible in Figure 6.13, particularly in the y -direction. It can be seen that in the descending part of the quadrotor's trajectory, the y -displacement somewhat remains constant, i.e., the quadrotor only makes a downward movement. This is possibly caused due to the fact that during the descent, the Parrot AR Drone has to move through the turbulent air generated by the rotors. Such turbulence affects the rotors thrust and torque, making tracking significantly more difficult and consequently losing position accuracy.

6.5 Concluding Remarks

In this chapter, the proposed output feedback controller has been tested in a realistic simulation environment with the aim to verify the closed-loop behaviour in the absence of perfect measurements and unconsidered dynamics. Hereto, a numerical model in which the sensory behaviour, external disturbances and actuator dynamics are incorporated, is used. A simulation has been performed in which it is desired for the quadrotor to track a three dimensional circular reference trajectory. The results show that the closed-loop system remains stable and sufficient tracking performance is achieved. It is furthermore observed that delayed position measurements have some significant effect on the tracking performance in the sense that the estimated states are delayed, resulting in a delayed control action.

The controller has subsequently been implemented within the Parrot AR Drone. In order to validate the usefulness of the available software and hardware, first an experiment is performed in which it is desired for the drone to hover. From the experiments it follows that the controlled quadrotor is capable of hovering within a small vicinity of the desired location. A constant deviation in the pitch angle is observed, which is possibly the result from a misalignment in the rotors. In a second experiment, the Parrot AR Drone is subject to a time-varying, three dimensional circular reference trajectory, similar as in the simulations. From the flight results it is concluded that the drone is able to perform a stable circular maneuver, however, a significant deviation between the quadrotor's position and reference trajectory remains present during flight. The following causes for this diminishing tracking performance are identified.

- During fast motion, it appears that a translational damping effect is becoming more dominant within the system. This effect has been further analyzed in simulations, in which a generalized damping force is modeled as a quadratic function of the quadrotor's velocity, and added to the translational dynamics. It is observed that the simulation results are strongly in accordance with the experimental results.
- As a second source of losing position accuracy, damping within the quadrotor's attitude dynamics is identified. This damping is possibly caused by the protective hull of the Parrot AR drone, which is not a rigid structure and not rigidly attached to the frame. In addition, the air resistance during orientation might introduce a drag torque.

- Several other effects such as turbulence of the surrounding airflow, and decreasing functioning of the motor-rotor structure could contribute to a reduction of the performance.

For future research, it is suggested to add an algorithm for estimating the dominating damping effects on-line, such that these can be compensated for by means of a feedforward structure.

Chapter 7

Conclusions and Recommendations

The use of unmanned aerial vehicles for automating several commercial or logistic processes is an interesting concept. In many of such automated processes it is required for the drone to autonomously track a certain trajectory. For achieving such a task, the design of appropriate tracking controllers is a crucial element. This thesis addresses the tracking control problem for a particular type of unmanned aerial vehicle: the quadrotor. Nonlinear tracking control laws are designed with the aim for sufficient tracking, not only in case of simple trajectories, but also for more aggressive acrobatic maneuvers.

7.1 Conclusions

We first state the main results regarding the theoretical research on modeling and tracking control of a quadrotor, and subsequently present our main conclusions concerning simulations and experiments.

Modeling and Control

A simplified mathematical model of a quadrotor has been derived, in which the attitude is parameterized by means of a rotation matrix, rather than minimal coordinates, resulting in a singularity free, global attitude representation. From this model description it is clear that the translational motion of a quadrotor is strongly affected by its attitude. This typical system property reveals a natural cascaded structure which serves as a critical element in tracking control design.

As a tracking control objective, it has been chosen to let a set of position and velocity tracking errors converge to zero. By expressing these error coordinates within a frame fixed to the reference quadrotor, independence of the choice of inertial frame of reference is provided. Moreover, within the resulting tracking error dynamics a convenient combination of the input thrust and quadrotor's orientation appears, which is subsequently used as a new virtual control input channel. This approach eventually allows to divide the overall control problem into the stabilization of two subsystems: a time-varying position tracking error system and a consequent attitude error system. Due to its definition, the latter subsystem is well-defined if the control input to the first subsystem remains within certain bounds. Considering this constraint, deliberate controllers are designed. By means of Lyapunov stability theory it has been shown that the closed-loop position subsystem and attitude error subsystem are *globally uniformly asymptotically* stable and *almost-globally uniformly asymptotically* stable, respectively. The complete closed-loop system is found to admit a cascaded, in which the position subsystem is coupled with the output of the attitude subsystem through a nonlinear coupling term. From cascaded

system theory it is known, however, that the asymptotic stability properties of each subsystem do not necessarily guarantee asymptotic stability of the complete closed-loop cascaded system. One additionally needs uniform boundedness of the solutions. It has ultimately been shown by means of cascaded stability theory that the complete closed-loop system is *almost-globally uniformly asymptotically* stable. Using a signal chasing approach, it has furthermore been shown that in addition to the position and velocities, the attitude and angular velocities of the quadrotor completely converge to the reference behaviour.

The proposed full state feedback control framework is subsequently used for output feedback control design. Regarding the absence of direct velocity measurements, a proportional integral Luenberger observer, driven by position measurements, has been designed for estimating the position tracking errors. Using standard Lyapunov techniques, *global uniform exponential* convergence of the estimated errors to the actual errors has been shown. Similar to the state feedback case, the complete closed-loop system admits a cascaded structure for which *almost-global uniform asymptotic* stability properties are derived by means of cascaded stability theory.

Simulations and Experiments

The proposed cascaded output feedback controller has been implemented in a numerical model of a quadrotor, in which the sensory behaviour (including noise and delays) and actuator dynamics of a Parrot AR Drone 2.0 are incorporated. Simulations are conducted in which it is desired for the quadrotor to track a three-dimensional circular reference trajectory. The results show sufficient tracking in case of corrupted measurements and saturation effects. In addition, it has been observed that a delay in the position measurements has some significant influence on the observer performance.

Since the simulations show successful results, the output feedback control structure has subsequently been embedded within a real Parrot AR Drone 2.0. Hovering experiments demonstrate the effectiveness of the proposed control law for the case of a simple time-invariant reference trajectory. In second experiments, it is desired for the drone to track a more challenging, three-dimensional circular reference trajectory. The results show that the controlled Parrot AR Drone is indeed capable of autonomously performing a stable three-dimensional circular maneuver. However, a large deviation from the reference trajectory remains in the sense that the quadrotor is unable to track the specified amplitudes in all directions. Unmodeled damping in the quadrotor's dynamics has been identified as a main cause of this effect. This has been confirmed by a comparison between the experimental results and the simulation results in which the generalized damping is added to the dynamics. This illustrates that the simplified model is inaccurate in case fast maneuvers are performed. We further remark several other effects such as turbulence of the surrounding air and decreasing motor-rotor functioning as possible other factors for making tracking considerably more difficult.

7.2 Recommendations

This final section presents some recommendations for future work, regarding modeling, control and hardware.

Modeling

- In order to improve the accuracy of the mathematical model of a quadrotor, dominant motion dependent (damping) effects should be added to the system description. Although these effects could be modeled, another interesting approach is to determine these effects during flight by means of an on-line estimation algorithm. Additional system identification experiments can be performed, for example, for mapping unconsidered effects of the rotors in turbulent air.

Control

- In order to improve the tracking performance, it is first and foremost suggested to add a feedforward structure to the proposed control scheme for compensating the previously mentioned dominant effects. Hereto, (dynamic) cancellation terms could be added to the proposed position and attitude feedback control laws.
- A certain degree of conservativeness is introduced in the state-feedback controller through the stability analyses. For example, the closed-loop stability analysis in the proof of Proposition 4.2.1 restricts the choice of gain matrices to $k_i I$. It is therefore recommended to examine other stability methods for obtaining possibly less conservative matrices (e.g. non-diagonal matrices). A similar recommendation is made for the proposed Luenberger observer.
- The necessity for the input thrust f to be larger than zero for letting the desired orientation be well defined in all cases, imposes some limitations on the control. Whereas in this work a saturation approach is chosen to satisfy this requirement, it is recommended to investigate other methods, for example a hybrid approach, for possibly improving the performance of the position control loop.
- The proposed attitude controller is somewhat redundant as for position tracking only the last column of the quadrotor's rotation matrix is of importance. It is therefore interesting to examine reduced attitude control methods, which can possibly provide certain benefits regarding control efficiency. Furthermore, the addition of integral control to the attitude control loop can be explored.
- It is suggested to further improve the proposed observers, for example by explicitly taking into account measurement delays.

Experimental Setup

- Within the experimental setup, a main source for delayed position measurements is the image processing algorithm. It is recommended to improve this algorithm and possibly use a different programming language (e.g. C) for reducing the processing time.
- The topcam used for position measurements has some limitations during large angle maneuvers of the quadrotor as the LEDs might disappear from the camera's view. In order to be able to accurately determine the position during aggressive maneuvers, alternative

positioning systems such as VICON, SLAM, GPS and the use of the internal cameras should be explored.

Bibliography

- [1] E. Semsch, M. Jakob, D. Pavlicek, and M. Pechoucek, "Autonomous UAV surveillance in complex Urban Environments," *2009 IEEE/WIC/ACM international Conference on Web Intelligence and Intelligent Agent Technology Workshops*, pp. 82 – 85, September 2009.
- [2] Y. Naidoo, R. Stopforth, and G. Bright, "Development of an UAV for search and rescue applications," *Africon 2011*, pp. 1–6, September 2011.
- [3] J. Han, Y. Xu, L. Di, and Y. Chen, "Low-cost multi-UAV technologies for contour mapping of nuclear radiation field," *J. Intell. Robot. Syst.*, pp. 401–410, April 2013.
- [4] A. Ahmad, K. Tahar, W. Udin, K. Hashim, N. Darwin, M. Hafis, M. Room, N. Farhah, N. Azhar, and S. Azmi, "Digital Aerial Imagery of Unmanned Aerial Vehicle for various Applications," *2013 IEEE International Conference on Control System, Computing and Engineering*, pp. 535–540, November 2013.
- [5] J. Cione, E. Kalina, E. Uhlhorn, A. Farber, and B. Damiano, "Coyote unmanned aircraft system observations in Hurricane Edouard (2014)," *Earth and Space Science*, pp. 370–380, September 2016.
- [6] M. Russon, "DHL to launch Parcelcopter medicine drone delivery service to remote German island," *International Business Times*, September 2014.
- [7] P. Tripicchio, M. Satler, G. Dabisias, E. Ruffaldi, and C. Avizzano, "Towards smart farming and sustainable agriculture with drones," *International Conference on Intelligent Environments*, pp. 140–143, 2015.
- [8] H. Fernando, A. De Silva, M. De Zoysa, and K. Dilshan, "Modelling, simulation and implementation of a quadrotor UAV," *2013 8th IEEE International Conference on Industrial and Information Systems (ICIIS)*, pp. 207–2012, December 2013.
- [9] Y. Choi and H. Ahn, "Nonlinear Control of Quadrotor for Point Tracking: Actual Implementation and Experimental Tests," *IEEE/ASME transactions on Mechatronics*, pp. 1179–1192, June 2015.
- [10] A. Brandao, M. Filho, and R. Carelli, "High-level underactuated nonlinear control for rotorcraft machines," *2013 IEEE International Conference on Mechatronics (ICM)*, pp. 279–285, February 2013.
- [11] R. Mahony, V. Kumar, and P. Corke, "Modeling, estimation and control of quadrotors," *IEEE Robotics and Automation Magazine*, pp. 20–32, 2012.
- [12] V. Parra-Vega, A. Sanchez, and C. Izaguirre, "Toward force control of a quadrotor UAV in SE(3)," *Conference on Decision and Control*, pp. 1802–1809, 2012.
- [13] T. Lee, "Exponential stability of an attitude tracking control system on SO(3) for large angle rotational maneuvers," *Systems and Control Letters*, pp. 231–237, December 2011.

-
- [14] G. Hoffmann, S. Waslander, and C. Tomlin, "Quadrotor helicopter trajectory control," *Proceedings of the AIAA Guidance, Navigation and Control Conference and Exhibit*, pp. 1–14, 2008.
- [15] R. Garcia, F. Rubio, and M. Ortega, "Robust PID Control of the Quadrotor Helicopter," *IFAC Conference on Advances in PID Control*, pp. 229–234, March 2012.
- [16] M. Belkheiri, A. Rabhi, A. El Hajjaji, and C. Pegard, "Different linearization control techniques for a quadrotor system," *2012 2nd International Conference on Communications, Computing and Control Applications (CCCA)*, pp. 1–6, December 2012.
- [17] X. Heng, D. Cabecinhas, R. Cunha, C. Silvestre, and X. Qingsong, "A trajectory tracking LQR controller for a quadrotor: design and experimental evaluation," *TENCON 2015 - 2015 IEEE Region 10 Conference*, pp. 1–7, November 2015.
- [18] S. Bouabdallah and R. Siegwart, "Backstepping and Sliding-mode Techniques Applied to an Indoor Micro Quadrotor," *Proceedings of the 2005 IEEE international Conference on Robotics and Automation*, pp. 2247–2252, April 2005.
- [19] T. Madani and A. benallegue, "Backstepping Control for a Quadrotor Helicopter," *Proceedings of the 2006 IEEE/RSJ*, pp. 3255–3260, October 2006.
- [20] H. Dang, B. Mohamed, and H. Rafaralahy, "Trajectory-tracking control design for an under-actuated quadrotor," *2014 European Control Conference (ECC)*, pp. 1765–1770, June 2014.
- [21] R. Skjetne and T. Fossen, "On integral control in backstepping: Analysis of different techniques," *Proceedings of the 45th IEEE Conference on Decision and Control*, pp. 1899–1904, 2004.
- [22] K. Benzaid, N. Mansouri, and O. Labbani-Igbida, "Robust Trajectory Tracking Control of a Quadrotor UAV," *Proceedings of the 3rd International Conference on Systems and Control*, pp. 206–211, October 2013.
- [23] G. Raffo, M. Ortega, and F. Rubio, "Robust nonlinear control for path tracking of a quadrotor helicopter," *Asian Journal of Control*, pp. 142–156, December 2013.
- [24] S. Islam, M. Faraz, K. Ashour, J. Dias, and L. Seneviratne, "Robust Adaptive control of Quadrotor Unmanned Aerial Vehicles with Uncertainty," *2015 IEEE International Conference on Robotics and Automation*, pp. 1704–1709, May 2015.
- [25] Z. Weidong, Z. Pengxiang, W. Changlong, and C. Min, "Position and attitude tracking control for a quadrotor UAV based on terminal sliding mode control," *Proceedings of the 34th Chinese Control Conference*, pp. 3398–3404, 2015.
- [26] R. Rashad, A. Aboudonia, and A. El-Badawy, "Backstepping Trajectory Tracking Control of a Quadrotor with Disturbance Rejection," *2015 XXV International Conference on Information, Communication and Automation Technologies (ICAT)*, pp. 1–7, October 2015.
- [27] A. A. J. Lefeber, *Tracking Control of Nonlinear Mechanical Systems*. PhD thesis, Twente University, April 2000.
- [28] G. Falconi, O. Fritsch, B. Lohmann, and F. Holzapfel, "Admissible Thrust Control Laws for Quadrotor Position Tracking," *American Control Conference*, pp. 4844–4849, June 2013.

- [29] B. van Aert, “Control and Coordination Algorithms for Autonomous Multi-Agent Quadrotor Systems,” Master’s thesis, University of Technology Eindhoven, 2016. Department of Mechanical Engineering, CST 2016.070.
- [30] T. Madani and A. Benallegue, “Sliding Mode Observer and Backstepping Control for a Quadrtor Unmanned Aerial Vehicle,” *Proceedings of the 2007 American Control Conference*, pp. 5887–5892, July 2007.
- [31] B. Xian, C. Diao, B. Zhao, and Y. Zhang, “Nonlinear robust output feedback tracking control of a quadrotor uav using quaternion representation,” *Nonlinear Dynamics*, vol. 79, no. 4, pp. 2735–2752, 2015.
- [32] D. Abeywardena, S. Kodagoda, G. Dissanayake, and R. Munasinghe, “Improved State Estimation in Quadrotor MAV’s: A Novel Drift-Free Velocity Estimator,” *IEEE Robotics and Automation Magazine*, pp. 1–8, September 2015.
- [33] R. Leishman, J. Macdonald, and R. Beard, “Quadrotors and Accelerometers: State Estimation with an Improved Dynamic Model,” *IEEE Control Systems*, pp. 28–41, January 2014.
- [34] B. Siciliano, L. Sciavicco, L. Villani, and G. Oriolo, *Robotics Modeling, Planning and Control*. Springer, 2009.
- [35] N. Chaturvedi, A. Sanyal, and N. H. McClamroth, “Rigid-Body Attitude Control,” *IEEE Control Systems*, vol. 31, pp. 30–51, May 2011.
- [36] M. Spong, S. Hutchinson, and M. Vidyasagar, *Robot Modeling and Control*. John Wiley and Sons, 2006.
- [37] N. van de Wouw, *Multibody Dynamics, Lecture Notes and Exercises*. Eindhoven University of Technology, September 2013.
- [38] H. K. Khalil, *Nonlinear Systems*. Prentice Hall, 3 ed., December 2001.
- [39] A. Micaelli and C. Samson, “Trajectory tracking for unicycle-type and two-steering-wheels mobile robots,” *Rapport de recherche 2097, INRIA*, 1993.
- [40] E. Lefeber and H. Nijmeijer, “Globally bounded tracking controllers for rigid body systems,” *Proceedings of the 4th European Control Conference*, 1997.
- [41] B. Paden and R. Panja, “Globally asymptotically stable PD+ controller for robot manipulators,” *International Journal of Control*, pp. 1697–1712, 1988.
- [42] E. Panteley and A. Loria, “On global uniform asymptotic stability of nonlinear time-varying systems in cascade,” *Systems and Control Letters*, vol. 33, pp. 131–138, 1998.
- [43] E. Panteley and A. Loria, “Growth rate conditions for uniform asymptotic stability of cascaded time-varying systems,” *Automatica*, vol. 37, pp. 453–460, September 2000.
- [44] P. Garcia, R. Lozano, and A. Dzul, *Modelling and Control of Mini-Flying Machines*. Springer-Verlag London, 1 ed., 2005.
- [45] P. Pounds, R. Mahony, P. Hynes, and J. Roberts, “Design of a four-rotor aerial robot,” *Australasian Conference on Robotics and Automation*, pp. 145–150, 2002.

- [46] Q. Li, “Grey-Box System Identification of a Quadrotor Unmanned Aerial Vehicle,” Master’s thesis, Delft University of Technology, September 2014. Faculty of Mechanical, Maritime and Materials Engineering.
- [47] A. Das, K. Subbarao, and F. Lewis, “Dynamic inversion with zero-dynamics stabilisation for quadrotor control,” *IEEE international Conference on Control Applications*, pp. 1189–1194, September 2008.
- [48] Y. Kanayama, Y. Kimura, F. Miyazaki, and T. Noguchi, “A stable tracking control method for an autonomous mobile robot,” *Proceedings of the IEEE Conference on Robotics and Automation*, pp. 384–389, 1990.
- [49] L. Rundqwist, *Anti-reset windup for PID controllers*. PhD thesis, Lund Institute of Technology, Sweden, March 1991. Department of Automatic Control.
- [50] Y. Peng, D. Vrancic, and R. Hanus, “Anti-windup, bumpless, and conditioned transfer techniques for PID controllers,” *IEEE Control Systems Magazine*, pp. 48–57, 1996.
- [51] L. Ranran and H. Khalil, “Conditional integrator for non-minimum phase nonlinear systems,” *IEEE Conference on Decision and Control*, pp. 4883–4887, 2012.
- [52] M. Hua and C. Samson, “Time sub-optimal nonlinear PI and PID controllers applied to longitudinal Headway car control,” *International Journal of Control*, pp. 1717–1728, 2011.
- [53] M. Hua, T. Hamel, P. Morin, and C. Samson, “A control approach for thrust-propelled underactuated vehicles and its application to VTOL drones,” *IEEE Transactions on Automatic Control*, vol. 54, no. 8, pp. 1837–1853, 2009.
- [54] P. Crouch, “Spacecraft attitude control and stabilization: an application of geometric control theory to rigid body models,” *IEEE Transaction on Automatic Control*, vol. 29, no. 4, pp. 321–331, 1984.
- [55] S. Bhat and D. Bernstein, “A topological obstruction to continuous global stabilization of rotational motion and the unwinding phenomenon,” *Systems and Control Letters*, vol. 39, pp. 66–73, 2000.
- [56] A. Sanyal and N. Chaturvedi, “Almost global robust attitude tracking control of spacecraft in gravity,” *Proc. AIAA Conf. Guidance, Navigation, and Control*, May 2008.
- [57] A. Weiss, G. Cruz, and K. Agarwal, “Inertia-free attitude control laws based on rotation matrices for spacecraft with torquers, thrusters and wheels,” *Meemorial Symposium on Estimation, Navigation, and Spacecraft Control*, pp. 322–391, 2012.
- [58] T. Lee, “Global exponential attitude tracking controls on $SO(3)$,” *IEEE Transactions on Automatic Control*, vol. 60, pp. 2837–2834, October 2015.
- [59] N. Chaturvedi, N. McClamroth, and D. Bernstein, “Asymptotic smooth stabilization of the inverted 3D pendulum,” *IEEE Transactions on Automatic Control*, vol. 54, no. 6, pp. 1204–1215, 2009.
- [60] A. Sanyal and Z. Lee-Ho, “Attitude tracking control of a small satellite in low earth orbit,” *AIAA Guidance Navigation and Control*, 2009.

-
- [61] T. Lee, M. Leok, and N. McClamroth, “Stable manifolds of saddle points for pendulum dynamics on S and $SO(3)$,” *Proceedings of the 50th IEEE Conference on Decision and Control*, December 2011.
- [62] V. Van Assche, T. Ahmed-Ali, C. Hann, and F. Lamnabhi-Lagarrigue, “High gain observer design for nonlinear systems with time-varying delayed measurements,” *IFAC World Congress*, pp. 692–696, 2011.
- [63] T. Ahmed-Ali, V. Van Assche, H. Massieu, and P. Dorleans, “Continuous-discrete observer for state affine systems with sampled and delayed measurements,” *IEEE Transactions on Automatic Control*, vol. 58, pp. 1085–1091, 2013.
- [64] M. Farza, M. Saad, M. Fall, E. Pigeon, O. Gehan, and R. Mosrati, “Continuous-discrete time observer for a class of MIMO nonlinear systems,” *IEEE Transactions on Automatic Control*, pp. 1060–1065, 2014.
- [65] S. Zhang, S. Yu, C. Liu, X. Yuan, and S. Liu, “A dual-linear Kalman filter for real-time orientation determination system using low-cost MEMS sensors,” *Sensors*, pp. 1–17, 2016.
- [66] N. Jeurgens, “Identification and control implementation of an AR Drone 2.0,” Master’s thesis, Eindhoven University of Technology, 2017. Department of Mechanical Engineering DC 2017.013.
- [67] N. Jeurgens, “Implementing a simulink controller in a AR Drone 2.0,” tech. rep., Eindhoven University of Technology, December 2015. Department of Mechanical Engineering DC 2016.005.
- [68] S. Piskorski, N. Brulez, P. Eline, and F. Haeyer, *AR Drone developer guide*, December 2012.

Appendix A

Observer Extension: Proof

In this appendix we present the exponential convergence result of the continuous-discrete observer (5.30) which is based on the proof given in [64]. Let us first recall the continuous-discrete observer structure as

$$\dot{\hat{e}}(t) = A(t)\hat{e}(t) + Bu(t) + L_p(\varphi(t) - \hat{y}(t)) - By_I(t) \quad (\text{A.1a})$$

$$\dot{y}_I(t) = -S(\omega_r(t))y_I(t) - L_I(\varphi(t) - \hat{y}(t)) \quad (\text{A.1b})$$

$$\hat{y}(t) = C\hat{e}(t) \quad (\text{A.1c})$$

where $\varphi(t)$ is the prediction of the system output, which is continuous in the interval $t \in (t_k, t_{k+1})$ and is updated with the available output at time t_k . The output predictor is defined as a hybrid system of the form

$$\begin{cases} \dot{\varphi}(t) = -S(\omega_r(t))\hat{e}_\rho(t) + \hat{e}_\nu(t) \\ \varphi(t_k^+) = y(t_k) \end{cases} \quad (\text{A.2})$$

where $y(t_k)$, $k \in \mathbb{N}$ is the output of the system, sampled at time t_k . We define the observer error $e_o(t) = e(t) - \hat{e}(t)$ and an auxiliary error function as $\psi(t) = \varphi(t) - \hat{y}(t)$. Using the translational error dynamics (4.7) and the augmented state $\xi(t) = (e_o(t), y_I(t))^T \in \mathbb{R}^9$, the following observer error dynamics are obtained

$$\dot{\xi} = (A_\xi(t) - \bar{L}\bar{C})\xi + \bar{L}(\bar{C}\xi(t) - \psi(t)) \quad (\text{A.3})$$

with

$$A_\xi(\omega_r(t)) = \begin{bmatrix} A(t) & B \\ 0 & -S(\omega_r(t)) \end{bmatrix}, \quad \bar{L} = \begin{bmatrix} L_p \\ L_I \end{bmatrix} \quad \text{and} \quad \bar{C} = [C \ 0]. \quad (\text{A.4})$$

Let us then consider these dynamics in the interval $t \in (t_k, t_{k+1})$ and define

$$y_e(t) = \bar{C}\xi(t) - \psi(t) \quad (\text{A.5})$$

which corresponds to the output estimation error. The dynamics of this error within the considered interval are derived as

$$\begin{aligned} \dot{y}_e(t) &= \bar{C}\dot{\xi}(t) - (\dot{\varphi}(t) - C\dot{\hat{e}}(t)) \\ &= C(\dot{e}(t) - \dot{\hat{e}}(t)) - (\dot{\varphi}(t) - C\dot{\hat{e}}(t)) \\ &= C\dot{e}(t) - \dot{\varphi}(t) \\ &= -S(\omega_r(t))(e_\rho(t) - \hat{e}_\rho(t)) + (e_\nu(t) - \hat{e}_\nu(t)) \\ &= Y(t)\xi(t) \end{aligned} \quad (\text{A.6})$$

with $Y(t) = [-S(\omega_r(t)) \quad I \quad 0]$. Furthermore, since $e_\rho(t)$ is continuous, it follows that $e_\rho(t_k) = e_\rho(t_k^+)$ and $y_e(t_k) = e_\rho(t_k^+) - \varphi(t_k^+) = 0$.

It is straightforward to verify that the first part of (A.3) corresponds to the continuous observer error dynamics (5.6) for which exponential stability of the origin is shown by means of the quadratic Lyapunov function $V(\xi) = \xi^\top P \xi$. Let us consider this function as a candidate Lyapunov function for the perturbed system (A.3) and choose the observer gains as $\bar{L}^\top = [l_1 I \quad l_2 I \quad l_3 I]$ with $l_1, l_2 > 0$ and $l_1 l_2 > l_3 > 0$. An upper bound for the time-derivative of V along the solutions of (A.3) within the interval $t \in (t_k, t_{k+1})$ then satisfies

$$\dot{V}(\xi) \leq -\|\xi\|^2 + 2\lambda_{\max}(P)\|\bar{L}\|\|\xi\|\|y_e\|. \quad (\text{A.7})$$

where we have used $Q = I$. Integration of the y_e -dynamics (A.6) over the sampling interval yields the following upper bound

$$\|y_e(t)\| \leq \sup_{t \in \mathbb{R}} \|Y(t)\| \int_{t_k^+}^t \|\xi(s)\| ds, \quad t \in (t_k, t_{k+1}). \quad (\text{A.8})$$

Note that $\sup_{t \in \mathbb{R}} \|Y(t)\|$ exists due to the assumption that $|\omega_r(t)| \leq \omega_{\max}$ for all $t \geq t_0$. Using this estimate and the well-known upper and lower bounds of a quadratic Lyapunov function, an estimate of the bound in (A.7) then follows as

$$\dot{V}(\xi) \leq -\alpha V(\xi) + 2\beta \sqrt{V(\xi)} \int_{t_k^+}^t \sqrt{V(\xi(s))} ds \quad (\text{A.9})$$

with

$$\alpha = \frac{1}{\lambda_{\max}(P)} \quad \text{and} \quad \beta = \sup_{t \in \mathbb{R}} \|Y(t)\| \|\bar{L}\| \frac{\lambda_{\max}(P)}{\lambda_{\min}(P)}. \quad (\text{A.10})$$

Applying the chain-rule $\frac{\dot{V}}{2\sqrt{V}} = \frac{d}{dt} \sqrt{V}$ to (A.9) and integrating the resulting expression within the sampling interval yields the following estimate for the decrease of the Lyapunov function

$$\sqrt{V(\xi(t))} \leq \sqrt{V(\xi(t_k^+))} + \left(\beta \delta_{\max} - \frac{\alpha}{2} \right) \int_{t_k^+}^t \sqrt{V(\xi(s))} ds, \quad t \in (t_k, t_{k+1}) \quad (\text{A.11})$$

where $\delta_{\max} = \max_{k \in \mathbb{N}} (t_{k+1} - t_k)$. Since $V(\xi(t))$ is positive definite, it then follows that

$$V(\xi(t)) \leq V(\xi(t_k^+)) \quad \text{if} \quad \delta_{\max} \leq \frac{\alpha}{2\beta} \quad (\text{A.12})$$

with α and β defined in (A.10), and consequently the observer error remains bounded within the sampling interval. Using (A.12) in (A.9), we obtain

$$\dot{V}(\xi) \leq -\alpha V(\xi) + 2\beta \delta_{\max} V(\xi(t_k^+)). \quad (\text{A.13})$$

Integrating this differential inequality on the sampling interval yields

$$V(\xi(t)) \leq \left(\left(1 - \frac{2\beta \delta_{\max}}{\alpha} \right) e^{-\alpha(t-t_k^+)} + \frac{2\beta \delta_{\max}}{\alpha} \right) V(\xi(t_k^+)). \quad (\text{A.14})$$

In order to find an exponential decay-rate for the Lyapunov function, in [64] it is proposed to define an auxiliary error function as

$$\varepsilon(t) = \left(\left(1 - \frac{2\beta\delta_{\max}}{\alpha} \right) e^{-\alpha(t-t_k^+)} + \frac{2\beta\delta_{\max}}{\alpha} \right) - e^{-\gamma(t-t_k^+)} \quad (\text{A.15})$$

and demand that $\varepsilon(t) \leq 0$. Hereto we use the property that the time-derivative of $\varepsilon(t)$ must be decreasing, i.e. $\dot{\varepsilon}(t) \leq 0$ and the observation that $\varepsilon(t_k) = 0$. An exponential decay rate is found as

$$V(\xi(t)) \leq e^{-\gamma(t-t_k^+)} V(\xi(t_k^+)) \quad \text{with} \quad \gamma = (\alpha - 2\beta\delta_{\max}) e^{-\alpha\delta_{\max}}. \quad (\text{A.16})$$

Since only the inter sample predictor is updated at the sampling time-instances, it is clear that the observer dynamics, and therefore the ξ -dynamics are only initialized at $t = t_0$, and then resolved for all t . This yields the (numerical) solutions to be continuous (non-smooth). Due to the definition of V , this function is continuous with respect to its arguments and hence $V(\xi(t_k^-)) = V(\xi(t_k))$. As a result we may conclude that

$$V(\xi(t)) \leq e^{-\gamma(t-t_0)} V(\xi(t_0)) \quad \forall t \geq t_0, \quad (\text{A.17})$$

and the estimated states exponentially converge to the actual states.

Appendix B

Attitude Reconstruction Algorithm

In this appendix the reconstruction of the quadrotor's attitude is discussed in more detail. Hereto, we first consider the estimation of the roll and pitch angles in Section B.1, and subsequently present the estimation of the yaw angle B.2.

B.1 Roll and Pitch Angles

For the reconstruction of the roll and pitch angles of the quadrotor, we use the accelerometer and gyroscopic data (cf. Figure 5.1). As a first step, we define the following state vector

$$x = g_{\mathcal{B}}, \quad (\text{B.1})$$

which represents the gravitational acceleration vector expressed with respect to the body fixed frame \mathcal{B} . Next, we define the output vector as

$$y = S_a, \quad (\text{B.2})$$

which corresponds to the output of the accelerometer. Recall that in Section 5.5 a theoretic description of this output in the absence of noise and bias was given as

$$S_a = R^\top(\ddot{\rho} + g e_3), \quad (\text{B.3})$$

where g is the gravitational acceleration expressed in an inertial frame of reference and is assumed to be constant and known. In [65, 67] it was shown that the unified discrete-time dynamics of the state x (B.1) could be expressed as

$$x_n = \Phi x_{n-1} + \mu_{n-1} \quad (\text{B.4})$$

$$y_n = H x_n + \nu_n, \quad (\text{B.5})$$

where μ_n and ν_n are the process and measurement noise vectors respectively. Moreover, the state transition matrix and output matrix are defined as

$$\Phi = \exp(-S(\omega) T_s) \quad \text{and} \quad H = I. \quad (\text{B.6})$$

Here, $S(\omega)$ is a skew-symmetric matrix containing the elements of the body-fixed angular velocity vector $\omega = [p, q, r]^\top$, expressed as

$$S(\omega) = \begin{bmatrix} 0 & -r & q \\ r & 0 & -p \\ -q & p & 0 \end{bmatrix}, \quad (\text{B.7})$$

and T_s is the sampling time. In order to estimate the body-fixed angular acceleration, a standard linear Kalman filter algorithm is proposed as [66, 67]

$$\bar{x}(k) = \Phi(k)\hat{x}(k-1) \quad (\text{B.8})$$

$$P^-(k) = \Phi(k)P(k-1)\Phi(k)^\top + Q(k) \quad (\text{B.9})$$

$$K(k) = P^-(k)H^\top \left(HP^-(k)H^\top + \lambda W \right)^{-1} \quad (\text{B.10})$$

$$\hat{x}(k) = \bar{x}(k) + K(k)(y(k) - H\bar{x}(k)) \quad (\text{B.11})$$

$$P(k) = \frac{1}{\lambda} (I - K(k)H) P^-(k), \quad (\text{B.12})$$

where we have defined $Q = LR_\omega L^\top$ as the process noise covariance matrix with

$$R_\omega = \text{diag}([\sigma_p^2, \sigma_q^2, \sigma_r^2]) \quad \text{and} \quad L = -S(\omega_m). \quad (\text{B.13})$$

Here, R_ω consists of the variances of the angular velocity measurements ω_m . Moreover, W is the sensor covariance matrix for the accelerometer. From the sensor description (B.3) it is clear that in case the drone is subject to small accelerations (i.e. $\ddot{p} = 0$), the measurements can be useful for estimating the body fixed gravitational acceleration. However, for large accelerations, these measurements could result in inaccurate state estimation. In order to overcome this issue, and still provide good attitude estimation during flight, in [65] a so-called decisive algorithm is proposed.

B.1.1 Decisive Algorithm

The decisive algorithm determines whether to use or disregard the accelerometer data for state estimation. Hereto, an error variable is introduced as

$$\alpha = \||S_a\| - \|g_B\|. \quad (\text{B.14})$$

Note that since $\|g_B\| = g$, in case of no accelerations and noise the error variable is zero. Furthermore, if S_a is subject to noise, α is rather small. The sensor covariance matrix is then defined as follows:

$$W = \begin{cases} W_0 & \text{for } \alpha \leq \delta \\ W_0 + k\alpha^2 I & \text{for } \delta < \alpha \leq \Delta \\ \gamma I & \text{for } \alpha > \Delta \end{cases} \quad (\text{B.15})$$

where $W_0 = \text{diag}([\sigma_x^2, \sigma_y^2, \sigma_z^2])$, δ is the noise threshold suggested as $\delta = \sqrt{\sigma_x^2 + \sigma_y^2 + \sigma_z^2}$ and Δ is some experimentally determined value. Moreover, γ is a parameter which must be set sufficiently large (e.g. $\gamma = 1 \cdot 10^8$) and k is a tuning parameter. Note that in this decisive algorithm, a distinction is made between large accelerations and sensor noise. Furthermore, for $W = \gamma I$, the Kalman gain K in (B.10) is temporarily set to zero, such that we only rely on the gyroscopic measurements for state estimation.

The estimated body-fixed gravitational acceleration is then obtained as $\hat{x} = \hat{R}^\top g e_3$, such that the last column of \hat{R} is determined by \hat{x}/g . If we then parametrize the rotation matrix R as

a sequence of rotations around the x , y and z axes of a fixed frame respectively, the roll and pitch angles are determined as

$$\hat{\phi} = \text{atan2}(\hat{x}_2, \hat{x}_3) \quad (\text{B.16})$$

$$\hat{\theta} = -\text{atan2}\left(\hat{x}_1, \sqrt{\hat{x}_2^2 + \hat{x}_3^2}\right). \quad (\text{B.17})$$

B.2 Yaw Angle

The reconstruction of the yaw angle is done in a similar manner as reconstructing the roll and pitch angle. Here, we have defined the state vector $x = m_{\mathcal{B}}$, and the augmented output vector

$$y = [S_m, S_c], \quad (\text{B.18})$$

where S_m corresponds to the magnetometer output, which for the ideal case is defined as

$$S_m = R^\top m_{\mathcal{I}}, \quad (\text{B.19})$$

with $m_{\mathcal{I}}$ the earth's magnetic field vector, expressed with respect to the inertial frame of reference. Furthermore, since we have access to data from an external camera, we have defined [66]

$$S_c = R_c^\top(\hat{\phi}, \hat{\theta}, \psi_c) m_{\mathcal{I}}, \quad (\text{B.20})$$

in which ψ_c is the heading angle of the quadrotor according to the camera. The body-fixed magnetic field vector is then estimated by means of a similar Kalman filter algorithm, with $H = [I, I]^\top$. Furthermore, the sensor covariance matrix W is defined as

$$W = \begin{bmatrix} W_m & 0 \\ 0 & W_c \end{bmatrix} \quad (\text{B.21})$$

in which W_m is the sensor covariance matrix of the magnetometer, and W_c the sensor covariance matrix related to the camera measurements. In order to prevent unreliable data to be used for yaw estimation, we again adopt a decisive algorithm, which determines the covariance matrices according to

$$W_m = \begin{cases} W_{m0} & \text{for } \alpha \leq \Delta \\ \gamma I & \text{otherwise} \end{cases} \quad (\text{B.22})$$

and

$$W_c = \begin{cases} W_{c0} & \text{if } \exists \psi_c \text{ and } \psi_c^k \neq \psi_c^{k-1} \\ \gamma I & \text{otherwise.} \end{cases} \quad (\text{B.23})$$

Here, $W_{m0} = \text{diag}([\sigma_{m1}^2, \sigma_{m2}^2, \sigma_{m3}^2])$ and $W_{c0} = \text{diag}([\sigma_{c1}^2, \sigma_{c2}^2, \sigma_{c3}^2])$. Furthermore, the comparison variable α is defined as $\alpha = \||S_m\| - \|m_{\mathcal{I}}\|$ and Δ is some threshold value. The yaw angle is subsequently determined as

$$\hat{\psi} = -\text{atan2}(m_2^*, m_1^*), \quad (\text{B.24})$$

where m_i^* are the respective components of the vector

$$m^* = R_y(\hat{\theta})R_x(\hat{\phi})\hat{m}_{\mathcal{B}}. \quad (\text{B.25})$$

A standard transformation from roll, pitch and yaw angles to a rotation matrix can then be done to obtain \hat{R} , which is used for attitude tracking control.

Acknowledgements

First and foremost, I would like to express my sincere gratitude to my supervisor prof. dr. H. Nijmeijer for providing me the opportunity to work on this project and for the continuous support, motivating enthusiasm and immense knowledge. I am grateful for the monthly meetings and discussions which led to valuable insights and new ideas.

Furthermore, I would like to thank my coach, dr. ir. A.A.J. Lefeber. Dear Erjen, thank you for the useful feedback, valuable guidance, and for always being there whenever I needed your advice.

A special thanks goes to my colleague student Niels Jeurgens for all his help and patience during the experimental parts of this project. Niels, it was a pleasure working with you.

I would like to thank my girlfriend Simone who has always believed in me and whose presence lights up my world. Finally, a special word of thanks goes to my parents for their everlasting support and unconditional encouragement during my studies. Dear Mom and Dad, this work is entirely dedicated to you.

Sebastiaan van den Eijnden
January 9, 2017